

The University of Maine

DigitalCommons@UMaine

Electronic Theses and Dissertations

Fogler Library

Summer 8-18-2023

Exploring the Impact of PQN-75 and GLH-1/Vasa on Germline Development, Maintenance, and GSC Reprogramming Using *Caenorhabditis elegans* as a Model

Jesse D. Rochester

University of Maine, jesse.rochester@maine.edu

Follow this and additional works at: <https://digitalcommons.library.umaine.edu/etd>



Part of the [Developmental Biology Commons](#)

Recommended Citation

Rochester, Jesse D., "Exploring the Impact of PQN-75 and GLH-1/Vasa on Germline Development, Maintenance, and GSC Reprogramming Using *Caenorhabditis elegans* as a Model" (2023). *Electronic Theses and Dissertations*. 3850.

<https://digitalcommons.library.umaine.edu/etd/3850>

This Open-Access Dissertation is brought to you for free and open access by DigitalCommons@UMaine. It has been accepted for inclusion in Electronic Theses and Dissertations by an authorized administrator of DigitalCommons@UMaine. For more information, please contact um.library.technical.services@maine.edu.

**EXPLORING THE IMPACT OF PQN-75 AND GLH-1/VASA ON GERMLINE DEVELOPMENT,
MAINTENANCE, AND GSC REPROGRAMMING USING *CAENORHABDITIS ELEGANS* AS A MODEL**

By

Jesse David Rochester

B.S. University of Maine Fort Kent, 2016

A DISSERTATION

Submitted in Partial Fulfillment of the

Requirements for the Degree of

Doctor of Philosophy

(in Biomedical Science)

The Graduate School

The University of Maine

August 2023

Advisory Committee:

Dustin Updike, Associate Professor, Mount Desert Island Biological Laboratories, Advisor

Christopher Baker, Assistant Professor, The Jackson Laboratory

Ewelina Bolcun-Filas, Associate Professor, The Jackson Laboratory

Joel Graber, Senior Staff Scientist, Mount Desert Island Biological Laboratories

Aric Rogers, Associate Professor, Mount Desert Island Biological Laboratories

© 2023 Jesse David Rochester

All Rights Reserved

**EXPLORING KEY GERM GRANULE COMPONENT'S ROLE IN FERTILITY AND GERMLINE STEM
CELL PLURIPOTENCY USING CAENORHABDITIS ELEGANS AS A MODEL**

By Jesse Rochester

Dissertation Advisor: Dr. Dustin Updike

An Abstract of the Dissertation Presented
in Partial Fulfillment of the Requirements for the
Degree of Doctor of Philosophy
(in Biomedical Science)
August 2023

This thesis combines research on PQN-75 expression, functional motifs of GLH-1/Vasa, and germ granule components in *Caenorhabditis elegans* to provide a comprehensive understanding of germline development, maintenance, and reprogramming, while also examining the role of pharyngeal gland cells in stress resistance and thermotolerance. In *C. elegans*, pharyngeal gland cells secrete mucin-like proteins, such as PQN-75, with similarities to human PRB2. The expression of PQN-75 in gland cells confers stress resistance and thermotolerance but does not affect fertility, instead it plays a role in the organism's ability to adapt to varying environmental conditions. While, GLH-1/Vasa, an ATP-dependent DEAD-box helicase, plays a critical role in safeguarding the germline by regulating translation and amplifying piwi-interacting RNAs. To elucidate the functions of GLH-1 and its role in germline development, CRISPR/Cas9 technology was employed to investigate its functional motifs in *C. elegans* by analyzing 28 endogenous mutant alleles. Results demonstrate that helicase activity is essential for GLH-1's association with P granules, and removing glycine-rich repeats diminishes P-granule interactions at the nuclear periphery. Additionally, mass spectrometry

reveals an affinity between GLH-1 and three structurally conserved PCI complexes, along with a reciprocal aversion for assembled ribosomes and the 26S proteasome. Suggesting that P granules compartmentalize the cytoplasm to exclude large protein assemblies, effectively shielding associated transcripts from translation, contributing to germline maintenance. Germ granules are essential for maintaining germline integrity and stem cell totipotency. Depletion of core germ granule components in *C. elegans* leads to germ cell reprogramming and sterility. To better understand the initiation of somatic reprogramming and the role of GLH-1 in this process, total mRNA (transcriptome) and polysome-associated mRNA (translatome) changes in a precision full-length deletion of *glh-1* were examined. Here two significant changes were observed: first, GLH-1 suppresses the expression of neuropeptide-encoding transcripts, suggesting a role in repressing somatic reprogramming and maintaining germline integrity; second, GLH-1 promotes Major Sperm Proteins levels, repressing spermatogenic expression during oogenesis and promoting MSP expression to drive spermiogenesis and sperm motility, highlighting its importance in fertility. Our findings contribute to understanding the roles of PQN-75 and GLH-1/Vasa in *C. elegans* germline development, maintenance, and germline stem cell reprogramming, while also shedding light on the organism's stress resistance and thermotolerance mechanisms. With broader implications identifying early stem cell reprogramming processes and provides a platform for future research on germline biology in *C. elegans*.

ACKNOWLEDGEMENTS

I would like to take this opportunity to express my deep appreciation to the people who have been an integral part of my academic journey and have played a crucial role in my success.

First and foremost, I would like to express my heartfelt gratitude to my loving parents Dave and Michelle Rochester. Their unwavering love, encouragement, and support have been the foundation of my achievements. Their sacrifices have helped me pursue my dreams and complete this thesis. Without them, this accomplishment would not have been possible.

I am also indebted to my fiancé Maren Leach, whose belief in me and unwavering support have been a constant source of inspiration and motivation. Your encouragement during the highs and lows of this journey have been the driving force behind my accomplishments. Your constant reminders to prioritize work-life balance have helped me maintain my mental and physical health, enabling me to stay focused on my research.

To my brother Jonathan Rochester, who has always been there for me, thank you for being my biggest cheerleader and never doubting my capabilities. Your ability to maintain a healthy work-life balance has been an inspiration to me, and I am grateful for the advice and support you have provided throughout my academic journey.

To my friends and family, thank you for your support and encouragement along the way. Your presence in my life has been invaluable, and I am grateful for the laughter, joy, and memories that we have shared.

I extend my heartfelt gratitude to all the members of my thesis committee Dr. Aric Rogers, Dr. Christopher Baker, Dr. Ewelina Bolcun-Filas, and Dr. Joel Graber; for their guidance, feedback, and invaluable support throughout this process. Your insights and knowledge have

been critical in shaping my research and helping me achieve my goals. I have learned so much from all of you, and I will carry these lessons with me throughout my career.

Finally, to my Ph.D. mentor Dr. Dustin Updike, thank you for believing in me and guiding me throughout this journey. Your mentorship has been instrumental in my academic growth and development. Your expertise, guidance, and encouragement have been invaluable, and I am grateful for the opportunities that you have provided me.

This thesis is dedicated to all of you, and I hope to make you proud with my future endeavors.

TABLE OF CONTENTS

ACKNOWLEDGMENTS.....	iii
LIST OF TABLES.....	viii
LIST OF FIGURES.....	ix
LIST OF ABBREVIATIONS.....	xi
Chapter I.....	1
Introduction	1
1.1 Stem cells.....	1
1.1.1 The history of stem cells.....	1
1.1.2 Stem cell classification.....	2
1.1.3 Somatic cell nuclear transfer and Stem cell induction	4
1.1.4 Stem cell medical applications and boundaries	6
1.1.5 Germline stem cells	7
1.2 <i>C. elegans</i> as a model organism	9
1.2.1 <i>C. elegans</i> life cycle.....	10
1.2.2 Anatomy of <i>C. elegans</i>	11
1.2.3 <i>C. elegans</i> Germline.....	19
1.2.3.1 Regions of the <i>C. elegans</i> germ line.....	20
1.2.4 Spermatogenesis in <i>C. elegans</i>	22
1.2.4.1 Spermatozoa morphology and activation	24
1.2.4.2 Major Sperm Proteins (MSPs) and sperm mobility	25
1.2.5 Genome editing in <i>C. elegans</i>	26
1.3 Germ plasma and granules	28
1.3.1 Germ granule conservation	30
1.3.1.1 Germ granules' structure and composition.....	32
1.3.2 DEAD-box RNA helicases	35
1.3.2.1 Role of GLH-1 in the <i>C. elegans</i> germline	37
1.4 Somatic reprogramming of germ cells.....	39
1.5 Review of the current state of research	41
1.6 Overview of dissertation	43
1. CHAPTER II: MATERIALS AND METHODS.....	46
2.1 Strains used	46
2.1 <i>C. elegans</i> maintenance	48
2.2 CRISPR strain construction	48
2.3 Live imaging of germline	50

2.4	Fixation and immunostaining.....	50
2.5	Liquid Cultures.....	51
2.5	Polysome profiling.....	52
2.7	RNA-Sequencing.....	53
2.8	qRT-PCR.....	53
2.9	Sequence analysis and data deposits.....	54
2.10	Growth assays	56
2.10.1	larval development size assay	56
2.10.2	Vulva development.....	56
2.10.3	Grinder size.....	56
2.11	Germline integrity	57
2.11.1	Variable Temperature Fertility counts	57
2.11.2	RNAi Fertility counts	57
2.12	Sperm functionality assays.....	57
2.12.1	Sperm migration	57
2.12.2	Sperm counts.....	58
2.12.3	In Vitro Sperm activation.....	58
2.13	Embryonic lethality	59
2.14	Proteotoxic stress assays	59
2.14.1	Oxidative stress	59
2.14.2	Osmotic stress	59
2.14.3	Heat stress	59
2.15	Biofilm formation	60
2.	CHAPTER III: CHARACTERIZATION OF THE GERMLINE DISPENSABLE PQN-75	61
3.1	Chapter summary.....	61
3.2	Introduction.....	62
3.3	Results	63
3.4	Discussion.....	77
3.	CHAPTER IV: GLH-1 IS REQUIRED TO MAINTAIN GERMLINE FERTILITY	82
4.1	Chapter Summary.....	82
4.2	Introduction.....	83
4.3	Results	86
4.4	Discussion	109

4. CHAPTER V: GLH-1 PREVENTS EARLY SOMATIC REPROGRAMMING	114
5.1 Chapter Summary.....	114
5.2 Introduction.....	116
5.3 Results	120
5.4 Discussion	136
5. CHAPTER VI: CONCLUDING DISCUSSION AND FUTURE DIRECTIONS	140
6.1 Chapter Summary.....	140
6.2 Concluding Discussions	141
6.2.1 PQN-75.....	141
6.2.1.1 Future Directions	143
6.2.2 GLH-1	144
6.2.2.1 Future Directions	145
6.2.3.1 Future Directions	148
6.3 Concluding Remarks.....	150
REFERENCES	151
APPENDICES	177
APPENDICE A: SUPPLEMENTAL TABLES AND FIGURES	177
APPENDICE B: DEPOSITED DATA	182
BIOGRAPHY OF THE AUTHOR	182

LIST OF TABLES

Table 1: List of all <i>C. elegans</i> strains used in this thesis.	48
Table 2: CRISPR/Cas9 reagents for generating <i>glh-1</i> alleles.	181

LIST OF FIGURES

Figure 1: <i>Caenorhabditis elegans</i> life cycle.....	11
Figure 2: Nematode body anatomy	13
Figure 3: Anatomy of the <i>C. elegans</i> pharynx.....	14
Figure 4: Cells of the <i>C. elegans</i> pharynx	16
Figure 5: Gland cells of the pharynx	18
Figure 6: Anatomy of the <i>C. elegans</i> hermaphrodite germline	21
Figure 7: Sperm Development	23
Figure 8: Activated sperm	24
Figure 9: Cladogram of the evolution of germ plasma	31
Figure 10: P granules FG size exclusion barrier	34
Figure 11: DEAD-Box helicases domains.....	36
Figure 12: PQN-75 protein domains	64
Figure 13: Germline phenotypes of <i>pqn-75</i>	67
Figure 14: PQN-75 expression	71
Figure 15: Larval development of <i>pqn-75</i>	73
Figure 16: Proteotoxic stress and immunity in <i>pqn-75</i>	76
Figure 17: GLH proteins in the <i>C. elegans</i> germline.	89
Figure 18: Level and distribution of mutant forms of GLH-1 in <i>C. elegans</i>	92
Figure 19: Consequences of GLH-1 mutant alleles.....	95
Figure 20: Colocalization of P-granule components in wild-type and GLH-1 mutants.	98
Figure 21: Glycine-rich FG repeats tether GLH-1 to the nuclear periphery.	101

Figure 22: GLH-1 protein associations.	105
Figure 23: Ribosomes and the size exclusion properties of P granules.....	108
Figure 24: GLH-1 functionality summary.	110
Figure 25: GLH-1 RNA-seq graphical summary.....	115
Figure 26: GLH-1 impact on the transcriptome and translome.	125
Figure 27: GLH-1 impact on fertility and MSP-142 expression.....	128
Figure 28: Male germline dependence on GLH-1.	131
Figure 29: GLH-1 impact on sperm activation.	134
Figure 31: Amino acid sequence conservation between DEAD-box helicase proteins.....	177
Figure 32: All images used to quantify granularity and expression in Figure 19.....	178
Figure 33: GLH-1 Immunoprecipitation.	179

LIST OF ABBREVIATIONS

ABBREVIATION	FULL FORM
BMPS	bone morphogenic proteins
C. ELEGANS	Caenorhabditis elegans
CAS	CRISPR-associated
CLIP	crosslinking immunoprecipitation
CRISPR	clustered regularly interspaced short palindromic repeats
DD	dimerization domains
DIC	differential interference contrast
DNC	dorsal nerve cord
DTC	Distal tip cells
EIF4E	eukaryotic translation initiation factor 4E
EMS	ethyl methane sulfonate
ESC	embryonic stem cells
FG	phenylalanine-glycine
FH	Formin Homology domain
GFP	green fluorescent protein

GLH-1	Germline Helicase 1
GSCS	germline stem cells
IDR	intrinsically disordered region
IPSCS	induced pluripotent stem cells
IP	immunoprecipitation
LC	liquid chromatography
MSPS	major sperm proteins
MO	membranous organelle
MS	mass spectrometry
MSCS	multipotent stem cells
NGM	nematode growth medium
NPC	nuclear pore complexes
NUP	nucleoporin
OSC	oligopotent stem cells
PQN-75	prion-like (Q/N-rich)-domain-bearing protein
PSCS	pluripotent stem cells

PROK	Proteinase K
QPCR	quantitative polymerase chain reaction
RDRPS	RNA-dependent RNA polymerases
RFP	Red fluorescent protein
RIP	RNA immunoprecipitation
RNAI	RNA interference
SMFISH	single-molecule fluorescence in situ hybridization
TALENS	transcriptional activator-like nucleases
TSCS	Totipotent stem cells
TSSCS	tissue-specific stem cells
TS	temperature-sensitive
UNC	uncoordinated
USCS	unipotent stem cells
VNC	ventral nerve cord
WT	wild type

Chapter I

Introduction

1.1 Stem cells

The genesis of an organism's life journey begins with dividing a fertilized egg into multiple cells. These cells multiply and divide, giving rise to all cell lineages of the organism. They are similar at inception, but as they mature, they become progressively specialized, losing their potency in the process. These primal, undifferentiated cells, known as stem cells, can generate every cell lineage in an organism. Unraveling the mechanisms that steer stem cells' fate can revolutionize advancements in medical applications such as fertility, regeneration, cancer research, neurological diseases, and many more. In this thesis, we explore the functionality of highly conserved proteins in the *C. elegans* germline and their impact on maintaining the immortality of germline stem cells.

1.1.1 The history of stem cells

The term "Stammzelle" (German for stem cells) was first introduced in literature in 1868 by Ernst Haeckel (Haeckel 1868). August Weismann later proposed the idea of differentiated cells originating from a single cell in his theory of the continuity of germ plasma, claiming that germ plasma was passed down to the next generation through specialized cells (Weismann 1885). Valentin Häcker and Theodor Boveri further developed Weismann's theory by describing two cell lineages, one giving rise to somatic cells and the other to the germline (Boveri 1892; Häcker 1892). Later the English term "stem cell" would arise, popularized by Edmund Wilson in his book "The Cell in Development and Inheritance" (Wilson 1896).

Stem cell properties remained largely undefined until the mid-1900s due to experimental limitations. Leroy Stevens of the Jackson Laboratory first described the mouse model 129Sv, which demonstrated the occurrence of testicular cancer (Stevens and Little 1954). The tumors were found to have embryonic-like attributes, containing multiple cell types (Stevens 1960). While the exact attribution to the discovery of stem cells is difficult to define, James Till and Ernest McCulloch's work on 129Sv bone marrow cells (later known as hematopoietic stem cells), transplanted into irradiated spleens marked the first widely accepted recognition and description of stem cell properties (Till and McCulloch 1961). This discovery led to the identification of stem cells in various tissue types, including embryonic stem cells (ESC), first isolated and characterized in mice (Martin 1981) and later in humans (Thomson et al. 1998).

Recently, work has focused on reprogramming somatic cells into pluripotent stem cells or induced pluripotent stem cells (iPSCs) (Takahashi and Yamanaka 2006). Discovering that mouse fibroblasts can exhibit embryonic stem properties by overexpressing just four transcription factors, KLF4, MYC, OCT4, and SOX2, revolutionized and opened the door for medical applications in the field of regenerative therapy. However, many challenges remain before stem cells and iPSC can be widely used in clinical applications.

1.1.2 Stem cell classification

Stem cells are unspecified cells that have not yet taken on a specific cell type's structural and protein characteristics. Instead, they retain the ability to self-renew or produce identical stem cells during cellular divisions. These cells are capable of developing into any specific cell type of an organism and play a crucial role in maintaining the health, regenerative capabilities, and sexual reproduction of an organism. Stem cells are categorized into four main types:

totipotent, pluripotent, multipotent, and unipotent; These categories are based on the cell types' specialization and developmental potential, each becoming increasingly specialized as they lose their developmental potency.

Totipotent stem cells (TSCs) have the greatest potency, as they can divide into all specialized cells of the organism, and all primary germ cell layers, including the placenta. The zygote formed after gamete fertilization is an example of a totipotent stem cell that gives rise to the blastocyst containing the source of pluripotent stem cells.

Pluripotent stem cells (PSCs) can develop into all three embryonic cell types, including the germline, but cannot produce cells for the placenta or extra-embryonic tissue. PSCs and TSCs are commonly referred to as embryonic stem cells (ESC). One example of a PSC is induced pluripotent stem cells (iPSCs) produced in the laboratory. iPSCs are considered a valuable source for stem cell research and regenerative medicine due to their ability to give rise to multipotent stem cells.

Multipotent stem cells (MSCs) are a class of stem cells found in specialized tissues, including neural stem cells, mesenchymal stem cells, and hematopoietic stem cells. For example, hematopoietic stem cells found in bone marrow develop into various blood cells and give rise to oligopotent stem cells.

Unipotent stem cells (USCs) possess the narrowest potency potential, as they only divide into a single cell type forming a single lineage, such as an epidermal stem cell that gives rise to skin cells and no other cell type. USCs include germline stem cells (GSCs) that give rise to male and female gametes. USCs, oligopotent stem cells (OSC), and MSCs are generally referred to as somatic or adult stem cells.

After embryogenesis, subsequent cell divisions result in classes of cells with reduced potency, creating a hierarchy of stem cells that compose an organism. However, cellular division alone is insufficient to develop an organism. Regulation factors controlling self-renewal and differentiation must be in place for proper development and functionality.

1.1.3 Somatic cell nuclear transfer and Stem cell induction

Advancements in stem cell research have resulted in the emergence of two novel ways to make stem cells, somatic cell nuclear transfer (SCNT) and induced pluripotent stem cells (iPSCs). Induced stem cells are generated in the laboratory through the reprogramming of somatic cells, leading to cells that display properties characteristic of both pluripotent stem cells (PSCs) and tissue-specific stem cells (TSSCs).

The initial approach to producing induced stem cells was somatic cell nuclear transfer (SCNT). This technique involves the removal of the nucleus from a donor somatic cell and its transfer into an egg cell, a process first demonstrated in frogs (*Xenopus laevis*) by Dr. John Gurdon in 1962. The findings indicated that the replacement of the nucleus of a blastula with that of a somatic cell results in normal organism development and the generation of a clone of the donor somatic cell (Gurdon 1962). Gurdon's discovery transformed our understanding of the plasticity of somatic cells and paved the way for subsequent cloning studies, including the production of Dolly the sheep in 1997 (Wilmut et al. 1997). Although SCNT has primarily been used for animal cloning and the generation of patient-specific stem cell lines for therapeutic purposes, its low success rate and the requirement for human egg cell donors have posed challenges to its utilization in clinical applications.

On the other hand, iPSCs are produced by reprogramming adult cells back to a pluripotent state, with morphology and proliferation rates similar to ESCs. The discovery of iPSCs was made by Dr. Shinya Yamanaka in 2006; who found that by transferring four transcription factors (KLF4, MYC, OCT4, and SOX2) present in mouse embryonic fibroblasts into adult somatic cells, the cells could be reverted to a pluripotent state (Takahashi and Yamanaka 2006). This finding has revolutionized the field of stem cell research; however, further research is needed to unlock the potential of iPSCs fully. For instance, iPSCs do not have the same gene expression, DNA methylation patterns, or germ transmission capacity as ESCs (Takahashi and Yamanaka 2006; Okita, Ichisaka, and Yamanaka 2007). These differences result in an innate memory of the cells' previously differentiated state, preserving some transcriptional and epigenetic markers of the cells' previous lineage (Polo et al. 2010; Eguchi et al. 2014; J. H. Lee et al. 2014). These effects tend to diminish with the passage of iPSC cell lines over time (J. H. Lee et al. 2014). Current research is focused on directing cell lineage development of iPSCs; the two prominent approaches are recreating the in vivo condition of the desired cell type by incorporating morphogen and growth factors (Cohen and Melton 2011; Nolbrant et al. 2017; Kriks et al. 2011) or through induced expression for lineage-specific transcription factors (Hikichi et al. 2013; K. P. Kim et al. 2021; Raabe et al. 2022).

Past studies of both iPSCs and SCNT have highlighted the significance of transcription factors and methylation control in ESCs. Understanding these underlying epigenetic and transcriptional differences and their role in directing stem cell lineage development is crucial for developing and successfully utilizing iPSCs in the medical field.

1.1.4 Stem cell medical applications and boundaries

Regenerative medicine is one of the most recent emerging fields of medical applications, propelled by the growth of stem cell research; it offers alternative therapeutic options for many diseases that cannot be cured with traditional medical techniques. The pluripotent nature of stem cells, which allows them to divide into various cell types, suggests that, in theory, there is an almost limitless range of diseases that can be treated through stem cell therapies. Some of the most promising applications of stem cell therapies include treating neurodegenerative disorders (Fang et al. 2018; Swistowski et al. 2010; Kikuchi et al. 2017), organ repair (Vadakke-Madathil and Chaudhry 2021), macular degeneration (Dor et al. 2004; Assinck et al. 2017; Mazzini et al. 2018), blood and immune system disorders (De Luca et al., 2019; Delemarre et al., 2016; Trounson & McDonald, 2015; Xu et al., 2012), among others (Antonov and Novosadova 2021; Zakrzewski et al. 2019). Despite the tremendous potential of stem cells for clinical applications, several boundaries and limitations need to be addressed.

Some concerns have already been partially addressed with the discovery of iPSC (Takahashi and Yamanaka 2006), such as the difficulty in obtaining and sourcing stem cells, the ethical concerns that go with it, and to some degree, immunological rejection. However, other significant factors must be overcome, such as early recognition of tumor formation, defining the stem cell niche, maintaining quiescent cell lines, and directing cell lineages.

The stem cell microenvironment, also called the stem cell niche, is a complex research area with significant potential for advancing regenerative medicine. The stem cell niche comprises a complex array of molecular and cellular components that provide essential signals to stem cells, guiding self-renewal (Daadi 2022), and differentiation (Strome and Updike 2015;

Updike et al. 2014; Yamada et al. 2019), maintenance, and migration (Matsuo et al. 2021). Dysregulation of the microenvironment can lead to various diseases (Mazzola & di Pasquale, 2020; Yamada et al., 2019), underscoring the importance of understanding the microenvironment's role in stem cell fate.

Various biochemical and mechanical factors are critical regulators of stem cell fate. Mechanical factors directed by biochemical signals act in a cascade response to initiate and direct differentiation as stem cells progress toward reduced potency. This process yields increasingly diverse stem cell lines with unique microenvironments comprising distinct biochemical and mechanical factors. By establishing a baseline understanding of stem cells in a totipotent state, we can elucidate the fundamental functions of the stem cell niche and those of decreased potency. Therefore, focusing on stem cells in a totipotent state represents a particularly underdeveloped yet essential field for advancing regenerative medicine.

1.1.5 Germline stem cells

Germline stem cells (GSCs) are a subtype of adult stem cells. They are unique in maintaining their pluripotency, an attribute crucial for preserving the germline integrity and the genetic information of future generations (Lehmann 2012; C. G. M. Extavour 2007). DNA replication during each cellular division can lead to various degrees of replication fidelity, causing the buildup of deleterious mutations in the genome (Willemsen et al. 2023; Vassilev and DePamphilis 2017). Since GSCs give rise to both male and female gametes and are responsible for passing genetic information to the next generation, the fate of GSCs must be determined early in embryogenesis to minimize the accumulation of deleterious mutations passed to the next generation (Cinalli, Rangan, and Lehmann 2008).

The precursor cells of GSCs are called primordial germ cells (PGCs), characterized by germ plasma's presence (disused later), often described as the ultimate stem cell because of their ability to develop into all cells of an organism. There are two models of PGC formation: preformation and induction (C. G. Extavour and Akam 2003; Hansen and Pelegri 2021). In species such as *C. elegans*, *Drosophila melanogaster* (Fruit flies), *Danio rerio* (zebrafish), and *Xenopus laevis* (frogs), germline specification occurs through preformation, where germline identity is continuously passed on from one generation to the next through asymmetric inheritance of germline precursors during the first cellular divisions of the oocyte post-fertilization. Specified PGCs will remain quiescent until later in embryonic development when they divide to form GSCs and be incorporated into the gonadal niche.

On the other hand, in species such as *Gryllus bimaculatus* (crickets), *Parasteatoda tepidariorum* (spiders), *Pelodiscus Sinensis* (turtles), and interestingly unlike other amphibians that rely on germ cell preformation *Ambystoma mexicanum* (salamanders) germ cell specification occurs through induction (Chatfield et al., 2014). Additionally, in mammals such as *Mus musculus* (mice) and *Homo sapiens* (humans), germ cell specification also occurs through induction (Nicholls et al., 2019), initiated by bone morphogenic proteins (BMPs) and WNT signaling from somatic cells (Fujiwara et al., 2001; Lawson et al., 1999; Ying et al., 2000). In mice, PCGs develop in the proximal epiblast before migrating along the genital ridge to be incorporated into the testis or ovaries (Richardson & Faulkner, 2018).

The early determination of PGCs through preformation or induction is critical for preventing the transmission of excessive mutations to offspring. However, even after PGCs are specified, they remain susceptible to mutations and require protective mechanisms that

regulate transcription, chromatin state, and the translation of germline-specific transcripts (Updike et al. 2014; Knutson et al. 2017). Factors such as Piwi, Nanos, Tudor, and Vasa (discussed later) all preserve and control PGSs and GSCs throughout development (Shukalyuk et al. 2012; Voronina et al. 2011; Ewen-Campen, Schwager, and Extavour 2010). Determining the functionality of these germline proteins and how they function in the germline holds significant potential in addressing the challenges faced in applying stem cells in medical treatments, such as maintaining a quiescent state, proliferation of new stem cells, and early detection of undesirable stem cell specification through the evaluation of transcriptome and translome.

Unfortunately, studying PGCs and GSCs in mammalian models and humans is complex due to various factors, such as their location in the body, ethical concerns, and experimental limitations. However, germline proteins are highly conserved throughout evolution. Therefore, utilizing various animal organisms such as *C. elegans* can shed light on the molecular functions and mechanisms involved in preserving the germline, contributing to the advancement of stem cell research and its applications in the medical field.

1.2 *C. elegans* as a model organism

The *Caenorhabditis elegans* (*C. elegans*) is a free-living nematode that has become a prominent animal model due to its various advantages including its small size (1mm), transparent epidermis, low maintenance cost, self-fertilization, ability to survive long-term freezing for storage, and short lifespan (reviewed in Meneely et al., 2019). Emile Maupas first described this organism in 1899 (Maupas, 1899). However, it was only when Sydney Brenner adopted it in the 1960s and popularized its use as a model organism in genetic, reproductive, neurobiology, and developmental biology that its significance became widely recognized. The

N2 strain, the first isolated population of *C. elegans* originating in Bristol, England, is still used as the original wild-type reference strain.

1.2.1 *C. elegans* life cycle

The first 48 hours of the *C. elegans* lifespan involve various developmental stages that must be completed before reaching sexual maturity, including both the embryonic and larval phases (Figure 1). Embryogenesis starts with the fertilization of the oocyte and ends once the embryo hatches, typically taking around 14 hours. After the embryo hatches, the organism enters the first larval development stage, L1, and an additional 12 hours are typically required for the L1 larva to reach the L2 stage. If environmental conditions cause stress, such as lack of food, the *C. elegans* can enter an alternative stage of development called Dauer. During the Dauer stage, the organism can remain quiescent without eating for several months, returning to normal development once adverse environmental conditions subside. Under normal developmental conditions, germ cells enter meiosis during the L3 and L4 stages while the gonad elongates, which lasts around 18 hours. If the *C. elegans* enters the Dauer stage, L2 and L3 developmental stages will be bypassed, entering directly into L4 development. The L4 stage eventually gives rise to adult nematodes, which become sexually mature and can lay eggs approximately 72 hours post-hatching at permissive temperatures. A single adult *C. elegans* can produce approximately 100 embryos per day, most of which are hermaphrodites, making it easy to continue lines of genetic mutants. However, small numbers of males (0.01-0.1% of offspring) also make genetic crosses possible.

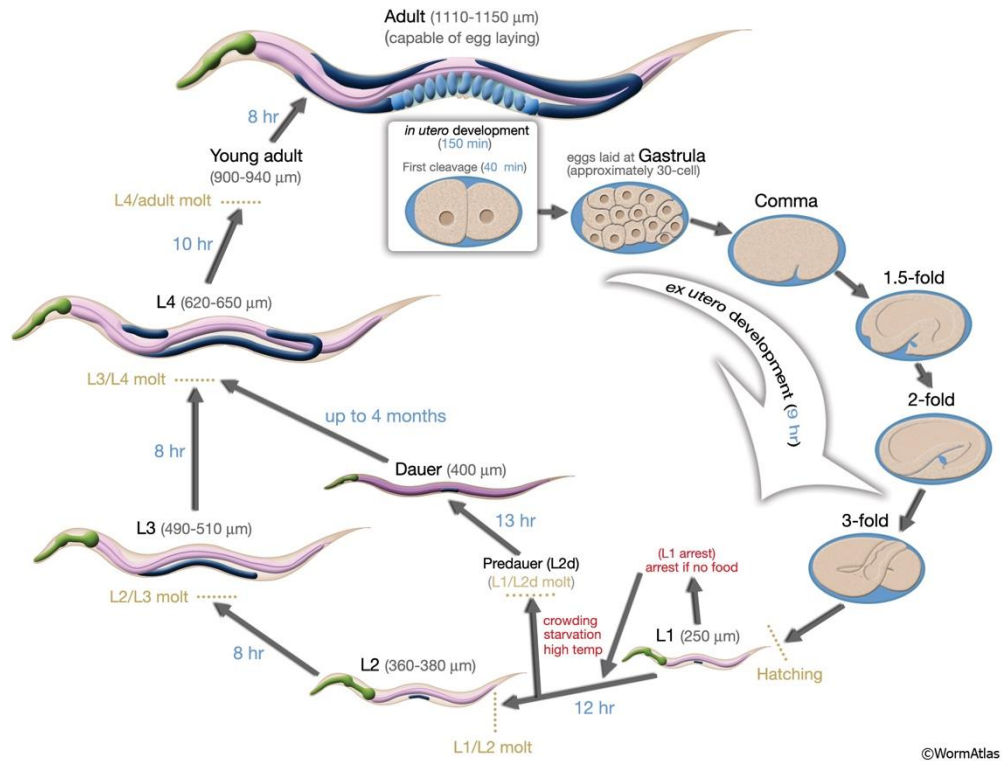


Figure 1: *Caenorhabditis elegans* life cycle

The image follows the *C. elegans* life cycle at 22°C. The moment of fertilization is marked as 0 minutes. Blue numbers along the arrows indicate the duration of each stage. The first cleavage takes place roughly 40 minutes after fertilization. Around 150 minutes after fertilization and during the gastrula phase, eggs are laid externally. The animal's size is indicated in micrometers (μm) next to the name of each stage. Figure reproduced from WormAtlas (www.wormatlas.org).

1.2.2 Anatomy of *C. elegans*

The anatomy of *C. elegans* has been comprehensively documented by John Sulston, providing lineage tracing and characterization for all 959 somatic cells of the adult hermaphrodite nematode, 302 of which are neurons (Sulston et al., 1983; Sulston & Horvitz, 1977). The body wall of *C. elegans* is unsegmented and cylindrical, a characteristic shared by

other free-living Rhabditida (Figure 2). The organism comprises two primary tubes separated by the pseudocoelomic cavity. The inner tube consists of the pharynx, intestine, and gonad, while the outer tube includes the cuticle, hypodermis, excretory system, neurons, and muscles. The gastrointestinal system of *C. elegans* includes the feeding tube, pharynx, and intestine that run the length of the body.

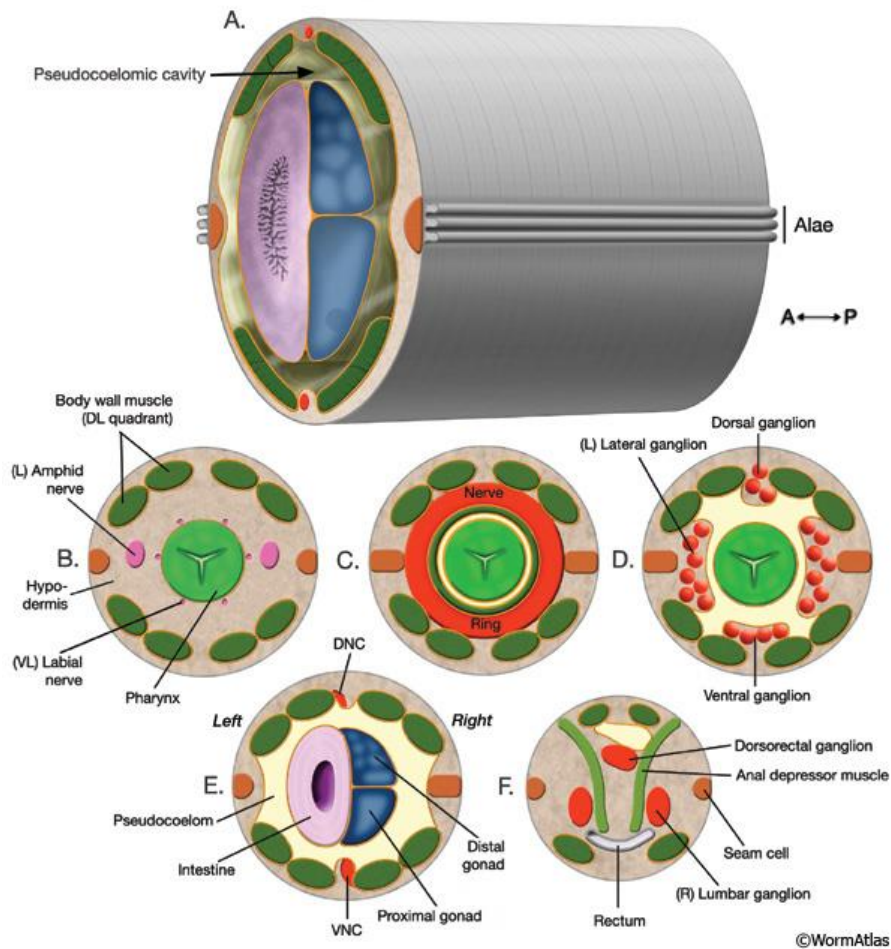


Figure 2: Nematode body anatomy

Nematode body sections start from the head to the tail. A. The posterior region of the body is characterized by the separation of the outer tube, i.e., the body wall, from the inner tube comprising the alimentary system and gonads by a pseudocoelom. B. A section through the anterior head shows a narrow space between the pharynx and the adjacent tissues. C. A cross-section through the middle of the head. D. Section through the posterior head. E. Section through the posterior body, highlighting the dorsal nerve cord (DNC) and ventral nerve cord (VNC). F. Depicts a section through the tail. Figure reproduced from WormAtlas (www.wormatlas.org).

The pharynx, located at the anterior end of *C. elegans*, is of particular interest to this thesis and will be discussed in subsequent sections. Functioning as a simple pump-like organ involved in feeding, the pharynx is a distinctively shaped feature. In the wild, *C. elegans* prey on various bacteria in decaying organic matter, such as leaf litter or fruit. However, *Escherichia coli* OP50 is used as a food source in the laboratory. The pharynx of *C. elegans* employs two large pharyngeal muscles, the anterior and posterior bulbs, to act as a pump, propelling bacteria from the buccal cavity through the pharyngeal lumen to the posterior of the pharynx, where a grinder breaks down bacteria prior to entry into the digestive tract. The pharynx comprises 69 cells, including 20 neurons, 20 muscle cells, 9 epithelial cells, 9 marginal cells, 6 valve cells, and 5 gland cells. The basal surface of the pharyngeal cells is lined with a specialized basal lamina, which effectively separates the pharynx from the pseudocoelom and the rest of the organism.

The pharynx consists of five distinct sections, the buccal cavity, corpus, metacarpus, isthmus, and terminal bulb (Figure 3). The terminal or posterior bulb is the most substantial

portion of the pharynx, acting as the pharyngeal “pump” containing the grinder at its posterior end. This specialized cuticle structure serves as a tooth to break down bacteria before passing through the pharyngeal intestinal valve and entering the intestine for further digestion. The pharynx contains many neurons and muscular tissue initiating the “pumping” of the pharynx (Figure 3).

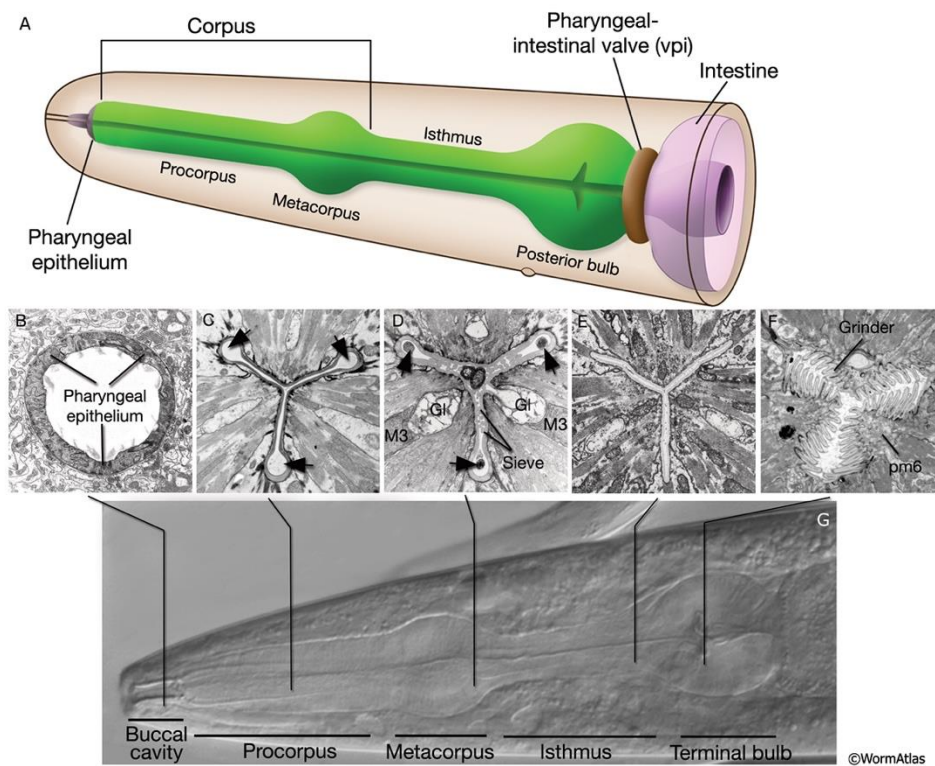


Figure 3: Anatomy of the C. elegans pharynx

A graphic rendition of the pharynx illustrating its significant features. B-F. TEM sections display different parts of the pharyngeal lumen. The section levels are labeled in G. Figure reproduced from WormAtlas (www.wormatlas.org).

In addition, to muscular and neural tissue, the posterior bulb also includes two distinct classes of pharyngeal gland cells: g1 and g2 (Smit et al., 2008). These gland cells project cuticle-lined ducts that terminate at various points within the lumen. The g1 class for cells consists of three cells, each extending ducts towards the anterior of the pharynx, with the right ventral and left ventral g1 ducts passing through the isthmus and emptying into the parapharyngeal lumen just before the anterior bulb. While the dorsal g1 gland duct extends beyond the anterior bulb and empties into the lumen just before the buccal cavity. The g2 gland cells, on the other hand, consist of two cells with significantly shorter ducts emptying directly into the lumen of the primary bulb. These cells are believed to play a critical role in the breakdown and digestion of bacteria (Albertson & Thomson, 1976; Hall & Hedgecock, 1991).

All five gland cells have been found to be connected to the M4 or M5 motor neurons, suggesting that excretion is stimulated during contractions for digestion and is thought to also play a role in cuticle digestion during the molting periods of the *C. elegans* larval stages (Albertson & Thomson, 1976; Hall & Hedgecock, 1991). Additional evidence of increased expression of excretion elements observed both within the ducts and throughout the muscle during molting periods also supports this theory (Rochester et al., 2017). However, the specifics of gland excretion function and their role in aiding digestion, cuticle breakdown, and immune response remain poorly understood, as noted by several studies (Albertson & Thomson, 1976; Hall & Hedgecock, 1991; Rochester et al., 2017).

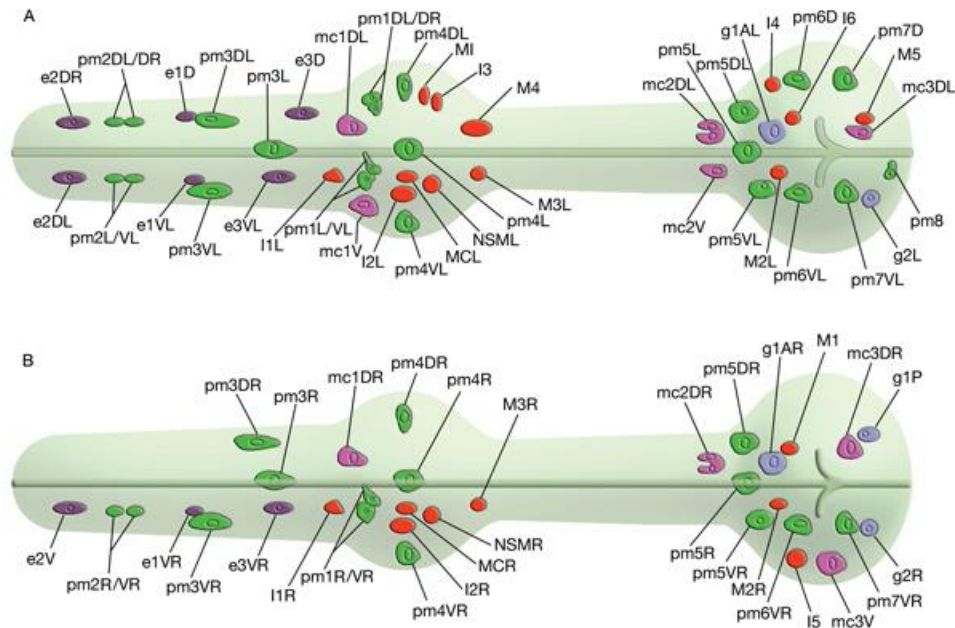


Figure 4: Cells of the *C. elegans* pharynx

Figure is based on a drawing by Ron Ellis reproduced from WormAtlas (www.wormatlas.org). Showing the nuclei of different types of cells in the nematode. Neuron nuclei are colored in red, pharyngeal muscle nuclei are in green, gland nuclei are in lavender, marginal cell nuclei are in fuchsia, and epithelial nuclei are in purple. A graphic rendition of the left lateral view of the ventral, left-side, and dorsal nuclei is shown in panel A, while panel B shows the left lateral view of the right-side nuclei.

The gastrointestinal system of *C. elegans* continues from the feeding tube and pharynx to the intestine, which runs the length of the body, excreting the waste through the anus located at the posterior end of the *C. elegans*.

The reproductive system of *C. elegans* differs slightly from that of other Rhabditida, with primarily self-fertilizing hermaphroditic individuals and a low occurrence of males. While the male and hermaphrodite anatomy is similar, some differences exist in the gonad arms

(discussed below) and reproductive and tail morphological differences. The male possesses a male copulatory apparatus in the posterior half of the body and a tapered posterior. At the same time, the hermaphrodite has a vulva along the ventral midline for egg-laying and copulation.

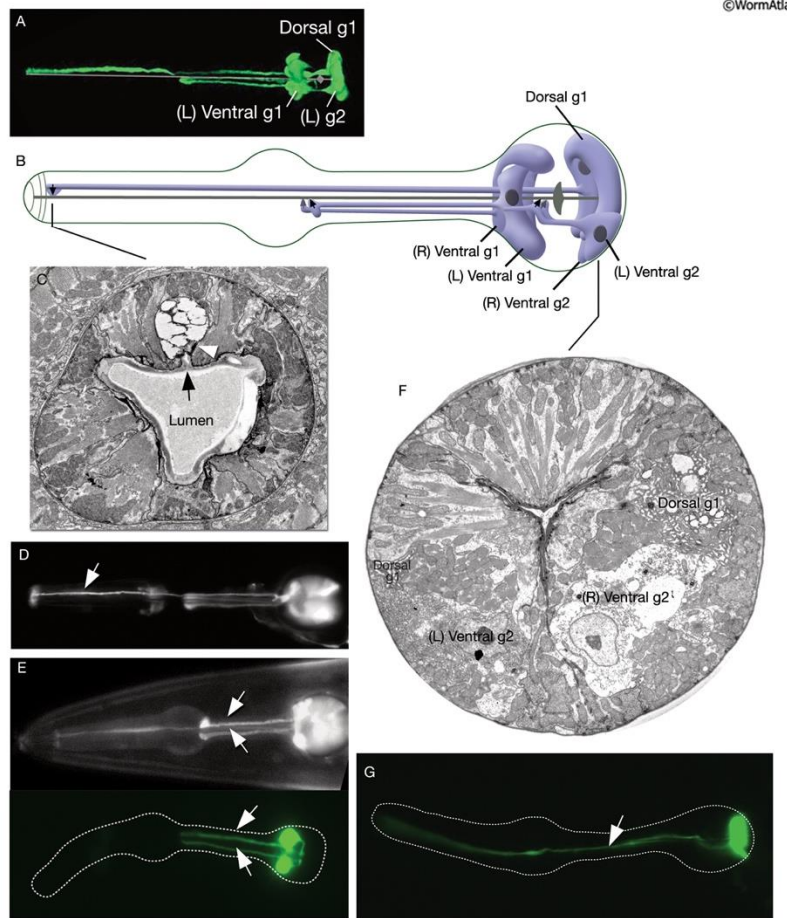


Figure 5: Gland cells of the pharynx

A) Left lateral oblique view epifluorescent image of gland cells expressing the reporter gene B0280.7::GFP, showing five gland cells: two posterior g2 cells, one right and one left g1 cells, and a dorsal g1 cell. B) Graphic representation of gland cells, with black ovals indicating gland cell nuclei and short arrows indicating gland openings to the lumen. C) The dorsal g1 gland duct lies within the dorsal nerve cord and opens to the lumen through a short cuticular duct (arrow) close to the buccal cavity. Adherens junctions (white arrowhead) attach nearby muscles to the duct. D and E) Epifluorescent images of gland cells expressing the reporter genes F20B10.1::GFP or phat-1::GFP, with arrows indicating the dorsal and ventral g1 processes. F) Transmission

electron microscopy image of transverse section through the posterior terminal bulb, showing that the g1 cells have lamellar cytoplasm, whereas the g2 cells have lighter cytoplasm with vesicles. G) Epifluorescent images of dorsal gland cells expressing the reporter gene Y8A9A.2::GFP, with an arrow indicating the dorsal g1 process. Figure reproduced from WormAtlas (www.wormatlas.org).

1.2.3 *C. elegans* Germline

C. elegans has been recognized for its potential to study embryonic and germline development since its discovery by Maupas (Maupas 1900). Maupas provided detailed illustrations of the hermaphrodite and male germline. In the 1970s, studies characterizing the hermaphrodite gonad structure and oogenesis (Hirsh, Oppenheim, and Klass 1976), spermatogenesis and cellular structure in both the hermaphrodite and male germline (Samuel Ward and Carrel 1979), and lineage tracing of germline development (Kimble and Hirsh 1979) established *C. elegans* as a prominent reproductive model.

C. elegans undergo rapid development, reaching sexual maturity in approximately 3-3.5 days at permissive temperatures (20 degrees Celsius) after passing through four larval developmental stages (Figure 1). The adult hermaphrodite germline comprises two major gonad arms, consisting of 143 somatic cells and approximately 1000 germ cells. The development of the gonad arms commences during the L1 stage with the Z2 and Z3 germ line precursor cells and the Z1 and Z4 somatic precursors. These cells divide to form Distal tip cells (DTC) that extend the gonad arms and determine the sex of the animal through signaling during the L3 stage of development (Figure 1). The *C. elegans* hermaphrodite germline is equivalent to the female germline of other *Caenorhabditis* species. Hermaphrodite *C. elegans* will produce

approximately 300 sperm during the L4 stage of development, with about 150 in each gonad arm stemming from 35-40 male germ cells. Developing sperm are stored in the spermatheca during the young adult stage of development when *C. elegans* reaches sexual maturity and oogenesis begins.

1.2.3.1 Regions of the C. elegans germ line

The germline, the lineage of cells that give rise to gametes, is organized in a highly ordered and intricate manner. In hermaphrodites, the germline consists of two gonad arms each in a cylindrical loop, while in males, it consists of a single gonad arm. The gonad arm in hermaphrodites comprises five distinct primary zones, including the mitotic progenitor zone, transition zone, pachytene zone, loop, and developing oocytes (Figure 6).

Germ cells perpetually arise from the DTC located at the end of the gonad and maintain a state of self-renewal through mitotic divisions. Germ cells of the DTC remain in constant contact with the mesenchymal DTC. This sustained contact activates the GLP-1/Notch signaling pathway in germ cells, transcribing essential stem cell regulatory elements that maintain GSCs in a stem cell-like state. This process is vital for producing functional gametes (Shin et al. 2017; Kershner et al. 2014).

As the germ cells move proximally toward the transition and pachytene zone, the GLP-1 signal gradually diminishes, resulting in the cessation of cellular division (C. H. Lee et al. 2016). During this time GSCs remain in contact with the germline core, or rachis, through ring channels, which enable cytoplasmic exchange and maintain the GSCs in a quiescent state via critical components of the stem cell niche, such as GLP-1, SYGL-1, and LST-1 (C. H. Lee et al. 2016; Shin et al. 2017).

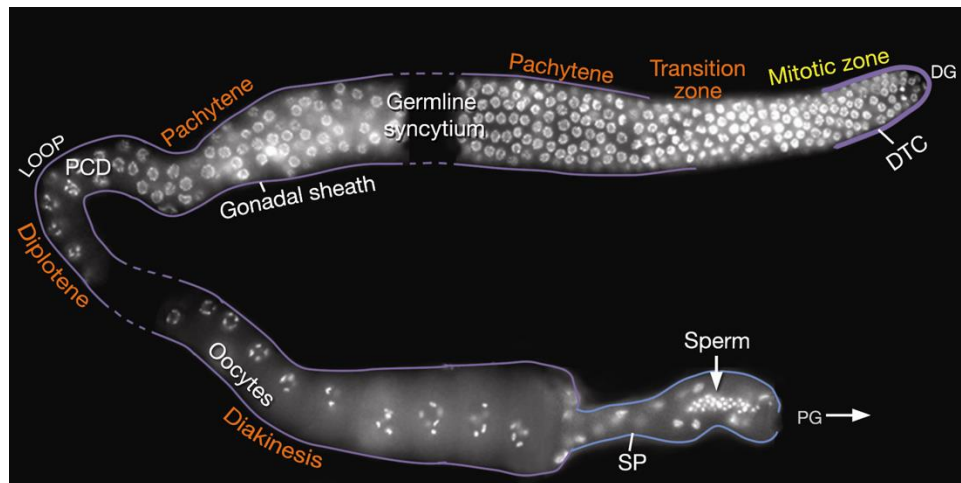


Figure 6: Anatomy of the *C. elegans* hermaphrodite germline

Epifluorescent visualization of one DAPI-stained adult hermaphrodite gonad (dissected) sourced from J. Maciejowski and E.J. Hubbard. Yellow text marks the Mitotic zone; orange text marks stages of meiotic prophase I. White text defines the region of the germline. Figure reproduced from WormAtlas (www.wormatlas.org).

Once GSCs round the bend or loop region of the gonad (fig), the ring channels begin to close, and the germ cells begin to expand, resulting in the deposition of cytoplasmic components containing essential germline proteins into developing oocytes. Once the gonad loop is rounded, the oocytes become entirely enclosed, and oogenesis initiates. In hermaphrodites, however, spermatogenesis must first commence during the L4 larval stage before the onset of oogenesis, producing a finite number of sperm stored in the spermathecas (Figure 6).

1.2.4 Spermatogenesis in *C. elegans*

Spermatogenesis is the process of producing sperm cells from an undifferentiated germ cell. In the *C. elegans*, spermatogenesis occurs during the L4 stage of development; during this time, male and hermaphrodite germ lines undergo spermatogenesis. Marking the completion of sexual maturity. Throughout sexual maturity, the male germline exhibits continuous production. In contrast, hermaphrodites generate a finite amount of approximately 250 sperm cells that are stored in the spermatheca (Figure 6). For hermaphrodites, sperm is the limiting factor for fertility unless male insemination occurs. The onset of oogenesis in hermaphrodites depends on the presence of major sperm proteins (MSPs), depending on the presence of sperm in the spermatheca. If sperm are absent, the expression of MSPs is inhibited, resulting in reduced germ cell production and, ultimately, impeding oogenesis.

In hermaphrodites, the process of spermatogenesis begins at the proximal end of the germline during the L4 stage of development. Primary spermatocytes connect to the rachis, with each primary spermatocyte giving rise to two secondary spermatocytes that develop into haploid spermatids by budding off the residual body (Figure 7). Following the formation of spermatids, oogenesis is initiated, and the spermatids are propelled into the spermatheca during the first ovulation, where they undergo activation and transform into fully activated spermatozoa.

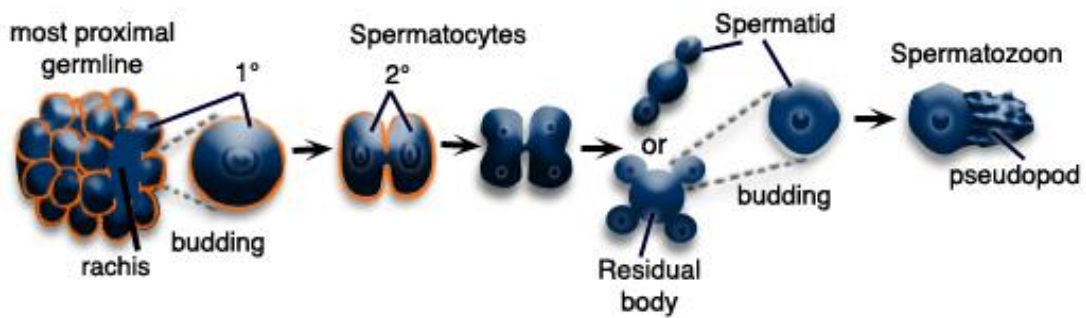


Figure 7: Sperm Development

illustrating the stages of spermatogenesis from germ cell (Left) to activated spermatozoon (Right). Adapted from WormAtlas (www.wormatlas.org).

While the development of sperm and the morphology of the gonads in males are similar to that of hermaphrodites, there are distinct differences. Spermatogenesis in males occurs in the distal end of the germline, perpetually originating from the DTC (Figure 6). The male sperm remains inactive until mixed with seminal fluid during the insemination of a hermaphrodite. Activated sperm crawl into the spermatheca, where they outcompete hermaphrodite sperm due to their larger size (LaMunyon and Ward 1998).

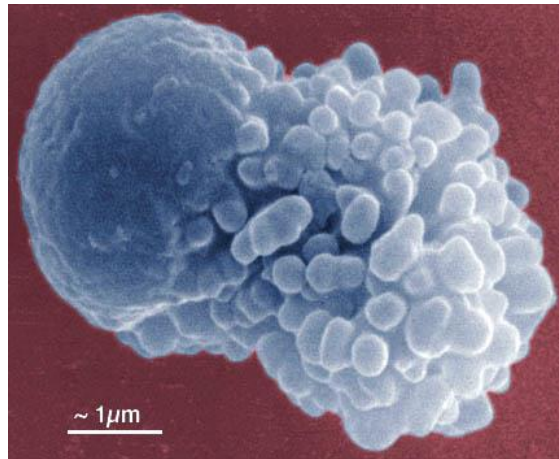


Figure 8: Activated sperm

This scanning electron micrograph shows a mature *C. elegans* sperm cell or spermatozoon. On the right is the pseudopod, and the left is the cell body. Adapted from WormAtlas (www.wormatlas.org)

1.2.4.1 Spermatozoa morphology and activation

Prior to sperm reaching full maturity, sperm must undergo sperm activation. This transformation is characterized by the conversion of round spermatids to a spikey intermediate or irregular shape phase, resulting in the total motility of the spermatozoa via the extension of pseudopods (Singaravelu et al. 2011) (Figure 8). Despite advances in the field, the precise factors involved in this process still need to be discovered. *C. elegans* sperm distinguish themselves from their mammalian counterparts in that they do not possess a flagellum for mobility but instead develop into an amoeboid cell type that propels itself using a pseudopod. This appendage is supported by a cytoskeleton made up of MSPs, which in conjunction with a dynamic cytoplasm, enable the sperm cell to crawl through the extension and retraction of the pseudopod. Through this mode of locomotion, the sperm can gather in the spermatheca after

copulation or ovulation, when some of the residing sperm is pulled into the ovary (Rochester et al. 2022).

The direction of travel is dictated by the sperm's capacity to sense and respond to chemical cues resulting in changes in mobility. Chemo-attractive molecules, such as the F-series prostaglandins - a family of lipid signaling molecules produced by the oocyte - play a critical role in mediating the direction of sperm travel (Hoang et al. 2013; Kubagawa et al. 2006a). These molecules are derived from polyunsaturated fatty acid components (PUFAs) within the insulin signal pathway. As food surplus is transferred to the oocytes as yolk (Hall et al. 1999; Kimble and Sharrock 1983), PUFAs are converted into F-series prostaglandins. The release of F-series molecules by the oocyte mediates sperm navigation toward the spermatheca and developing oocytes (Watts and Browse 2002; Watts 2009).

1.2.4.2 Major Sperm Proteins (MSPs) and sperm mobility

C. elegans genome encodes 28 MSP genes along with a multitude of pseudogenes. These MSPs exhibit significant sequence similarity, with isoforms bearing a maximum of 3% genetic variation (Burke and Ward 1983; Roberts, Pavalko, and Ward 1986). One characteristic feature of these MSPs is their small size, with a protein weight of approximately 14 kDa, ubiquitously present throughout *C. elegans* spermatids, representing 15% of the total proteins in the cell type and 40% of total soluble proteins (S. Ward et al. 1986; Nelson, Roberts, and Ward 1982). MSPs play a pivotal role in the atypical crawling motion of the spermatozoon, which is distinctive to nematodes and has not been found in other phyla. Ameboid cells generally use actin as a pseudo backbone for cell extension, but the nematode spermatozoon lacks actin and relies on MSPs for this function (Nelson, Roberts, and Ward 1982). Despite

similarities in function, actin and MSPs bear neither sequence homology nor structural similarity (K. L. King et al. 1992; Bullock, Roberts, and Stewart 1996). MSP fibers extend from the tip of the pseudopod to grip the uterus wall and pull the spermatozoa in the direction of the most potent chemical signal towards the spermatheca (Sepsenwol, Ris, and Roberts 1989; Nelson, Roberts, and Ward 1982).

Notably, the assembly of MSPs and sperm locomotion heavily depend on intercellular pH levels. High pH gradients from within the pseudopod at the leading edge (6.8 pH) facilitate MSP filament assembly and gripping of the surrounding surface structures. Lower pH levels are observed at the base of the pseudopod (6.2 pH), where filaments disassemble (Karen L. King et al. 1994). The continuous assembly and disassembly of MSP filaments serve as a treadmill-like mechanism, which drags the trailing cell body (reviewed in Baker et al., 2002). In vitro observations have indicated that pH gradients do not affect MSP polymerization, suggesting that the direction of travel is influenced by internal mechanisms activated through PUFA chemical signals rather than extracellular pH changes (Kubagawa et al., 2006).

1.2.5 Genome editing in *C. elegans*

As discussed above, *C. elegans* has emerged as a preeminent model organism for many reasons. It has remained one of the top model organisms due to its distinction as the first multicellular organism to have its entire genome sequenced (Consortium* 1998). The *C. elegans* genome comprises approximately 20,359 protein-coding genes, of which 38% or 7,663 genes are predicted to have human orthologs (W. Kim et al. 2018), implying a considerable degree of evolutionary conservation (WormBase referential freeze WS250, November 2015). This striking feature has made *C. elegans* a valuable and simplistic model organism, providing a

foundation for fundamental studies and a critical resource for translated findings across phylogeny.

Various methods have been implemented to generate genetic mutants to elucidate the functional roles of proteins in *C. elegans*. Initially, forward genetic screens such as ethyl methane sulfonate (EMS) were used to encourage DNA damage, resulting in random genetic mutations (Hartman et al. 2014; Brenner 1974). Later, reverse genetics methods, including RNAi, were employed, which enabled the targeted knockdown of specific transcripts (Fire et al. 1998). However, RNAi is a powerful genetic tool, but its effectiveness is only temporary, providing a partial gene knockdown and prompting additional genetic methods. Genome editing solutions, such as zinc-finger nucleases (ZFNs) and transcriptional activator-like nucleases (TALENs), could incorporate mutations into the genome capable of being passed to the next generation (Lo et al. 2013; Wood et al. 2011; Morton et al. 2006). Despite their time-consuming nature and relatively low success rates, these methods have proven useful.

However, recent advancements using clustered regularly interspaced short palindromic repeats (CRISPR) has emerged as a transformative tool in genetic engineering (Jinek et al. 2012; Mojica et al. 2005). Initially discovered in *Escherichia coli* (Ishino et al., 1987), the CRISPR-Cas9 gene editing system relies on naturally occurring bacterial immune system components that protect against invading viruses. Short RNA molecules guide CRISPR-associated (Cas) proteins to locate and cut specific viral DNA or RNA target sequences. These bacterial components incorporate segments of viral DNA into CRISPR domains to enable recognition and recall of threats to the cell. The CRISPR-Cas9 system can easily be manipulated by constructing a single guide RNA (sgRNA) to direct the Cas9 protein to a specific DNA sequence; the Cas9 enzyme

then cuts the DNA at the desired location, after the cell's natural DNA repair mechanisms can then be utilized to delete or replace the DNA sequence, providing a simple, precise, and efficient approach to introducing targeted mutations and uncovering gene functions (Jinek et al. 2012).

While these methods can be used in any organism, animal models such as *C. elegans* are crucial for investigating germline proteins and their functions, as ethical considerations preclude direct germline mutations in humans. *C. elegans* is particularly advantageous due to its transparency, which permits visualization of germline proteins labeled with fluorescent tags in vivo throughout development. Here we adopted the early use of the CRISPR-Cas9 system in *C. elegans* requiring several adaptations to the methods used throughout our publications (described in chapter II). Using three different CRISPR protocols, we created targeted mutations of critical germline proteins in *C. elegans*. In doing so, we aimed to assess the dynamic movements of these proteins throughout development and determine how mutations in critical domains affect localization, transcript interaction, and fertility.

1.3 Germ plasma and granules

Germ plasma is a unique cytoplasmic compartment that embodies specialized ribonucleoprotein organelles unique to germ cells. Discovered in the early 20th century by Hegner (Hegner, 1908), germ plasma represents a critical defining feature in the cytoplasm of PGCs. It comprises non-membrane-bound organelles with amorphous properties, consisting of RNA and protein. Germ granules exhibit diverse phenotypes dispersed throughout the cytoplasm or condensed into aggregates. Exhibiting dynamic, liquid-like properties capable of rapidly changing size and location within the cytoplasm or assuming a specific position during

various stages of development. The germ granules' complexity and dynamic properties make them challenging to study *in vivo*. For example, in *C. elegans*, germ granules detach from the nucleus of developing oocytes before fertilization and become cytoplasmic. Following fertilization, polarization ensues, and the germ plasma migrates to the posterior end of the dividing germline blastomere P1 (discussed later) (Strome & Wood, 1982).

When condensed over NPCs, these granules create cytoplasmic condensates that extend the NPC microenvironment, promoting proteins associated with germ granules' interaction with mRNA transcripts as they exit the nucleus before entering the germ cells' cytoplasm (Strome & Updike, 2015). Helicases associated with germ granules can suppress transcripts unlicensed for germline expression through direct mRNA suppression, mRNA promotion, or via the ping-pong cycle, suppressing transcripts with piRNA (Marnik et al., 2019; Rochester et al., 2022; Strome & Updike, 2015). This complex environment is critical to understanding how germ granules preserve PGCs in their characteristic totipotent state. For example, complete loss of germ granules results in sterility, and even partial loss of core germ granule components such as Germline Helicase 1 (GLH-1) in *C. elegans* can compromise germline function. With GLH-1 deletions lines demonstrating slight decreased fertility rates at permissive temperatures (20°C) and are completely sterile at higher temperatures (26°C) (Marnik et al., 2019; Strome & Updike, 2015; Updike et al., 2014). The compromised germ cells begin to exhibit somatic markers that are foreign to the germline, demonstrating the loss of their characteristic totipotent state; as a result, germ plasma proteins remain relatively conserved throughout evolution (Campbell & Updike, 2015; Kawasaki et al., 1998; Knutson et

al., 2017; Marnik et al., 2019; Marnik & Updike, 2019; Rochester et al., 2022; Strome & Updike, 2015).

1.3.1 Germ granule conservation

Germ plasma, or germ granules, are essential for maintaining GSCs functionality and have been observed across phylogeny from worms to humans, as depicted in (Figure 9). Homologs of key germ granule components, such as GLH/VASA, have been identified in various organisms, including VASA in Fruit flies (*Drosophila melanogaster*), DDX4 in zebrafish (*Danio rerio*) (Knaut et al., 2000; Koen Braat et al., n.d.; Weidinger et al., 1999; Yoon et al., 1997), DDX4 previously called Mvh in mice (*Mus musculus*) (Carrera et al., 2000; Y. Fujiwara et al., 1994; Tanaka et al., 2000), and DDX4 the human (*Homo sapiens*) germline ortholog (Castrillon et al., 2000) reviewed in (Raz, 2000). The joint function of conserved germ granule proteins can be found throughout these phyla, including sequence similarity. The conserved *C. elegans* GLH-1 protein or DDX4 in humans share a (~40%) homology. The high degree of both functional and sequence conservation across phylogeny highlights the critical role of these proteins in maintaining fertility and preventing deleterious mutation accumulation in GSCs. Any loss or mutation to key germ granule components can lead to sterility. However, in *C. elegans* there are four other GLH proteins (GLH-1, GLH-2, GLH-3, and GLH-4). GLH-1 and GLH-2 have the closest sequence resemblance to the mammalian DDX4. However, some redundancy between them prevents the complete loss of sterility in the absence of another (Marnik et al., 2019; Marnik & Updike, 2019). While this adds some complexity, it also allows for mutations to be made to GLH without resulting in complete sterility.

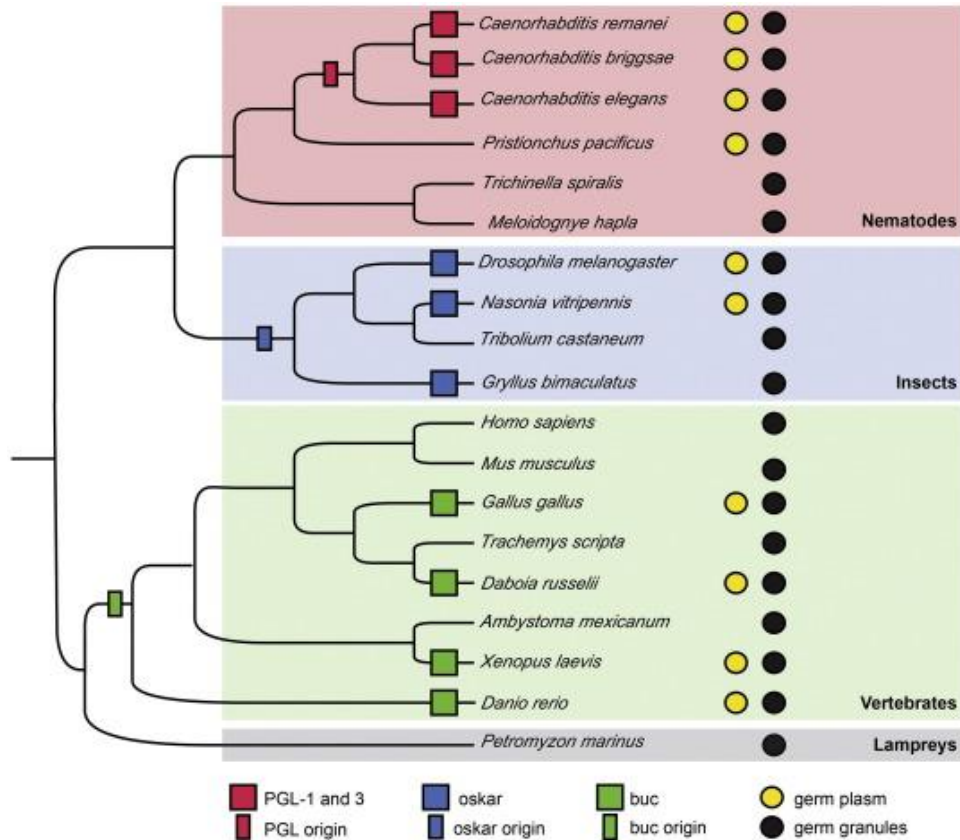


Figure 9: Cladogram of the evolution of germ plasma

Cladogram of the evolution of germ plasma for different animal lineages (nematodes in red, insects in blue, and vertebrates in green). Species that inherit germ plasma maternally are shown in yellow. Image from (Kulkarni & Extavour, 2017)

Although differences exist in establishing germ cells through induction or inheritance and nucleating proteins (reviewed in Kulkarni & Extavour, 2017), the Helicases interacting with RNA have remained primarily conserved. Model organisms, such as insects like *Chrysomelidae multipunctata* or *Drosophila melanogaster*, have been instrumental in establishing fundamental research about germ granules. Nevertheless, in vivo phenotypes of germ granules in adult or larval development remain challenging to observe. Here we utilize the *C. elegans* to study conserved germ granule components throughout development to address this.

1.3.1.1 Germ granules' structure and composition

Germ granules, as previously mentioned, are noted for their remarkable fluidic attributes, capable of swift size and positional adjustments within the germ cell cytoplasm, and precise localization during specific developmental stages. For instance, in *C. elegans*, germ granules detach from the nuclei of developing oocytes before fertilization and migrate to the cytoplasm. Post-fertilization results in germ plasma polarization and migration of the germ plasma towards the posterior end of the dividing germline blastomere P1 (Strome & Wood, 1982). Asymmetric divisions are governed by MEG-3 and MEG-4, which bind to and guide maternal mRNA and germ granule components (Wang et al., 2014). During the initial four embryonic germline divisions, the resulting P4 cell divides into the Z2 and Z3 cells, from which the *C. elegans* germline arises (Sulston et al., 1983). Following these cellular divisions, germ granules or P granules in *C. elegans* condense over the nuclear envelope, covering approximately 75% of nuclear pore complexes (Pitt et al., 2000).

The formation and structure of P granules are initiated by PLG-1 and PGL-3, which facilitate the recruitment of RNA and other granule components, creating a scaffold complex through the C-terminal RGG box domain (Arg-Gly-Gly repeats) (Kawasaki et al., 1998, Hanazawa et al., 2011a). Unlike other core, P-granule components such as GLH-1, the P granule nucleators PGL-1 and PGL-3 are exclusive to the *Caenorhabditis* genome (Aoki et al., 2016; Updike et al., 2011). However, in addition to the RGG domains, both PGL-1 and PGL-3 have dimerization domains (DD) that were found to form homodimers contributing to the structural integrity of P granules (Aoki et al., 2016). DDs of PGL proteins initiate P-granule localization through the self-binding of PGL-1 and PGL-3, which subsequently recruits other P-granule components through

the RGG domain scaffolding (Aoki et al., 2016; Hanazawa et al., 2011; Marnik & Updike, 2019).

Although RGG domains are distinctive to *C. elegans*, DD domains can also be found in *Drosophila* Osk, which forms dimers and is thought to facilitate granule localization (Jeske et al., 2015; N. Yang et al., 2015).

Although PGLs are distinctive to *C. elegans*, the DD domains found in *Drosophila's* Osk, are thought to serve a similar role by forming dimers that facilitate granule localization (Jeske et al., 2015; N. Yang et al., 2015).

The sequential recruitment of binding proteins PGL-1 and PGL-3 provides the scaffold for subsequent components to localize to the granules. While germ granules comprise several components, two major constitutive RNA-binding proteins define them in *C. elegans*: the RGG-proteins, PGL-1, and PGL-3, as previously discussed, and the DEAD-Box helicase proteins, germline helicases; GLH-1, GLH-2, GLH-3, and GLH-4, helping to recruit over 90 other transient components (Reviewed in Phillips & Updike, 2022). Together these components display dynamic movements with liquid-like properties (Brangwynne et al., 2009) loosely held together through dynamic multivalent interactions of phenylalanine-glycine (FG). These interactions are initiated by the interactions with the RGG domains of PGLs, creating a framework for germ granules to localize over nuclear pore complexes and extrapolate through the FG recruitment (Reviewed in Marnik & Updike, 2019; Shinkai et al., 2021).

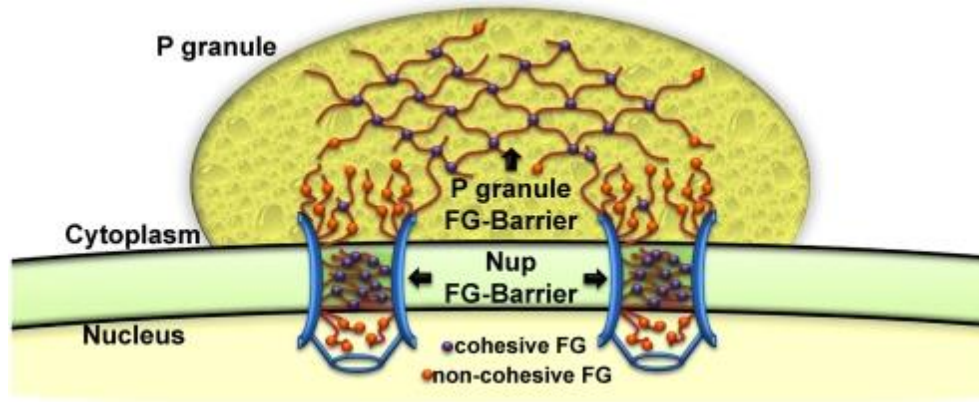


Figure 10: P granules FG size exclusion barrier

Illustrating how P granules could interact with NPCs to extend the nuclear pore environment through FG interactions. Adapted from (Updike et al., 2011).

Much like FG repeats found in the nuclear pore complexes (Sheth et al., 2010), germ granules act as a size exclusion barrier, enabling germline proteins to interact with mRNA transcripts as they exit the nucleus (Figure 10). FG repeats are found in several germline dispensable proteins, including GLH-1, GLH-2, GLH-4, Nucleoporins NNP-4 and NPP-10, DEAD box helicase Homolog (ddx-19), and RNAi defective (rde-12) (Sheth et al., 2010; Shirayama et al., 2014; Spike et al., 2008a). Other components in the germline containing FG repeats with unknown roles of phase separation include NPP-1, NNP-11, and prion-like (Q/N-rich)-domain-bearing protein (PQN-75) (Rochester et al., 2017).

The FG repeat meshwork, in conjunction with RGG domains, acts as the framework for the localization of germ granules over nuclear pore complexes (NPC), which together form a size-exclusion meshwork structure that is capable of interacting with those of NPC FG-NUPS (Marnik et al., 2019; Updike et al., 2011). This granular structure framework is essential for promoting the localization and increasing the coverage of germ granules over the nuclear periphery. Within this perinuclear microenvironment, germline helicases, such as GLH-1,

preferentially promote germline-authorized transcripts. This has been demonstrated through the RNAi knockdown of the core P granule components, including GLH-1, GLH-4, PGL-1, and PGL-3, resulting in a complete loss of P granule formation and the subsequent expression of somatic markers, including neural and muscle-like cell structures in GSCs (Updike et al., 2014). However, the knockdown of PGL-1 and PGL-3 alone is insufficient to cause a complete loss of sterility, indicating the critical role of germline helicases in maintaining GSC totipotent potential even when dispersed in the cytoplasm.

1.3.2 DEAD-box RNA helicases

RNA helicases constitute a highly conserved family of enzymes ubiquitously distributed across eukaryotic and prokaryotic cells and are indispensable for a multitude of RNA metabolic processes. Utilizing ATP-dependent remodeling ribonucleoprotein complexes to bind to and restructure mRNA into secondary structures. RNA helicases play a crucial and extensive role in gene expression, encompassing mRNA transport, degradation, processing, and transcript initiation, as reviewed by (Bourgeois et al., 2016b).

RNA helicases are diverse enzymes that play crucial roles in RNA metabolism. The majority of these enzymes are members of superfamily 2, which comprises eleven subfamilies. Among these subfamilies, the DEAD-Box helicases constitute a prominent group defined by 12 conserved domains forming the RNA helicase core (Figure 11) (Bourgeois et al., 2016a; Cordin et al., 2006; Linder & Jankowsky, 2011; P Linder et al., 1989). This helicase core structure comprises two significant RecA-like domains, one and two, connected by a flexible linker sequence. The DEAD-Box helicase subfamily is further characterized by the inclusion of motifs Q, I, II, and VI that are essential for ATP binding and hydrolysis, as well as motifs Ia, Ib, Ic, IV,

IVa, and V, which are required for RNA binding (Figure 11). While motifs III and Va mediate RNA and ATP binding (Linder & Jankowsky, 2011; P Linder et al., 1989).

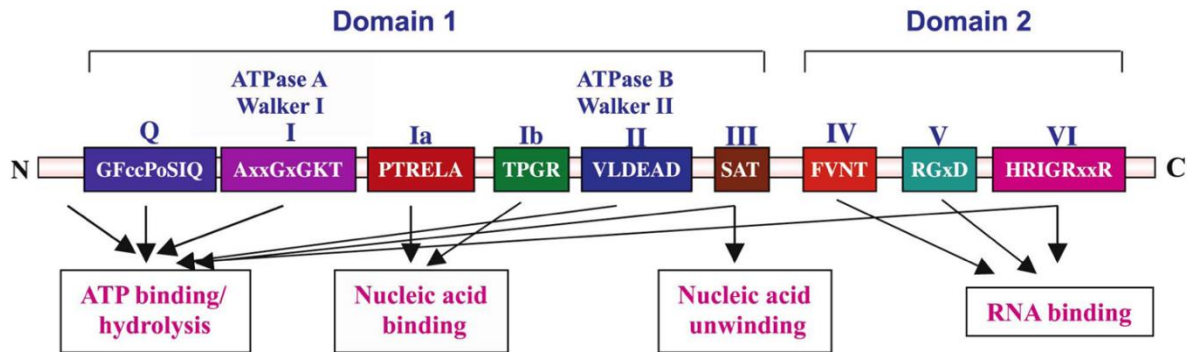


Figure 11: DEAD-Box helicases domains

Sequence Motifs of eIF4A/DEAD-box RNA Helicases of superfamily 2 and their functions.

eIF4A/DEAD-box RNA helicases contain conserved sequence motifs located in two domains:

motifs I, Ia, Ib, II, and III in domain 1 and motifs IV, V, and VI in domain 2. Motif II (also known as Walker B) contains the amino acids DEAD, characteristic of DEAD-box RNA helicases. The Q motif is specific to the family of DEAD-box proteins. These conserved motifs play important roles in the functions of eIF4A/DEAD-box RNA helicases.

The term "DEAD-box" is derived from the presence of a DEAD motif (asp(D)-glu(E)-ala(A)-asp(D)) located in RecA-like domain two. The first DEAD-box helicase identified was the eukaryotic translation initiation factor 4E (eIF4E), which consists solely of the DEAD-box helicase core components and a short N-terminal extension (P Linder et al., 1989).

Initially, the absence of N and C terminal extensions in the eIF4E gene was deemed a characteristic feature of DEAD-box helicases. However, subsequent discoveries showed that the majority of DEAD-box helicases possessed such extensions. While the core domains are highly conserved among all DEAD-box helicases, the N- and C-terminal regions exhibit variability,

leading to diverse affinities for RNA and proteins, and creating a dynamic network of overlapping functionality used to direct and regulate gene expression. Since DEAD-box helicases are involved in RNA transport, RNA stability, and translation initiation, GLH-1 and other DEAD-box helicases play a critical role in maintaining germline totipotency.

1.3.2.1 Role of GLH-1 in the *C. elegans* germline

The *C. elegans* GLH-1 is a ubiquitous DEAD-box helicase that has been evolutionarily conserved and is homologous to VASA in *Drosophila* and DDX4 in humans. This protein is exclusively expressed in developing male and female germ cells and participates in mRNA regulation as a constituent of the germ granule microenvironment. During early embryonic stages, GLH-1 can be either localized in P granules over NCPs or dispersed in the cytoplasm. Despite these variations in its distribution, GLH-1 can interact with its target transcripts while cytoplasmic, albeit to a lesser extent (Updike et al., 2014).

GLH-1 constitutes one of the key germline proteins in *C. elegans*, alongside Tudor domain and argonaut proteins, which constitute the core germ granule proteins. While GLH-1 shares high sequence and motif similarities with other species, there are some notable differences, such as the presence of the GLH-1 zinc finger domain. The functional role of this domain in the germline remains unknown and has been repeatedly excluded in evolution. Moreover, *C. elegans* has several paralogs, including GLH-2, GLH-3, and GLH-4. However, only GLH-1 and GLH-2 contain VASA homolog-defining motifs, including a glycine-rich flanking domain surrounding the N- and C-terminal DEAD-box helicase domain and a negatively charged domain preceding a terminal tryptophan.

Interestingly, GLH-4 also plays a crucial role in germline development. RNAi knockdown experiments revealed that individual knockdowns of GLH-1 or GLH-4 do not result in sterility changes. However, the knockdown of both proteins reduces fertility by 97% (Kuznicki et al., 2000a), indicating that GLH-4 shares some redundancy with GLH-1 in the *C. elegans* germ line. While GLH-2 and GLH-3 do not significantly impact fertility, they too likely serve as redundancies for GLH in the germline. It is worth noting that no more than one GLH/VASA homolog has been found in any vertebrate (Kuznicki et al., 2000b).

The proper development and stability of the germline are crucial for the continuity of species. GLH-1 has been identified as a key player in this process, with its loss resulting in increased sterility rates at permissive temperatures of 20° C. This phenotype is further emphasized under heat stress, with mutants becoming completely sterile at 26° C (Kuznicki et al., 2000b; Marnik & Updike, 2019). The sterility caused by GLH-1 deficiencies is also observed in *glh-1/glh-2* and *glh-1/glh-4* double mutants, resulting in infertility at permissive 20° C temperatures with a significant decrease or absence of germ cells and limited to no sperm production (Spike et al., 2008b). While GLH paralogs complicate their role in the *C. elegans* germline and overlap in functionality, it also provides a unique opportunity to study the function of GLH/Vasa.

DDX4 or VASA depletions result in infertility, making it challenging to resolve their roles and passage of mutant lines. However, in the case of *C. elegans*, the knock-out of GLH-1 and GLH-2 causes fertility defects while maintaining reduced but sustainable reproduction rates, thus offering a valuable opportunity to investigate the conserved GLH-1's role in the germline, including transcript affinity and its contribution to promoting spermatogenesis. Although GLH-1

has three other orthologs in the *C. elegans* genome, unlike other VASA homologs, this attribute can be advantageous to studying VASA functionality since the GLHs in *C. elegans* possess every functional domain found in VASA homologs. The various genes of GLH can be knocked out individually without detrimental fertility defects to evaluate their role in the germline, providing valuable insights into the role of GLH/VASA and increasing our understanding of the critical germline proteins that drive spermatogenesis and maintain germline immortality.

In this context, our research has precisely defined GLH-1's functional domains by analyzing 28 endogenous mutant alleles, their role in sperm development, and C and N terminal transcript affinity. These results demonstrate that loss or reduction of function in these domains leads to loss of embryo viability, sterility, compromised sperm functionality, and disoriented granule localization, furthering our understanding of the critical germline proteins driving spermatogenesis and maintaining germline immortality.

1.4 Somatic reprogramming of germ cells

Throughout development, germ cells undergo a unique potency transition. PGCs give rise to EGC precursors, which develop into sperm and oocytes while losing developmental potency. However, during a brief period after fertilization, oocytes are returned to their previous totipotent state, capable of developing into all cells of an organism. GSCs themselves, under typical development, are unable to develop into anything but gametes, which are in part safeguarded by germ granules. However, under atypical developmental circumstances, GSCs developing pluripotency can result in sterility, cancerous growths, and uncontrolled cellular specification.

An RNAi knockdown of a handful of core P granule genes, such as PGL-1, PGL-3, GLH-1, and GLH-4, reduces germ cell potency, beginning to express both genotypic and phenotypic traits of neurons (Updike et al., 2014). Here germ cells develop axon-like projections and express somatic pan-neuronal markers, such as uncoordinated 119 (*unc-119*), *unc-33*, and the body wall muscle myosin (*MYO-3*). However, germ cells are not terminally differentiated, demonstrating that germ granules help maintain germline potency by repressing somatic transcripts (Strome & Updike, 2015). Similar results are found when other germline proteins and transient germ granule localizers are knocked out, such as muscle excess 3 (*MEX-3*) and defective in germ development 1 (*GLD-1*). These knockouts result in germ cells undergoing an immediate induction to terminal somatic cells (R. Ciosk et al., 2006). Both results were later reaffirmed through RNA-seq studies, finding global increases in somatic transcripts in *GLH-1* deletion mutants (A. K. Knutson et al., 2017a). Together, these results demonstrate germ granules' ability to control and direct stem cell fate and the variability that individual germ granule components have on stem cell fate, suggesting a complex and dynamic epigenetic regulation suppressing and, at times, promoting mRNA in germ cells.

Germ granules act as safeguards or "gatekeepers" of germ cells, controlling epigenetic regulation within the germ line and maintaining GSC potency. When these safeguards are compromised, stem cells lose potency and express transcripts typically associated with somatic development. For instance, when germ granule safeguards are removed, germ cells often revert to pan-neuronal marker expression such as (*rab-3*, *unc-119*, *snb-1*, *unc-33*, and *unc-10*), including neuron subtype-specific transcripts (*gcy-5*, *ceh-36*, and *eat-4*) (reviewed in Marchal & Tursun, 2021). These markers have helped identify many factors that safeguard or preserve this

developmental type, such as the histone chaperone abnormal cell Lineage (LIN-53) (Cheloufi & Hochedlinger, 2017a; Tursun et al., 2011), Retinoblastoma protein Binding Protein (RBBP-5) (Kazmierczak et al., 2020), the facilitates chromatin transactions (FACT) complex member 3 (HMG-3) (Kolundzic et al., 2018a), and the chromodomain protein, mortality factor-related Gene (MRG-1) (Fujita et al., 2002; Gupta et al., 2015; Hajduskova et al., 2019). Several of these have conserved functions in higher organisms, such as CAF-1, Lin-53s ortholog in mice, and FACT homologs SSRP1 and SUPT26, found to help increase the efficiency of reprogramming human fibroblasts into iPSCs and induced neurons (Cheloufi & Hochedlinger, 2017b; Kolundzic et al., 2018b).

In the *C. elegans*, germ cells often default into neuron-associated cell fates when losing germ granules (A. K. Knutson et al., 2017b; Marchal & Tursun, 2021; Rochester et al., 2022), which could be attributed to over a third (37%) of *C. elegans* cells being neurons or glial-associated (Hobert, 2010; Sulston & Horvitz, 1977). It may also suggest that pan-neuronal expression is a marker of the earliest stages of germ cell differentiation (reviewed in Marchal & Tursun, 2021).

1.5 Review of the current state of research

The field of stem cell research holds great promise but also presents many challenges that must be addressed before its potential can be fully realized. These challenges include immunological rejection, undesired cellular differentiation, identification of early stages of cancerous growth, and development of a "fail-safe mechanism" for self-destruction in case of unintentional development (Itakura et al., 2017; Ivics, 2015; Lytle et al., 2018). Addressing these challenges through research focused on preserving and directing stem cell lineage has already

expanded and improved current methods of iPSC and regenerative therapies for use in the medical field (Kolundzic et al., 2018a).

Embryonic development is particularly interesting and offers a complex opportunity to evaluate stem cell development and differentiation governed by a network of epigenetic interactions. Understanding how ESCs are preserved in an undifferentiated state, induced and directed into specific lineages, and retain totipotent potential presents a particularly interesting yet challenging path due to the various networks of interactions governing stem cell fate. Fortunately, recent advances in genetic tools such as CRISPR have enabled researchers to start teasing apart various mechanisms in stem cells, including how germ granules and their components factor into maintaining a stem cell's totipotent state.

Germ granules have been identified as key contributors to the preservation of germ cell totipotency, fertility, pluripotent potential, and the direction of stem cell fate (Cinalli et al., 2008; Phillips & Updike, 2022; Strome & Updike, 2015). Their direct effect on preserving the germ line has created remarkable protein and sequence structure conservation throughout evolution, making translating model organism research to human medical applications particularly relevant (Kulkarni & Extavour, 2017). Current research efforts have been directed toward understanding germ granules' structural makeup (C. Y. S. Lee et al., 2020; Marnik et al., 2019; Updike et al., 2011), including the formation of sub-granules such as Z granules (Cipriani et al., 2021; Ishidate et al., 2018; Marnik et al., 2022; Wan et al., 2018) and Mutator foci (Phillips et al., 2012; Tsai et al., 2015; Uebel et al., 2018, 2020), as well as the recruitment, segregation, mixing, and how helicases interact with and control mRNA to direct GSC fate (reviewed in Phillips & Updike, 2022). Additionally, fundamental research that has been

established in model organisms such as *C. elegans* and *Drosophila* has begun to be explored in higher organisms such as Mice establishing translational relevancy of these conserved proteins throughout evolution (Fang et al., 2018; Hikichi et al., 2013; Kikuchi et al., 2017; Zakrzewski et al., 2019).

The emergence of CRISPR technology has facilitated recent progression in stem cell and germline research (Jinek et al., 2012). Recent advancements in CRISPR methodologies' efficiency have enabled researchers to address previously unanswerable questions hindered by experimental, time, or resource limitations. Particularly efficiency in the *C. elegans* germline has precisely edited thousands of new mutant lines (Schwartz et al., 2021). Although the function of VASA/GLH-1 has been a significant focus in the germline field in the past decade, the emergence of CRISPR technology at the start of this thesis work has provided a means for the rapid production of mutant lines, promoting further investigation into the structure and function of GLH-1 (Chen et al., 2020; Marnik et al., 2019; Rochester et al., 2022). Specifically, the domain functions of GLH-1, its affinity for P granules, and its interactions with mRNA.

1.6 Overview of dissertation

Stem cells have remarkable potential for various medical applications, including regeneration and cancer therapies. Among stem cells, GSCs are considered the ultimate stem cell type due to their ability to give rise to all cells of the next generation. However, GSCs possess the same genetic information as somatic cells. Conserved factors found in the cytoplasm of germ cells, called germ granules, are responsible for the differences in potency between germ cells and somatic cells—the mechanisms by which germ granules function is still poorly understood. Since germ granule components are conserved throughout evolution from

C. elegans to humans, determining their function is critical to developing stem cell medical applications.

In this thesis, I investigate the role of a central component of the germ granules' microenvironment, specifically the VASA/GLH-1 DEAD-box helicase, which is critical for maintaining fertility rates through the conservation of germline stem cells. By utilizing newly developed CRISPR protocols, we created over 30 precision edits to determine the functional domains of GLH-1/VASA and developed a toolkit of mutant lines for future studies.

Furthermore, I developed a liquid culture protocol that enables the simplified mass collection of *C. elegans*, allowing us to determine GLH-1 binding partners using immunoprecipitation and investigate how the presence of GLH-1 antagonizes somatic reprogramming. This approach involves RNA-seq with polysome profiling during young adult worms' targeted developmental time point. Making two significant discoveries. First, GLH-1 deletion lines demonstrated an upregulation of nearly all neuropeptide-encoding mRNAs. Second, GLH-1 promotes the translation efficacy of most major sperm-associated transcripts, driving spermatogenesis and sperm motility.

In chapter III, I investigate the role of an uncharted protein containing glycine-phenylalanine-rich (FG) repeats called PQN-75 since germ granules are composed of many proteins containing Glycine-rich domains regularly interspersed with phenylalanine. We used CRISPR to tag PQN-75s C terminal end with A GFP flag tag. Surprisingly, we found that PQN-75 was not expressed within the germline but in the pharynx's gland cells. Further characterization suggests it is a secreted protein that plays a role in digestion, thermotolerance, and innate immunity.

These findings provide novel insights into the role of PQN-75 and extend our understanding of GLH-1/VASA's functions. Specifically, our results show that GLH-1/VASA helps maintain germ cell pluripotency by suppressing neuropeptide mRNA transcripts while promoting spermatogenesis and sperm motility.

1. CHAPTER II: MATERIALS AND METHODS

2.1 Strains used

STRAIN	GENOTYPE
N2	wild type
DUP17	<i>ddEx16[pgl-1p::PGL-1::TY1::EGFP::3XFLAG(92C12)+Cb-unc-119(+)] I</i>
DUP36	<i>pqn-75(EMS) csr-1(sam18)IV/nT1[qIs51](IV;V); ddEx16[pgl-1p::PGL-1::TY1::EGFP::3XFLAG(92C12)+Cb-unc-119(+)] I</i>
DUP38	<i>pqn-75(sam20) IV</i>
DUP49	<i>ddEx16[pgl-1p::PGL-1::TY1::EGFP::3XFLAG(92C12)+Cb-unc-119(+)] I; pqn-75(sam20) IV</i>
DUP64	<i>glh-1(sam24[glh-1::gfp::3xFLAG]) I</i>
DUP66	<i>pqn-75[sam26(pqn-75::GFP::3xFLAG)] IV</i>
DUP73	<i>glh-1(sam31[glh-1::rla-1bicis::gfp::3xFlag]) I</i>
DUP 116	<i>pqn-75(tm6575) IV; samEx7(pqn-75 fosmid WRM0639dH02+pCFJ104)</i>
DUP121	<i>glh-1(sam24[glh-1::gfp::3xFLAG]) I; pgl-1(sam52[pgl-1::mTagRFPT::3xFLAG]) IV</i>
DUP124	<i>glh-1(sam54 - sam24[glh-1::gfp::3xFlag]) I</i>
DUP129	<i>samEx9(hlh-6::YFP+myo-3::mCh); pqn-75(tm6575) IV</i>
DUP130	<i>glh-1(sam57 - sam24[glh-1::gfp::3xFlag]) I</i>
DUP137	<i>glh-1(sam59 - sam24[glh-1::gfp::3xFlag]) I; dpy-10(coCRISPR) hets II</i>
DUP140	<i>glh-1(sam61 - sam24[glh-1::gfp::3xFlag]) I;</i>
DUP141	<i>glh-1(sam62 - sam24[glh-1::gfp::3xFlag]) I;</i>
DUP142	<i>glh-1(sam63 - sam24[glh-1::gfp::3xFlag]) I;</i>
DUP143	<i>glh-1(sam64 - sam24[glh-1::gfp::3xFlag]) I;</i>
DUP144	<i>glh-1(sam65 - sam24[glh-1::gfp::3xFlag]) I</i>
DUP145	<i>glh-1(sam66 - sam24[glh-1::gfp::3xFlag]) I</i>
DUP146	<i>glh-1(sam67 - sam24[glh-1::gfp::3xFlag]) I</i>

DUP147	glh-1(sam68 - sam24[glh-1::gfp::3xFlag]) I
DUP148	glh-1(sam69 - sam24[glh-1::gfp::3xFlag]) I
DUP149	glh-1(sam70 - sam24[glh-1::gfp::3xFlag]) I
DUP151	glh-1(sam71 - sam24[glh-1::gfp::3xFlag]) I
DUP152	glh-1(sam72 - sam24[glh-1::gfp::3xFlag]) I
DUP154	glh-1(sam74 - sam24[glh-1::gfp::3xFlag]) I
DUP156	glh-1(sam76 - sam24[glh-1::gfp::3xFlag]) I
DUP157	glh-1(sam77 - sam24[glh-1::gfp::3xFlag]) I
DUP160	glh-2(sam80) glh-1(sam78 - sam24[glh-1::gfp::3xFlag]) I/hT2[bli-4(e937) let-?(q782) qls48](I;III)
DUP162	<i>glh-1(sam24[glh-1::gfp::3xFLAG]) I ; itIs37[pie-1p::mCherry::H2B::pie-1 3'UTR, unc-119(+)] IV</i>
DUP163	<i>glh-1(sam92[glh-1(DQAD)::gfp::3xFLAG]) I ; itIs37[pie-1p::mCherry::H2B::pie-1 3'UTR, unc-119(+)] IV</i>
DUP164	glh-1(sam82 - sam24[glh-1::gfp::3xFlag]) I
DUP165	<i>glh-2(sam82[glh-2(DQAD)]) glh-1(sam92[glh-1(DQAD)::gfp::3xFLAG]) I ; itIs37[pie-1p::mCherry::H2B::pie-1 3'UTR, unc-119(+)] IV</i>
DUP168	glh-1(sam86 - sam24[glh-1::gfp::3xFlag]) I
DUP170	glh-2(sam89) glh-1(sam90 - sam24[glh-1::gfp::3xFlag]) I/hT2[bli-4(e937) let-?(q782) qls48](I;III)
DUP171	glh-2(sam91) glh-1(sam92 - sam24[glh-1::gfp::3xFlag]) I
DUP173	glh-2(sam91) glh-1(sam94 - sam24[glh-1::gfp::3xFlag]) I
DUP175	glh-2(sam87) glh-1(sam88 - sam24[glh-1::gfp::3xFlag]) I/hT2[bli-4(e937) let-?(q782) qls48](I;III)
DUP178	<i>glh-1(sam24[glh-1::gfp::3xFLAG]) prg-1(sam97[TagRFP::3xFLAG::PRG-1]) I</i>
DUP179	glh-2(sam91) glh-1(sam98 - sam24[glh-1::gfp::3xFlag]) I
DUP180	<i>glh-1(sam65[Δglh-1::gfp::3xFLAG]) prg-1(sam97[TagRFP::3xFLAG::PRG-1]) I</i>
DUP181	<i>glh-1(sam92[glh-1(DQAD)::gfp::3xFLAG]) prg-1(sam97[TagRFP::3xFLAG::PRG-1]) I</i>
DUP184	<i>glh-1(sam86[glh-1(_EAD)::gfp::3xFLAG]) prg-1(sam97[TagRFP::3xFLAG::PRG-1])</i>
KX197	glh-1(sam24 [glh-1::gfp::3xFlag]) I; ssq-1(sam120[V5::mCherry::ssq-1]) IV; him-5 (e1490) V
KX198	glh-1(sam24[glh-1::gfp::3xFlag]) I; msp-142(sam116[msp-142::mCherry::V5]) II; him-5 (e1490) V

KX199	<i>glh-1(sam24 [glh-1::gfp::3xFlag]) I; him-5 (e1490) V</i>
KX200	<i>glh-1(sam65 [Δglh-1::gfp::3xFlag]) I; him-5 (e1490) V</i>
DUP206	<i>glh-1(sam24[glh-1::gfp::3xFlag]) I; msp-142(sam116 [msp-142::mCherry::V5]) II</i>
DUP210	<i>glh-1(sam65 [Δglh-1::gfp::3xFlag]) I; msp-142(sam116[msp-142::mCherry::V5]) II</i>
DUP211	<i>glh-1(sam24 [glh-1::gfp::3xFlag]) I; ssq-1(sam120[V5::mCherry::ssq-1]) IV</i>
DUP216	<i>glh-1(sam65[Δglh-1::gfp::3xFlag]) I; ssq-1(sam120[V5::mCherry::ssq-1]) IV</i>

Table 1: List of all *C. elegans* strains used in this thesis.

2.1 *C. elegans* maintenance

Strains were maintained at 20 °C on nematode growth medium (NGM) agar plates seeded with *Escherichia coli* OP50 as previously described (Brenner, 1974).

2.2 CRISPR strain construction

Three CRISPR/Cas9 protocols were followed for strains created and used in this thesis. In (Rochester et al., 2017), strains were created following a protocol previously described in (Ward, 2014). To recreate the G to A base pair change in the *sam18* allele of *pqn-75*, plus silent mutation in the PA motif to prevent recleavage, the sgRNA (AATCCGCTAGCAGTTACACCT) was used to make the Cas9/sgRNA plasmid pDU54 and coinjected with a 60 bp HR oligo (TTGGCCTCCGAATCCGCTAGCAGTTACATCTT**G**ATTTCCACCGAATCCTCCATTGTTTCC) using the *rol-6* Co-CRISPR method (Ward, 2014). Bold letters indicate changes in the sequence. Edits were sequence confirmed and homozygosed.

Endogenous *pqn-75* was tagged with GFP::3xFLAG using the FP-SEC method (Dickinson et al., 2015), where the sgRNA (GCGAAGAATCCCTTCTTTGG) was used to make the Cas9/sgRNA plasmid pDU61, and coinjected with a GFP-SEC flanked with *pqn-75* sequence (pDU66) to make

the C-terminal insertion with 10 silent mutations to prevent Cas9 recleavage. The expected edits were sequence confirmed and homozygosed. The following strains were created for this study, and are available upon request: DUP17, DUP36, DUP38, *DUP49*, DUP 116, DUP66, DUP129.

In (Marnik et al., 2019) A co-CRISPR technique with *dpy-10* was used to create the mutant alleles as described (Paix et al., 2017). Table S1 lists the sequences for the guide RNA and repair templates for the strains created. A mTagRFPT::3xFLAG tag was added to the C-terminus of *pgl-1* and the N-terminus of *prg-1*, using the fluorescent protein-selection excision cassette (FP-SEC) method, to create *pgl-1* (*sam52*) and *prg-1* (*sam97*) alleles (Dickinson et al., 2015). The same method was modified to generate the *glh-1* (*sam31*) allele found in DUP73, which contains a bicistronic rSL2 GFP::3xFLAG transcriptional *glh-1* reporter. Additional strains created for this study include DUP121, DUP162, *unc-119*, DUP163, DUP165, DUP178, DUP180, DUP181, and DUP184.

Finally, in (Rochester et al., 2022) the CRISPR/Cas9 protocol was adapted from (Ghanta & Mello, 2020) and used on WT DUP64 and Δ *glh-1* DUP144 to create the following: DUP206, DUP210, DUP211, and DUP216. The *him-5(e1490)* allele was crossed into WT DUP64, Δ *glh-1* DUP144, DUP206, and DUP211 to generate KX199, KX200, KX197, KX198, KX199, KX200, KX197, and KX198.

All strains generated for this study, their associated sequence files, and GenBank files for each strain are available upon request.

2.3 Live imaging of germline

Transgenic male worms were placed into SM buffer (50 mM HEPES, 25 mM KCl, 45 mM NaCl, 1 mM MgSO₄, 5 mM CaCl₂, and 10 mM Dextrose; pH 7.8) containing 0.2 mM levamisole on a GCP (0.2% w/v gelatin, 0.02% w/v chrome alum, 0.05% w/v poly-L-lysine)-coated glass slide. To extrude spermatids, 5–6 worms were dissected from each strain and covered with a coverslip for live imaging with the Leica Thunder Imager, objectives, and camera described above. Fixed exposure conditions were used on all strains. Using ImageJ, a fixed circular ROI was applied to each spermatid, and the measurement tool was applied to obtain the integrated density. Mean pixel intensity was subtracted from the adjacent background to calculate the corrected total cell fluorescence (CTCF = Integrated Density – (area of cell * mean background fluorescence)).

2.4 Fixation and immunostaining

Two fixation methods were used as previously described (Huggins & Keiper, 2020; Min et al., 2016) with minor modifications. Briefly, to observe the expression of fluorescently labeled whole worms, they were fixed with 4% paraformaldehyde at room temperature for 20 min and further fixed with 70% ethanol. The specimens were stained with DAPI (Thermo Scientific, Germany, 62248) to stain DNA, and observed on a Leica Thunder Imager Live Cell microscope with an HC PL APO 63x/1.47 Oil CORR TIRF objective and DAPI, GFP, and TXR filter sets. Images were acquired with a Leica DFC9000 GT deep-cooled sCMOS camera and Leica LAS X imaging software. To observe the mitotic germ cells and progression of spermatogenesis in males, worms were dissected and fixed with 100% methanol at –20 °C for 10 min, followed by 100% acetone fixation at –20 °C for 10 min. The specimens were further counter-stained with

DAPI to stain DNA. The following primary and secondary antibodies were used: mouse monoclonal anti- α -tubulin (1:500; Sigma, T9026), rabbit anti-phospho-histone H3 (Ser10) (1:500; EMD Millipore, 06–570), Alexa Fluor 488-conjugated goat anti-mouse IgG (1:500, Invitrogen, A32723), Alexa Fluor 594-conjugated goat anti-rabbit IgG (1:500, Invitrogen, A32740).

2.5 Liquid Cultures

A substantial quantity of worms is required to conduct RNA-seq, polysome profiling, IP, and MS analysis on *C. elegans*. To collect a sufficient sample size, a liquid culture protocol was developed with the aim of simplifying and streamlining the process. This protocol's development required resolving several obstacles, including differences in *C. elegans* developmental timing, feeding behavior, and stress factors.

Although some stress factors are inherent to rearing worms in liquid media, significant stressors, such as feeding ability, were addressed using a freeze-dried and powdered OP50 instead of a standard OP50 live culture. That tends to aggregate, leading to inconsistencies in feeding behavior between liquid cultures. These inconsistencies are critical to address, as they can impact fertility, lifespan, and germline expression (Howard et al., 2021; Laws & Drummond-Barbosa, 2017). Any inconsistencies in germline development between samples are likely to directly affect the proteins of interest in (Marnik & Updike, 2019; Rochester et al., 2022).

To ensure even dispersal of the OP50 throughout the media and promote consistent feeding habits within the liquid culture, freeze-dried and powdered OP50 was selected and provided by the company LabTie. Developmental timing changes were also determined to

enable the collection of worms at a specific stage of development. The resulting protocol is described below.

C. elegans strains DUP64 *glh-1(sam24[glh-1::gfp::3xFlag])* and DUP144 *glh-1(sam65[Δglh-1::gfp::3xFlag])* (Marnik et al., 2019) were used in the polysome profiling experiments. With three replicates for each strain. For each replicate, 25 recently starved plates were added to 1L of S Media with 5 g of freeze-dried OP50 (LabTie, Leiden, The Netherlands). These cultures were separated into four 250 ml aliquots in 1L beveled flasks to improve aeration and incubated in shakers at 20 °C. Once worms were gravid, they were precipitated and washed with M9. After a bleach solution with (3 parts water, 1 part Clorox bleach, 0.1 parts 10M NaOH) was prepared and added to the worms for 3 min, followed by three washes to extract embryos. Embryos were hatched overnight on unseeded plates. Synchronized L1-staged worms were used to inoculate 1L of S Media with OP50, separated into four 250 ml flasks, and grown for approximately 40 h until the majority reached the young adult stage. Young adults were precipitated with a pear funnel, washed, pelleted, and flash-frozen in 1-ml aliquots.

2.5 Polysome profiling

For each strain and replicate, pelleted worms were lysed by grinding in solubilization buffer (300 mM NaCl, 50 mM Tris-HCL pH 8, 10 mM MgCl₂, 1 mM EGTA, 200 μg ml⁻¹ heparin, 400 U mL⁻¹ RNAsin, 1 mM PMSF, 0.2 mg ml⁻¹ cycloheximide, 1% Triton X-100, 0.1% sodium deoxycholate). Half of the sample was separated and used for total RNA isolation. The other half of the lysate was loaded onto a 10–50% sucrose gradient in high salt resolving buffer (140 mM NaCl, 25 mM Tris-HCL pH 8, 10 mM MgCl₂). Gradients were resolved by ultracentrifugation

in a Beckman SW41Ti rotor at $38\,000 \times g$ at $4\text{ }^{\circ}\text{C}$ for 2 h. Fractions of the gradients were continuously monitored at an absorbance of 254 nm using a Teledyne density gradient fractionator, collecting the polysome fraction. I would like to acknowledge Dr. Jared Rollins for his valuable training in using the profiler and Dr. Aric Rogers for providing the protocol and resources.

2.7 RNA-Sequencing

mRNA was isolated from the lysates total and polysome associated halves using a TruSeq RNAv2 kit (Illumina) following the manufacturer's protocol. RNA quality was assessed on an Allegiant 2100 Bio-analyzer (Agilent, Palo Alto, CA), requiring an A260/A208 > 1.7 and RIN > 8.0 . All 12 samples were sent to the Jackson Laboratory (Bar Harbor, ME) for sequencing using a KAPA stranded mRNA sequencing kit (Roche), followed by 75 cycles on the NextSeq HO Illumina sequencer.

2.8 qRT-PCR

RNA extraction - Worms were grown on chicken egg plates at $20\text{ }^{\circ}\text{C}$ and floated on 35% sucrose before flash freezing as pellets in liquid nitrogen with 14 mM E64 protease inhibitor (Sigma-Aldrich), 4 mM Vanadyl-RNC RNase inhibitor (Sigma-Aldrich), and 0.2% Tween 20 detergent (Sigma Aldrich). Four worm pellets were ground using mortar and pestle. Powdered worms were melted on ice, and the lysate was extracted with Trizol (Life Technologies) according to the manufacturer's protocol. This was followed by 0.7 vol isopropanol precipitation. The resuspended precipitate was further extracted with phenol-chloroform-isoamyl alcohol (25:24:1), and twice with chloroform-isoamyl alcohol (24:1), then ethanol precipitated. GlycoBlue (Invitrogen) was used as a co-precipitate according to the

manufacturer's instructions. RNA quality and quantity were determined using NanoDrop ND-1000 spectrophotometer.

qRT-PCR - Reverse transcription was performed on 0.5 µg of total RNA in a 20 µl reaction with the iScript Adv cDNA synthesis kit (Bio-Rad Laboratories) according to the manufacturer's instructions. qRT-PCR was performed in triplicate on an OPUS CFX-96 Real-Time System (Bio-Rad Laboratories) using Sso Fast Evagreen Supermix (Bio-Rad Laboratories), according to the manufacturer's instructions. Quantification of *msh-142* and *ssq-1* mRNA was normalized to *gpd-3* mRNA using $\Delta\Delta CT$ analysis.

2.9 Sequence analysis and data deposits

Final FASTQ data files were sent to the Mount Desert Island Biological Laboratories Bioinformatics Core. Sequences were preprocessed with TrimGalore version 0.67, using default options (<https://github.com/FelixKrueger/TrimGalore>). Quantification was performed with kallisto version 0.45.1 (Bray et al., 2016), using a custom target transcriptome that was based on the Ensembl release 105 (based on Wormbase Release 235), using the combined "cdna" and "ncrna" assigned transcript, and which also had two additional transcripts that correspond to the GLH-1-GFP fusion construct, and the associated GLH-1 deletion transcript. The resulting sample-specific expression files were joined into transcript- and gene-level expression matrixes using the R package tximport (Soneson et al., 2015), with a custom transcript-to-gene map that assigned the two GLH-1 constructs to the same gene as the endogenous GLH-1 (WBGene00001598). Differential expression analysis was carried out in R version 4.1.0 with the DESeq2 version 1.24.0. DESeq2 was also used to generate a rlog-matrix which was Z-transformed to normalize each gene across all samples. mRNA-seq datasets have been

deposited in the NCBI Gene Expression Omnibus database under accession number GSE148737 (BioProject ID PRJNA625528).

For comparative visualization of read coverage on specific genes, the trimmed fastq files were aligned to the previously mentioned *C. elegans* Ensembl genome using the STAR aligner version 2.6.1b (Dobin et al., 2013), with a splice junction overhang of 100 nt. The resulting BAM files were converted to bigwig with bamCoverage version 3.6 from the DeepTools2 suite (Ramírez et al., 2016) for visualization in IGV version 2.11.2 (Robinson et al., 2011).

The STRING database (v11) (string-db.org) was used to visualize clustered protein-protein networks and perform the gene ontology analysis in Supplemental table 1 (Szkłarczyk et al., 2019, 2021).

Gene categories were defined using published datasets. Soma-specific genes include the dataset described and used in (Knutson et al., 2017a, 2017b; Rechtsteiner et al., 2010) Oogenic, gender-neutral, and spermatogenic categories were described in (Ortiz et al., 2014). Neuronal genes and neuronal subclasses that include ion channels and neuropeptides were extrapolated from neuronal “threshold level 2” genes as defined in the CeNGEN (complete gene expression map of the *C. elegans* nervous system) (Taylor et al., 2021) Violin plots and unpaired *t*-test analysis were performed using GraphPad Prism version 9.4.0 for Windows, GraphPad Software, San Diego, California USA, www.graphpad.com. Sequence analyses were headed by Goel H. Graver, aided by Nathaniel J. Maki.

2.10 Growth assays

2.10.1 larval development size assay

Worm growth was evaluated by bleach synchronizing 100-200 N2 (wild type) and *pqn-75 (tm6575)*. The remaining embryos were hatched and plated onto OP50 lawn. Worm Tracker (Micro Bright Field Inc. Stable camera stand with WormLab software and ATV Stingray F504B camera attached to a Nikon macro lens) was used to monitor worm length every half hour for 51 h. The video was captured from within the bacterial lawn for 30 seconds and used to quantify worm length for 10-60 worms for each time point. Lengths captured are slightly shorter than usual due to the program's inability to capture the small diameter of the worm's tail accurately. A collective average was used to plot the lengths in R.

2.10.2 Vulva development

Bleach-synchronizing was used to monitor vulval development—the L1 larvae were then plated onto a bacterial lawn, each with 50 worms per plate. After 48 h of incubation at 20°C, worms were evaluated and removed when a fully developed vulva was evident. The observation ended when all worms reached full vulval development.

2.10.3 Grinder size

In order to assess grinder development, a method utilizing bleach synchronized L1s was employed. These individuals were placed on a bacterial lawn and imaged at hourly intervals from 15-20 h after feeding. At each time point, 20 nematodes from each strain were transferred onto an agar slide containing 5 mM levamisole, and the width of their grinder was measured via a 40× DIC objective and Leica imaging software (George-Raizen et al., 2014).

2.11 Germline integrity

2.11.1 Variable Temperature Fertility counts

For each strain, the fertility was determined by plating L4 worms at both 20° and 26°. Hatched F1 progeny were then picked to 10 plates with 25 worms on each plate. The percent of grotty (uterus filled with unfertilized oocytes and terminal embryos) and clean (germline atrophy with an empty uterus) sterile F1s were scored when they reached day 2 of adulthood. Previously described in (Marnik et al., 2019)

2.11.2 RNAi Fertility counts

Six L4 stage worms were picked to a plate to count brood size and passaged to new plates each day for six consecutive days. The number of progenies was totaled from each plate and averaged based on the replicates. Previous steps were repeated three times to gather average brood sizes for N2 and *pqn-75(tm6575)*. This assay was repeated with wild-type N2s on *pqn-75* RNAi plates and control empty vector plates. RNAi feeding was performed as previously described (Kamath et al., 2001).

2.12 Sperm functionality assays

2.12.1 Sperm migration

To assay sperm migration, synchronized MSP:mCherry-tagged transgenic males were used for mating as previously described (Hoang & Miller, 2017) with minor modifications. Males mated with *fog-2* females in a 10:1 ratio for 3 h. Mated *fog-2* animals were subsequently transferred to new NGM plates and examined for fluorescence under a fluorescence microscope (n = 30 mated with WT males, n = 26 mated with *Δglh-1* males). Fluorescence and

DIC images of the uterus were divided into three equal zones to analyze MSP-142:mCherry distribution. Hymin Min performed sperm migration assays.

2.12.2 Sperm counts

Sperm counts of synchronized young adults were collected by fixing in M9 with 8% PFA for 1 h, washed 3× with PBS, 1× with 95% ethanol for 1 min, and 3× with PBS. Worms were then mounted on a charged slide with mounting media containing DAPI. Sperm nuclei were imaged and counted in each spermatheca using a 60× objective on a Leica DMI6000B – 10 worms/strain, previously described in (Rochester et al., 2017).

2.12.3 In Vitro Sperm activation

In vitro sperm activation was performed as previously described (Tajima et al., 2019) with minor modifications. L4 males were isolated on OP50-seeded NGM plates and cultured on the plates at 20 °C for 48 h in the absence of hermaphrodites. Then, 10 of the virgin males were transferred to 10 µl of SM buffer (50 mM HEPES, 25 mM KCl, 45 mM NaCl, 1 mM MgSO₄, 5 mM CaCl₂, and 10 mM Dextrose; pH 7.8) with or without 200 µg/ml of proteinase K or 6 mM ZnCl₂ on a glass slide. Spermatids were released by cutting the tails. After incubating at RT for 5 min, a coverslip was gently overlaid and sealed with Vaseline. Activation of spermatids to spermatozoa was observed at 63X magnification under Nomarski differential interference contrast (DIC) microscopy on the Leica Thunder Imager. Hymin Min performed sperm activation assays

2.13 Embryonic lethality

Plating L4 worms determined embryonic lethality for each strain at 20°. Hatched F1s were grown to gravid young adults. Six worms were randomly selected, picked to new plates, and allowed to lay for 5 hr h. Embryos were marked and counted after the initial 5 hr period, and later unhatched embryos were counted again 18–24-hr later. Terminal phenotypes were imaged from these unhatched but still moving embryos, previously described in (Marnik et al., 2019).

2.14 Proteotoxic stress assays

2.14.1 Oxidative stress

Oxidative stress was induced in L4 worms by exposure to 100 mM Paraquat in a 96-well plate assay (N=10/well, 12 replicates/strain); survival was scored every hour as previously described in (Possik & Pause, 2015)

2.14.2 Osmotic stress

Osmotic stress was induced in L4 worms by growing on seeded OP50 NGM plates containing 51 mM NaCl (Control NGM levels) and higher NaCl concentrations of 400 mM, 500 mM, and 600 mM, survival was scored 24 h later as described (Lee et al., 2016).

2.14.3 Heat stress

Heat stress was induced in synchronized young adult worms (2 plates, 50 worms/plate/strain) by incubating them at 37°C. Plates were checked each hour, and dead worms (not responding to physical stimulation and no pharyngeal pumping) were removed from the plate.

2.15 Biofilm formation

Synchronized *pqn-75 (tm6575)* and wild-type worms were plated on GFP-expressing *X. nematophila* ATCC19061-007-GFP bacteria. At 24 and 48 h, worms were resuspended for five minutes 1× Egg Buffer (118 mM NaCl, 448 mM KCl, 2 mM CaCl₂, 2 mM MgCl₂, 25 mM HEPES) with 1 mM levamisole, mounted on an agar slide, and imaged on a Leica DMI6000B. Green bacteria were counted in the pharyngeal lumen (n=30worms/strain) for each strain at each time point.

2. CHAPTER III: CHARACTERIZATION OF THE GERMLINE DISPENSABLE PQN-

75

The contents of this chapter are adapted from Rochester et al., *Biology Open*, doi: 10.1242/bio.027987, Published 2 August 2017.

Author contributions:

Paige C. Tanner, Catherine S. Sharp, and Karolina M. Andralojc performed strain creation and validation—primary analysis and investigation performed by Jesse D. Rochester. Writing, review, and editing by Jesse Rochester and Dustin L. Updike. Supervision, administration, and funding from Dustin L. Updike.

3.1 Chapter summary

In *Caenorhabditis elegans*, five pharyngeal gland cells reside in the terminal bulb of the pharynx and extend anterior processes to five contact points in the pharyngeal lumen. Pharyngeal gland cells secrete mucin-like proteins thought to facilitate digestion, hatching, molting, and assembly of the surface coat of the cuticle, but supporting evidence has been sparse. Here we show pharyngeal gland cell expression of PQN-75, a unique protein containing an N-terminal signal peptide, nucleoporin (Nup)-like phenylalanine/glycine (FG) repeats, and an extensive polyproline repeat domain with similarities to human basic salivary proline-rich pre-protein PRB2. Imaging of C-terminal tagged PQN-75 shows localization throughout pharyngeal gland cell processes but not the pharyngeal lumen; instead, aggregates of PQN-75 are occasionally found throughout the pharynx, suggesting secretion from pharyngeal gland cells into the surrounding pharyngeal muscle. PQN-75 does not affect fertility and brood size in *C.*

elegans but confers some degree of stress resistance and thermotolerance through unknown mechanisms.

3.2 Introduction

Proteins with repeating phenylalanine/glycine (FG) units are known to create intrinsically disordered domains. The NPC is an example of this, where FG-nucleoporin (Nups) act as the permeability barrier facilitating transport between the nucleus and cytoplasm (reviewed in Beck & Hurt, 2017). In *C. elegans*, FG-repeat domains are also present in the P-granule proteins GLH-1, GLH-2, GLH-4, DDX-19, and RDE-12, extending the permeability barrier of NPCs into the cytoplasm of germ cells (Sheth et al., 2010b; Updike et al., 2011). The loss of P granules in the adult germline of *C. elegans* results in sterility and germ cell reprogramming, suggesting that P granules play a role in maintaining pluripotency (Campbell & Updike, 2015; A. K. Knutson et al., 2017b; Updike et al., 2014).

Apart from FG-Nups and the five P-granule FG-repeat proteins mentioned earlier, FG-repeats are also present in EGO-2, a regulator of GLP-1/Notch signaling in the germline, and in two undescribed proteins, K01A6.4 and PQN-75. EGO-2, K01A6.4, and PQN-75 are unique because their FG-repeats are glutamine/asparagine (Q/N)-rich; however, it was not known if these three proteins function in or associate with germline NPCs or P granules.

In this study, we used EMS mutagenesis to identify germline proteins influencing germ granule function. During this screen an allele of PQN-75 was isolated from an EMS mutagenesis screen, prompting an investigation into its potential role in regulating P-granule homeostasis. Interestingly, PQN-75 was found to be expressed in pharyngeal gland cells and was dispensable

for germline development. Secretions from the pharyngeal gland cell process have been observed just before hatching, suggesting they aid cuticle digestion (Singh & Sulston, 1978). Pharyngeal gland cell specification requires the transcription factor HLH-6, and worms without HLH-6 or pharyngeal gland cells exhibit delayed growth and partially penetrant larval arrest (Smit et al., 2008b).

HLH-6 is related to the mammalian salivary gland transcription factor Sng1; both mammalian salivary glands and gland cells in *C. elegans* secrete mucin-like proteins to aid in digestion, suggesting that these glands are evolutionarily related (Smit et al., 2008b). This study describes similarities between PQN-75 and the human basic salivary proline-rich pre-protein PRB2, further strengthening this evolutionary relationship. The function of PQN-75 within pharyngeal gland cells was explored by quantifying growth, larval development, and strain health in a *pqn-75* deletion strain, revealing subtle defects that potentially reflect a vestigial role of pharyngeal gland cells under laboratory growth conditions.

3.3 Results

In a search for effectors of P-granule assembly and distribution, (Andralojc et al., 2017) conducted an EMS mutagenesis screen which produced multiple mutant alleles of the Argonaute protein CSR-1 causing defects to P granule morphology. One of these identified alleles, *csr-1* (*sam18*), was found to have a linked Gly to Asp mutation in *pqn-75* (Figure 12A). It is worth noting that EMS mutagenesis typically generates over 300 variants per strain, with around 50 of them altering or disrupting gene function (Flibotte et al., 2010), making linked mutations a common occurrence following outcrossing. The discovery of the *pqn-75* mutation is intriguing due to its possession of domains found in several essential P-granule proteins. As a

factor binding sites for pharyngeal gland cell expression. (B) Location of the signal peptide, FG/QN and polyproline repeats in the PQN-75b sequence. A hydrophobicity plot (taller bars are more hydrophobic) demonstrates the regularity of FG (dark green) and QN (light green) and proline residues (dark blue) in PQN-75b. (C,D) Similarity of extended polyproline repeats in human PRB2 and FNM2 protein sequences.

PQN-75 includes a unique combination of protein motifs:

PQN-75 is an unusual protein. As its name suggests, the N-terminal half of PQN-75 contains a Q/N-rich 'prion' domain (Figure 12A,B) (Michelitsch & Weissman, 2000). What distinguishes the Q/N-rich region of PQN-75 is that these polar residues are separated approximately every ten amino acids by a hydrophobic phenylalanine (F) flanked by glycine (G), generating cycles of regular hydrophobicity within this FG/QN repeat domain (Figure 12B, green). In addition to the FG domain of PQN-75, three of its isoforms contain an N-terminal signal peptide (Figure 12A,B, pink) with a predicted cleavage site (Figure 12A,B, red diamond), suggesting that PQN-75 is a secreted protein. The C-terminal half is also unique in that it is proline-rich (i.e. 35% of the amino acids in the C-terminal half are prolines), primarily consisting of GSPP repeats (Figure 12A,B, blue). While high proline content is indicative of a collagen-related structural protein, PQN-75 lacks cysteine residues important for cross-linking elongated collagen fibrils.

Clear PQN-75 orthologs exist in other *Caenorhabditis* species (*Caenorhabditis remanei*, *Caenorhabditis brenneri*, *Caenorhabditis briggsae*, and to a lesser extent in (*Caenorhabditis japonica*) that contain the signal peptide, FG-repeat, and polyproline domains, but orthologs carrying all three of these domains are not apparent in the diplogastrid nematode *Pristionchus*

pacificus or beyond. Wormbase (*WormBase : Nematode Information Resource*, n.d.) lists the closest human homolog of PQN-75 as the human basic salivary proline-rich pre-protein PRB2 (e-value: 1.2e-45; % length: 54%). This secreted pre-protein has a signal peptide but lacks FG-repeats, and its function in the saliva is unknown (Figure 12C). Another protein similar to PQN-75 that has both an N-terminal Q/N domain and a sizable C-terminal proline-rich repeat is human Formin-2 (e-value: 3.7e-31), a perinuclear actin-nucleating protein that confers nuclear integrity during cell migration (Skau et al., 2016). Unlike Formin-2 and the six Formin proteins in *C. elegans* (CYK-1, DAAM-1, FRL-1, FHOD-1, EXC-6, and INFT-2) (Mi-Mi et al., 2012), PQN-75 contains only the proline-rich Formin Homology domain one (FH1), but not FH2 or FH3 domains (Figure 12D), making it unlikely that PQN-75 functions as a Formin.

PQN-75 is dispensable for germline development:

To determine the role of PQN-75 in the germline and whether the EMS-generated *pqn-75* allele affects P-granule size and distribution independent of *csr-1(sam18)*, these two linked mutations needed to be separated. This was done using CRISPR/Cas9 to recreate the single base pair mutation in *pqn-75* and included silent mutations to prevent Cas9 recleavage (Figure 12A); this new allele, *pqn-75(sam20)*, was crossed into a P-granule reporter (PGL-1::GFP). P granules in *pqn-75(sam20)* appeared indistinguishable from wild-type worms, suggesting the original EMS-generated mutation was collateral and had no bearing on the P-granule phenotype of *csr-1(sam18)* (Figure 13A). Sperm counts were compared in the predicted *pqn-75* null allele *tm6575* (see Figure 12A, red bar). No appreciable difference was found (Figure 13B). Brood sizes in the *pqn-75* mutant and with *pqn-75(RNAi)* were just as high as controls (Figure 13C), suggesting PQN-75 does not impact fertility and plays little or no role in the germline.

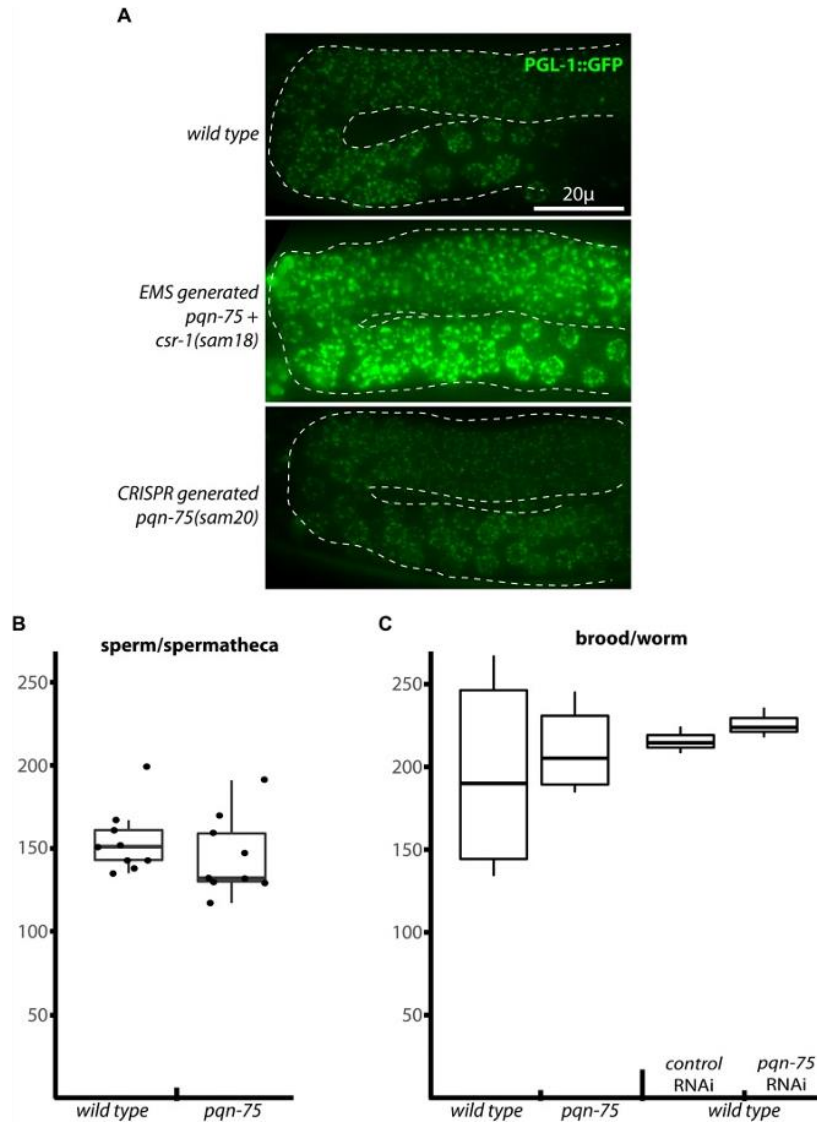


Figure 13: Germline phenotypes of *pqn-75*

(A) An EMS-generated Gly to Asp missense mutation in *pqn-75* does not contribute to the enlarged P-granule expression phenotype of *csr-1(sam18)* worms. Representative images show P granules surrounding germ cell nuclei navigating the bend in the gonad arm during the fourth larval stage. (B) DAPI-stained sperm nuclei/spermatheca in wild type and *pqn-75(tm6575)* mutants. (C) Brood size in wild type and *pqn-75(tm6575)* mutants, and in wild-type worms fed

empty vector control or pqn-75 RNAi. Box and whisker plots indicate the median, 1st and 3rd quartiles, and the minimum and maximum data points (excluding outliers - circles).

PQN-75 is expressed in pharyngeal gland cells:

Several FG-repeat containing proteins (e.g. GLH-1, GLH-2, GLH-4, DDX-19, and RDE-12) are enriched in germline P granules (Gruidl et al., 1996; Sheth et al., 2010a) however, expression profiling suggests that PQN-75 may not share this subcellular localization as its transcripts are minimally expressed in dissected germlines (0.3 FPKM; 12,155th of 20,259 genes ranked by germline expression) (Campbell & Updike, 2015). Lines carrying fluorescent pqn-75 reporters are available, showing expression in the terminal bulb of the pharynx but not the germline (Mounsey et al., 2002). Since the germline frequently silences repetitive reporters, CRISPR was used to tag pqn-75 with GFP::3xFLAG so endogenous gene expression in the germline could be examined. Again, an extremely faint expression was only observed in the posterior pharynx. To amplify the PQN-75::GFP::3xFLAG signal, worms were fixed and stained green with M2 anti-flag and a blue DAPI/DNA costain. Still, there was no evidence of germline expression (Figure 14A). PQN-75 staining was exclusively in the pharynx, starting in the threefold stage of embryogenesis (arrow), becoming progressively more pronounced through larval development. Within the pharynx, PQN-75 was most abundant in the pharyngeal gland cells and could be observed in gland-cell processes that extend along the pharyngeal lumen (Figure 14A, arrowheads). Poly Q/N and FG repeats have the propensity to promote self-assembly and aggregation in a number of proteins; similarly, punctate PQN-75 aggregates are found in the processes and pharyngeal gland cell bodies.

Pharyngeal gland cell function is heavily inferred from cell shape, position, and gene expression. It is thought that pharyngeal gland cell secretions lubricate the pharyngeal lumen and aid in molting or formation of the surface coat on the anterior cuticle (reviewed in Pilon, 2014). While worms are still viable following genetic ablation of gland cells, they exhibit delayed growth, development, and partially penetrant larval arrest (Smit et al., 2008b). Interestingly, PQN-75 staining was not detected within the pharyngeal lumen, buccal cavity, or on the anterior cuticle. Instead, 77% (n=200) of larval-staged worms had varying amounts of PQN-75 aggregates throughout the pharynx, suggesting that gland cells secrete PQN-75 into the surrounding pharyngeal muscle (Fig. 3A, red arrows). This is in contrast to the recently described *abu/pqn* paralog group (APPG) genes that encode poly Q/N proteins in pharyngeal muscle, which are excreted to form the anterior cuticle (George-Raizen et al., 2014). PQN-75 also differs from mucin-like PHAT-5, which is secreted from pharyngeal gland cells to line the pharyngeal lumen (Smit et al., 2008b).

Pharyngeal gland cell expression is enacted through combinatorial signaling of the sequence-specific transcription factors PHA-4 and HLH-6 (Gaudet & Mango, 2002; Raharjo & Gaudet, 2007). Correspondingly a short 22 base pair sequence at the beginning of the PQN-75 coding region contains two tandem PHA-4 consensus binding sites (TRTTKRY) and an HLH-6 consensus binding site palindrome (AACANNTGTT) that may promote gland cell expression of PQN-75 (Figure 12A). To determine if PQN-75 is required to drive pharyngeal gland cell specification or morphology, *hlh-6::YFP* arrays were introduced in wild type and *pqn-75(tm6975)* mutants to light up pharyngeal gland cells and their processes (Figure 14B). All five pharyngeal gland cells were present in wild type and *pqn-75* mutants, and no differences in cell

morphology or process extension could be distinguished between the two strains throughout larval development and in adults (>30 worms imaged for each strain). This suggests that PQN-75 is not required for gland cell survival or morphology.

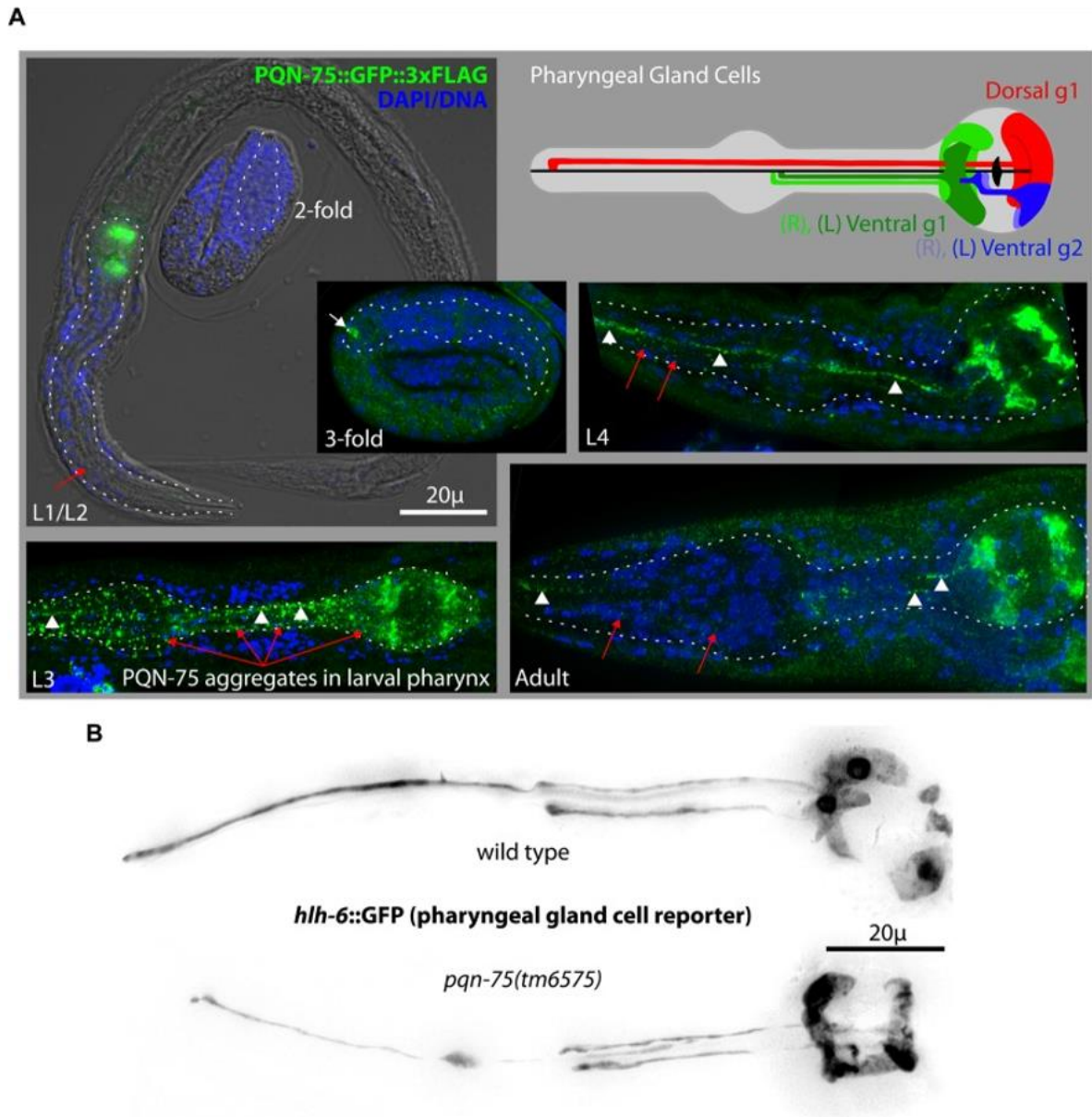


Figure 14: PQN-75 expression

(A) Cartoon (adapted from <http://wormatlas.org/>) shows the five pharyngeal gland cells extending processes into the anterior (red), mid (green), and posterior (blue) pharyngeal lumen (black). In fixed worms, anti-FLAG staining of PQN-75 (green) first appears in the threefold stage of embryogenesis (arrow) and PQN-75 aggregates persist in the pharyngeal gland cells and their processes (arrowheads) through larval stages and in the adult, and are frequently found

throughout pharyngeal muscle (red arrows). Dotted lines outline the pharynx of each worm. (B) Images of *hlh-6::GFP* expression in wild-type and *pqn-75(tm6575)* animals.

Pharyngeal gland cell expression may implicate a role for PQN-75 in feeding, digestion, or molting, all of which should be reflected in the growth rate. To test this, *pqn-75(tm6575)* and wild-type L1 worms were synchronized, and growth and time to sexual maturity were compared. Worm length was measured in approximately 30 worms every hour for 52 h using automated worm-tracking software. However, no difference could be observed between the two strains (Figure 15A). Sexual maturity was measured by the time to reach the young adult stage as marked by vulval maturation. While *pqn-75* mutants were delayed 1.5 h ($P < 1 \times 10^{-6}$), worms carrying *pqn-75* fosmid arrays did not rescue this delay in the mutant, suggesting this minor delay could be attributed to possible background mutations (Figure 15B). Obvious molting phenotypes were not apparent in *pqn-75(tm6575)*. To detect more subtle effects on growth and molting, the width of the grinder was measured as it grows in a salutatory fashion during each molt (George-Raizen et al., 2014). For each strain, grinder width was measured in 15 worms from synchronized cultures between 15 and 20 h to capture the window of the L1 to L2 molt (Figure 15C). Grinder width was comparable in wild type and *pqn-75(tm6575)* mutants, suggesting that PQN-75 has no significant or detectible role in molting.

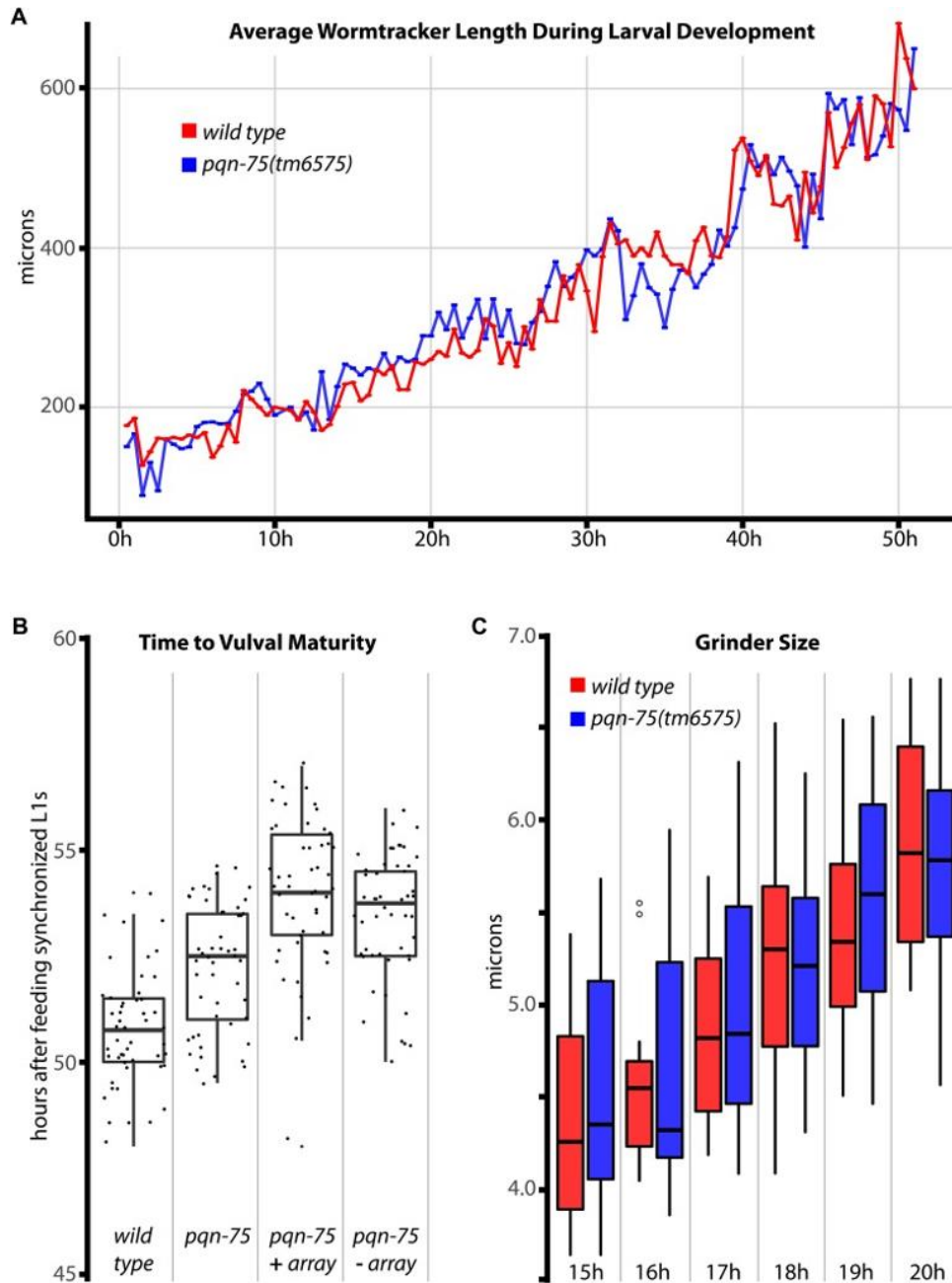


Figure 15: Larval development of *pqn-75*

(A) Wormlab software was used to capture the collective average length of wild-type and *pqn-75* worms ($n > 30$ worms/time point) every half hour for the first 51 h of larval development. (B) Time to vulval maturity in wild type, *pqn-75* mutants, *pqn-75* mutants rescued with a wild-type *pqn-75* array, and in the rescued worms after losing the array. (C) Grinder width of wild type

and pqn-75 mutants (n=20 worms/time point). Box and whisker plots indicate the median, 1st and 3rd quartiles, and the minimum and maximum data points (excluding outliers - circles). PQN-75 promotes thermotolerance, but minimally impacts innate immunity and proteotoxic stress:

Optimal conditions in the laboratory will often mask subtle defects caused by mutated genes. Proteins with Q/N prion-like domains, like those found in PQN-75, have a propensity to aggregate, which could burden cellular protein homeostasis machinery (Moronetti Mazzeo et al., 2012). To test whether PQN-75 impacts homeostasis, pqn-75 (tm6575) worms were challenged and their response to various forms of stress recorded. First, paraquat was used to induce oxidation/glutathione conjugation of proteins; no survival advantage or disadvantage was conferred after five hours of exposure by the presence of PQN-75 (Figure 15A). Second, osmotic stress was used to induce protein misfolding, and while there was a trend for survival rates of pqn-75 mutants to be lower after 24 h of growth in hyperosmotic environments, it was not significant (Figure 16B, $P > 0.05$). Third, protein misfolding was induced with heat stress. In this case, pqn-75(tm6575) viability decreased more rapidly than wild type when grown at 37°C (Figure 16C, $P < 0.001$, log rank). To test specificity, thermotolerance was observed in pqn-75 mutant worms carrying an array with wild-type pqn-75 sequence, which rescued survivability ($P < 0.001$). These results suggest that the presence of PQN-75's Q/N prion-like domains do not exacerbate proteotoxic stress; instead, the presence of PQN-75 confers some advantage when worms are stressed, primarily upon exposure to high temperatures.

Because the surface coat of the anterior cuticle provides innate immunity against pathogen biofilm and colonization, wild type and pqn-75 mutants were compared on plates

seeded with the bacteria *Xenorhabdus nematophila*. *X. nematophila* exists in a symbiotic relationship with soil nematodes that parasitize insects. When fed to *C. elegans*, it can produce a biofilm on the cuticle and the pharynx's lumen (Couillault & Ewbank, 2002). *X. nematophila* expressing green fluorescent protein (GFP) was fed to both wild-type and mutant worms. The number of bacteria in the pharyngeal lumen was quantified at 24 and 48 h (Figure 16D). The pharyngeal lumen of pqn-75 mutants was not more impacted than wild type; in fact, mutants had slightly fewer bacteria in the lumen at 24 h (6.2 bacteria in wild type versus 2.1 in pqn-75, $P < 1 \times 10^{-3}$) and 48 h (11.6 versus 7.9, $P = 0.35$), raising the possibility that PQN-75 negatively impacts innate immunity. This difference may be insubstantial, and the response to a larger panel of natural pathogens would be warranted before reaching a conclusion about PQN-75's role in innate immunity.

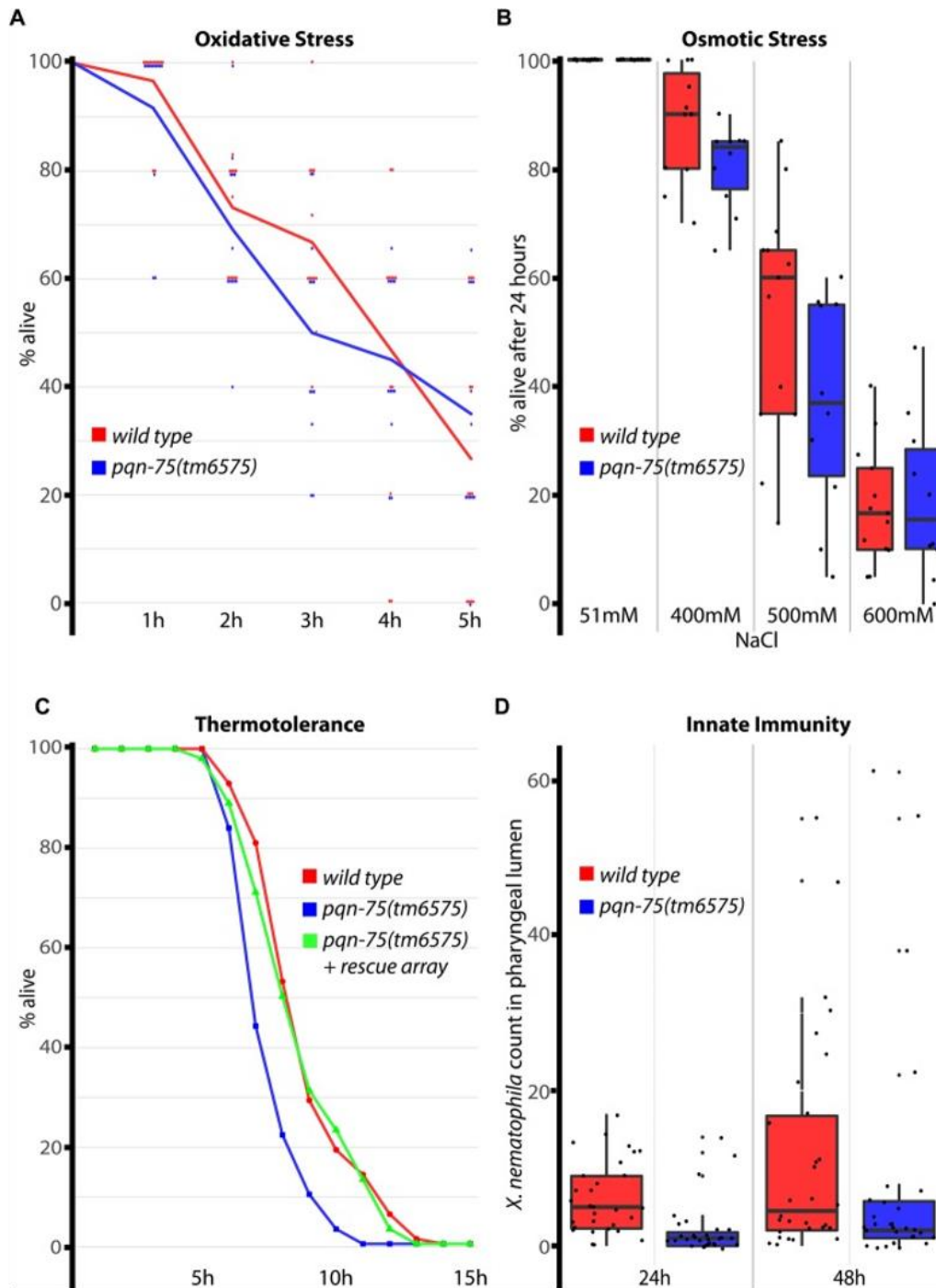


Figure 16: Proteotoxic stress and immunity in *pqn-75*.

(A) Oxidative stress was induced with Paraquat, and viability was monitored over a five-hour period. Data points are included for all 12 replicates of each strain. (B) Osmotic stress was induced by exposure to high salt, and viability was scored after 24 h. (C) Heat stress was

induced by growth at 37°C, and viability was monitored each hour for 15 h. (D) Innate immunity is measured by the accumulation of GFP-expressing *X. nematophila* in the pharyngeal lumen at 24 and 48 h. Box and whisker plots indicate the median, 1st and 3rd quartiles, and the minimum and maximum data points (excluding outliers).

3.4 Discussion

Unlike the majority of FG-repeat proteins, which associate with the nuclear pore complex or germline P granules, PQN-75 aggregates disperse throughout the cytosol of pharyngeal gland cells and appear to be secreted into surrounding pharyngeal muscle, although the function of PQN-75 aggregates in these cells remains unclear. We have demonstrated that PQN-75 does not affect brood size or growth rate, and minimally impacts osmotic stress and innate immunity. However, *pqn-75* mutants are more susceptible to heat stress, suggesting that PQN-75 protects the organism from acute temperature changes.

The surface coat of the anterior cuticle is thought to originate from pharyngeal gland cell secretions, and the mucin-like gland cell protein PHAT-5 associates with the cuticle when secreted (Smit et al., 2008b). While PQN-75 was not found on the cuticle or in the pharyngeal lumen, detection relied on a C-terminal GFP::3xFLAG tag on the endogenous gene and secretions would not be observed if the protein is subject to proteolysis, and there may be a precedence for this. The human salivary proline-rich-proteins (PRPs) are mammals' most conserved oral salivary proteins, representing 20-30% of proteins in saliva, but their function remains unknown (Manconi et al., 2016). Humans have six salivary PRPs that cluster on chromosome 12, and each undergoes proteolysis into much smaller peptides. PRB2 (Figure 12C) is one of these processed pre-proteins containing polyproline repeats like PQN-75. Both worm

PQN-75 and human PRB2 are expressed in gland cells of the upper digestive tract; therefore, one possibility is that PQN-75 also undergoes proteolysis, preventing the detection of N-terminal secretions in the lumen or cuticle with the C-terminal tag. If secreted to the lumen or cuticle, one could predict that PQN-75 promotes the digestion or prevents the pathogenesis of bacteria regularly encountered in its natural environment, or alternatively contributes to the structural integrity of the cuticle, making the worms less susceptible to fluctuations in temperature.

Investigations into the role of PRPs in mammals have shown they may help prevent caries. Evidence suggests they function as essential adhesion antigens, initiating an immunological response that can attach to bacteria such as *Streptococcus*, preventing plaque buildup on tooth enamel (Nobbs et al., 2011). Patients with type one or two diabetes have an increased risk of tooth decay (Ferizi et al., 2018; Novotna et al., 2015; Pachonski et al., 2020). Individuals with poorly regulated type one diabetes exhibit significant downregulation of PRPs, including PRB2 (fold change of ≈ -1.3) (Pappa et al., 2021), potentially increasing the risk of tooth decay by promoting pathological changes in tooth enamel (Cabras et al., 2010). If PQN-75 is secreted, it may similarly maintain the integrity of *C. elegans*' cuticle and/or grinder.

PQN-75, much like PRB2, is predominantly expressed in the upper digestive tract, indicating a potential role in the digestive process. The digestive system is a highly regulated microenvironment sensitive to pH alterations. *C. elegans*' natural habitat often contains tannins, an organic compound in various plants, such as fruits, trees, and leaves. Over time, hydrolysis can break down tannins, rendering them water-soluble. While tannins are generally weak acids, their potency varies significantly depending on the source, with many high-tannin

plants being unpalatable due to their bitter taste or anti-nutritive effects (Thakur et al., 2019). Recent studies on boars have demonstrated that the consumption of hydrolysable tannins, such as those in a controlled diet of 3% hydrolysable tannin-rich extract Farmatan[®], can result in parotid gland enlargement, along with significant increases in PRB2 (Mavri et al., 2022). This adaptation enables boars to avoid the anti-nutritive consequences of tannins. By secreting high amounts of proline-rich proteins, such as PRB2, in saliva, tannins can bind to these proteins, thereby preventing their interaction with other proteins in the digestive tract. It is plausible that the secretion of PQN-75 could serve a similar function for *C. elegans* in their natural environment (Schulenburg & Félix, 2017).

If the primary function of PQN-75 is within the gland cell itself, the propensity of PQN-75 to self-aggregate may be nucleating cytoskeletal structures. Polyproline helices are common in both globular and structural proteins and frequently serve as the interface between protein-protein interactions (Manconi et al., 2016). The long polyproline repeat (FH1 domain) of Formin-2 (12D) shares similarities with the polyproline domain of PQN-75. Formins use their FH1 domain to interface with profilin to nucleate actin polymerization (Schönichen & Geyer, 2010), and interestingly Formin-2 (FMN2) specifically nucleates actin filaments on the nucleus to maintain nuclear shape and integrity during cell migration (Skau et al., 2016). Three of the six formins expressed in *C. elegans* (EXC-6, INFT-2, and CYK-1) are expressed in the large excretory cell, which forms tubules along the worm's length and functions in osmoregulation (Shaye & Greenwald, 2016). In the excretory cell, these three formins polymerize actin to regulate tubulogenesis. Outside of the excretory cell, the formins CYK-1 and FHOD-1 associate with body-wall muscle sarcomere Z lines to promote muscle contractility (Mi-Mi et al., 2012).

Pharyngeal gland cells do not undergo tubulogenesis, but their long processes are like those of the excretory cell and may also require profilin-dependent actin nucleation during elongation. Alternatively, PQN-75 secreted into the surrounding pharyngeal muscle may stimulate muscle contractility. We used this reasoning to look for genetic interactions between *pqn-75* and the three profilins in *C. elegans* (*pfn-1*, *pfn-2*, and *pfn-3*) but did not find signs of enhanced lethality, sterility, or growth defects. PQN-75 appears not to affect pharyngeal gland cell process extension as viewed by the *hlh-6::YFP* reporter, so a clear role for this protein and actin polymerization in pharyngeal gland cells has yet to be determined.

Many genes with unknown functions (40% in *C. elegans*) are likely essential in natural settings (Petersen et al., 2015). *pqn-75* is one of these genes, and its growth under laboratory conditions may mask its functions, such as PQN-75's protective effect at higher temperatures. It is also worth noting that *pqn-75* expression increases in response to dietary restriction and pathogen exposure (Baugh et al., 2009; Engelmann et al., 2011; Heestand et al., 2013; Mueller et al., 2014; W. Yang et al., 2015, Jarod Rollins and Aric Rogers, personal communication), further suggesting a role for PQN-75 in feeding and innate immunity. Although our results with *X. nematophila* contradict this, PQN-75 could combat other bacteria present under natural conditions in the pharynx and potentially the digestive tract.

Another possibility is that PQN-75 plays a role in stress resistance through its excretion into the pharyngeal lumen, preventing the formation of small bacterial aggregations that could block the opening of the lumen or accumulate within it. Our observations revealed a noticeable increase in the presence of *X. nematophila* within the lumen of the wild-type (WT) worms, potentially indicating that the buildup of pathogenic bacteria around the buccal cavity might be

impeding feeding in the PQN-75 deletion lines resulting in dietary restriction. While additional assays are required to confirm this hypothesis, the findings would suggest that PQN-75 is in fact involved in dietary stress resistance through its interaction with bacterial aggregation dynamics and the regulation of feeding within the pharyngeal lumen. Once laboratory growth conditions better reflect the worm's natural diet and ecology, additional pqn-75 phenotypes will become apparent to clarify this gene's function.

3. CHAPTER IV: GLH-1 IS REQUIRED TO MAINTAIN GERMLINE FERTILITY

The contents of this chapter are adapted from Marnik et al., Genetics, doi:

10.1534/genetics.119.302670, Published 01 November 2019.

Author Contributions:

Elisabeth Marnik, Heath Fuqua, Emily Xu, Sarah Holbrook, and Catherine Sharp performed strain creation and validation. Jesse Rochester performed liquid cultures, fertility, and embryonic lethality assays. Elisabeth Marnik performed protein lysates, IP, and MS analyses. Graphs created by Elisabeth Marnik and Jesse Rochester. Writing, review, and editing by Elisabeth Marnik and Dustin L. Updike. Supervision, administration, and funding by Dustin L. Updike.

4.1 Chapter Summary

Vasa homologs, which are ATP-dependent DEAD-box helicases, multipotency factors, and critical components responsible for specifying and safeguarding the germline, have been found to regulate translation, amplify piwi-interacting RNAs (piRNAs), and act as RNA solvents. However, studying these factors has been complicated due to the limited availability of mutagenesis-derived alleles and their wide range of phenotypes. Fortunately, the development of clustered regularly interspaced short palindromic repeats (CRISPR/Cas9) has made it possible to overcome these limitations and explore why certain protein domains have been retained or lost throughout evolution. In this study, we utilized CRISPR/Cas9 to investigate the functional motifs of GLH-1/Vasa in *Caenorhabditis elegans* by analyzing 28 endogenous mutant alleles. Our results demonstrate that GLH-1's helicase activity is essential for its association with P granules. Even though changes were made outside of the helicase and flanking domains, GLH-1

remained in P granules, but fertility was still compromised. Furthermore, removing glycine-rich repeats from GLH proteins gradually diminished P-granule wetting-like interactions at the nuclear periphery. Mass spectrometry of GLH-1-associated proteins implies the conservation of a transient piRNA-amplifying complex and reveals a novel affinity between GLH-1 and three structurally conserved PCI (26S Proteasome Lid, COP9, and eIF3) complexes or “zomes,” along with a reciprocal aversion for assembled ribosomes and the 26S proteasome. These results suggest that P granules compartmentalize the cytoplasm to exclude large protein assemblies, effectively shielding associated transcripts from translation and associated proteins from turnover. Within germ granules, Vasa homologs may act as solvents, ensuring mRNA

4.2 Introduction

Germ cells and somatic cells from an individual carry identical copies of DNA, yet only germ cells have the potential to give rise to all the cell types of each subsequent generation. This suggests that epigenetic factors confer a germ cell’s totipotent and immortal potential. These epigenetic factors are not limited to chromatin modifications but also reside in the germ cell cytoplasm or germplasm. In some cases, germplasm alone has been sufficient to reprogram somatic nuclei to restore cellular potency and immortal potential (reviewed in Strome & Updike, 2015). Germplasm contains a heterogeneous mix of RNA and protein not expressed in differentiating somatic tissue. In some animals, these germ cell-specific ribonucleoproteins separate in the germ granules (reviewed in Marnik & Updike, 2019). Depletion of germ granules in *Caenorhabditis elegans* causes sterility and germ-to-soma transformation, suggesting that they contain the cytoplasmic components that preserve germ cell totipotency (A. K. Knutson et al., 2017b; Updike et al., 2014). A conserved protein consistently observed in the germplasm

and germ granules across species is collectively known as Vasa. Vasa and its homologs are required for germline specification and have been shown more recently to influence somatic multipotency during development, regeneration, and tumorigenesis (reviewed in Poon et al., 2016). Therefore, it is critical to understand Vasa's molecular function and complex role as a multipotency factor.

Vasa was cloned in *Drosophila* just over 30 years ago as a DEAD-box helicase with homology to the eukaryotic initiation factor-4A (eIF4A) (Hay et al., 1988; P. F. Lasko & Ashburner, 1988) and a binding partner to the translation initiation factor (eIF5B) (Carrera et al., 2000). These findings strongly suggested that Vasa and its homologs function to initiate and/or regulate translation in the germline, which was subsequently demonstrated by the eIF5B-dependent accumulation of Gurken and mei-P26 in *Drosophila* (Johnstone & Lasko, 2004; Liu et al., 2009). A more recent focus has been on Vasa's RNA-independent interactions with argonaute proteins through a transient amplifying complex that impacts ping-pong-mediated piwi-interacting RNA (piRNA) amplification (Dehghani & Lasko, 2016; Kuramochi-Miyagawa et al., 2010; Malone et al., 2009; Megosh et al., 2006; Wenda et al., 2017; Xiol et al., 2014). Other studies have demonstrated the ability of Vasa homologs (i.e., DDX4) to form phase-separated organelles in cell culture that melt nucleic acid duplexes and act as a solvent for single-stranded RNA (Nott et al., 2015, 2016). The roles of Vasa homologs in translational regulation, piRNA amplification, and as an mRNA solvent demonstrate the protein's diversity of functions within the germline (reviewed in P. Lasko, 2013).

Phenotypes of various mutant Vasa alleles in *Drosophila* reflect this diversity of function. Strong alleles exhibit recessive female sterility in homozygotes due to defective oocyte

development. Moderate Vasa alleles produce oocytes, but after fertilization, the resulting embryos arrest with posterior patterning defects and no germ cells. Mutants rescued with a Vasa transgene carrying weak alleles permit some embryos to hatch and develop into adults that exhibit a range of fertility defects (Dehghani & Lasko, 2016). Vasa phenotypes are also diverse across organisms. For example, Vasa mutations in *Drosophila* cause female-specific sterility, whereas Vasa homolog DDX4 cause male-specific sterility in mice (Wenda et al., 2017). Furthermore, while Vasa is conserved across metazoans, some animals, such as *C. elegans*, amplify piRNA silencing through RNA-dependent RNA polymerases (RdRPs) instead of the ping-pong method used by insects and mammals that lack RdRPs. Because of these differences, a comparative analysis of Vasa in different organisms is needed to determine conserved and divergent germline maintenance and specification functions.

The comparison of Vasa function in model organisms has traditionally been limited by available mutants, making it difficult or impossible to gain insight into structural motifs from available alleles exhibiting a wide range of phenotypes. This was especially true in *C. elegans*, where the function of one of its Vasa homologs, GLH-1, could only be inferred from a small handful of alleles that still made truncated proteins (Spike et al., 2008b). However, with the advent of CRISPR technology, it has become possible to modify endogenous genes to replicate informative alleles in conserved residues. Using this approach, over two dozen site-directed mutant alleles of *glh-1* were created in a strain where the endogenous gene carried a C-terminal GFP::3xFLAG fusion. Each modification was then examined to determine its influence on fertility and embryonic viability in the context of its effect on GLH-1 expression and distribution in the embryonic and adult germline. These results emphasize the role of GLH-1's

helicase activity in maintaining P granule association and provide insight into the functional domains that distinguish Vasa proteins from the dozens of other DEAD-box helicases encoded in the *C. elegans* genome.

Vasa protein interactions may be very transient, making them difficult to detect. Previous DEAD-box helicase studies have utilized mutations within the DEAD motif that are thought to either inhibit substrate binding or lock in bound substrates, with the idea of capturing different interaction partners at distinctive, and often transient, enzymatic steps (Cruciat et al., 2013; Pause & Sonenberg, 1992; Xiol et al., 2014; H. Yang et al., 2014). In this report, immunoprecipitation (IP) liquid chromatography (LC)-mass spectrometry (MS)/MS was used to identify proteins with increased GLH-1 association and examine what happens to those associations in the substrate-inhibited or locked states. These results suggest that GLH-1 associates with evolutionarily conserved PCI (26S Proteasome Lid, COP9 signalosome, and eIF3) scaffolding complexes or zones to regulate protein translation and degradation. In the locked state, GLH-1 shows an increased affinity for a handful of Argonaute proteins, suggesting that a form of the transient amplifying complex is conserved but that GLH-1 is not limited to piRNA amplification. This comparative approach represents a significant advance toward understanding how GLH-1/Vasa functions as a multipotency factor within and outside of the germline.

4.3 Results

GLH-1 is just one of several dozen proteins enriched in germ granules—also known as P granules—in *C. elegans*; like Vasa, it is part of a germ granule protein core that is conserved across multicellular animals. GLH-1 is a constitutive P-granule protein that is associated with P

granules at all stages of adult and embryonic development (Figure 1A). Other core germ granule proteins include Tudor domains and Argonaute proteins that bind small RNAs (Figure 1B). The function of this protein core in germ granules is intriguing and elusive. However, studies across systems have demonstrated a role for this core in regulating protein expression and small RNA biogenesis in ways that ensure germ cell integrity. GLH-1 has three close paralogs (GLH-2, GLH-3, and GLH-4), but only GLH-1 and GLH-2 contain all the domains that define Vasa proteins. Vasa-defining domains include a glycine-rich repeat domain, a flanking domain that wraps between N- and C-terminal DEAD-box helicase domains, and a negatively charged domain that precedes a terminal tryptophan (Figure 1C and Figure S1, A and B). A conserved zinc-knuckle domain can be found in most Vasa homologs but has been lost several times throughout evolution (Gustafson & Wessel, 2010) (Figure S1C). GLH-1 mutations, including nulls, are fertile at the permissive temperature of 20° but are sterile at 26° (Kuznicki et al., 2000a). This temperature-sensitive (ts)-sterile phenotype stems from redundancy with other GLHs, as both *glh-2 glh-1* and *glh-1; glh-4* double mutants are sterile at permissive temperatures, and exhibit a severe reduction or no germ cells, and little to no sperm (Spike et al., 2008b). The *C. elegans* genome encodes ~50 DEAD-box helicases. Of these, the GLHs, RDE-12, VBH-1, LAF-1, DDX-19, and DDX-17 have glycine-rich repeats and (except for DDX-17) have previously been shown to associate with P granules (Gruidl et al., 1996; Hubert & Anderson, 2009; Sheth et al., 2010b; Shirayama et al., 2014); however, outside GLH-1 and GLH-2, none contain an entire repertoire of Vasa domains (Figure 1C).

The structure of *Drosophila*'s Vasa-flanking and helicase domains have been determined, showing that the N- (blue) and C-terminal (green) RecA-like DEAD-box domains

interact upon RNA and ATP binding (Figure 17D, Sengoku et al. 2006). ATP hydrolysis is coupled with RNA helicase activity, destabilizing RNA duplexes in a nonprocessive manner. The flanking domain (red) wraps around the side when the helicase domains are in the closed conformation. Because of the high conservation between Vasa in *Drosophila* and GLH-1 in *C. elegans* (Figure 1E), iTasser was used to model the structure of GLH-1 based on Vasa (Figure 17D, third image overlay). Except for a GLH-specific loop (white), the predicted structure was nearly identical. From this, several key residues and their relation to ATP- and RNA-binding sites and helicase interphases can be identified (Figure 17D, fourth image).

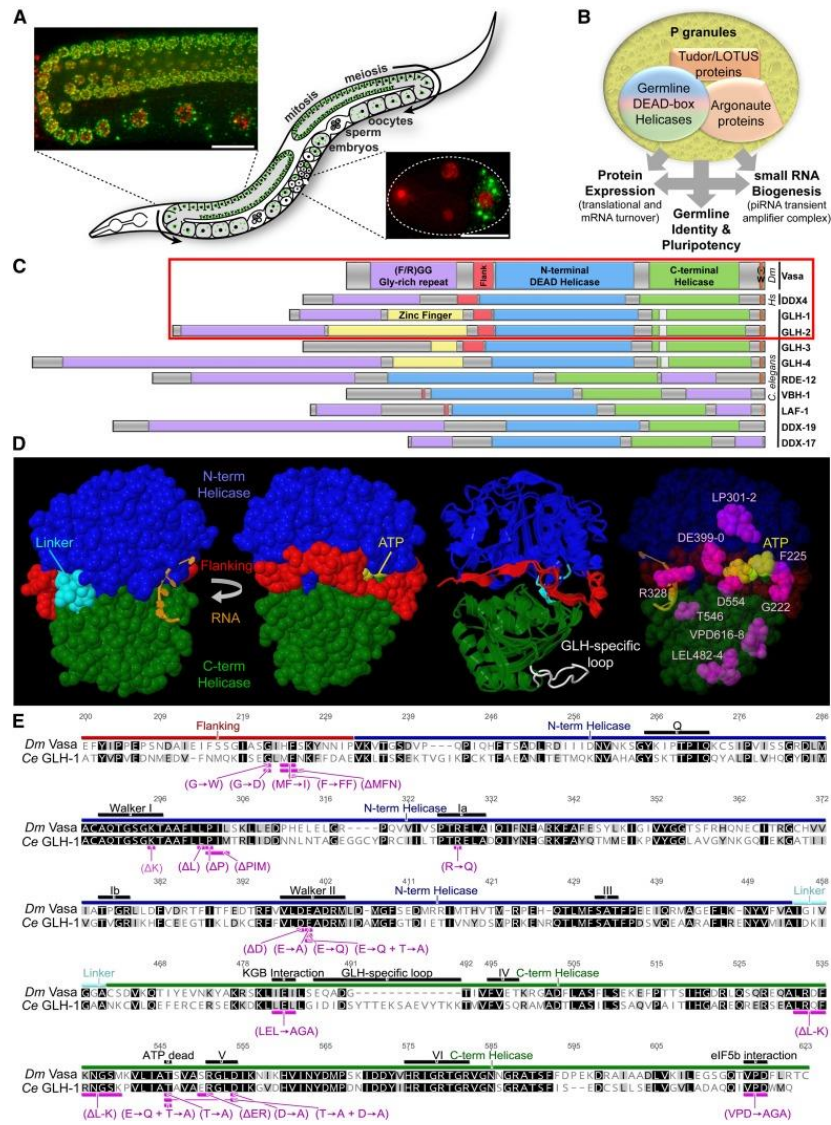


Figure 17: GLH proteins in the *C. elegans* germline.

(A) GLH-1::GFP::3xFLAG in P granules and mCherry:His2B-marked chromatin. Inserts provide context for expression in the germline loop and four-cell embryo. (B) Schematic depicting the function of core proteins in P granules. (C) Conservation of Vasa/DDX4-like DEAD-box helicases in *C. elegans*. A red box surrounds proteins that contain all four Vasa-defining domains (glycine-rich in purple, flanking in red, N- and C-terminal helicase in blue and green, and negatively charged residues before a terminal tryptophan in orange). The GLH-specific loop is shown in

white. (D) Crystal structure of Vasa showing front and back views of the flanking and helicase domains, in relation to ATP- and RNA-binding pockets (as determined by Sengoku et al., 2006). Image 3 is an overlay of Vasa (ribbon) with an iTasser-predicted model of GLH-1 (backbone) that shows the location of the GLH-specific loop (white). Image 4 shows key amino acid residues targeted in this study and their location within the Vasa protein structure. (E) Sequence alignment of the flanking and helicase domains in *Drosophila* Vasa with *C. elegans* GLH-1. Protein domains and mutations are indicated (purple). The K295A mutation was not obtained. The Δ ER550-1 was not sustainable. See also Figure 30. Ce, *C. elegans*; ; Dm, *Drosophila melanogaster*; Hs, *Homo sapiens*; piRNA, piwi-interacting RNA.

New alleles of *glh-1* were initially obtained from an EMS mutagenesis screen for P-granule phenotypes. Unlike previous screens that utilized transgenes expressed from an array, this screen was performed in a strain where endogenous GLH-1 was tagged with GFP::3xFLAG, allowing for the recovery of intragenic mutations. While most *glh-1* alleles from the screen reduced GFP expression, one allele dispersed GLH-1::GFP throughout the cytoplasm and resembled GLH-1 staining patterns previously associated with original *glh-1* alleles (Spike et al., 2008b). Sequencing *glh-1* revealed a Gly to Asp (G→D) change (Vasa position 222) caused by a single-base pair mutation within the flanking domain, suggesting that flanking domain function is required for GLH-1's association with P granules (Figure 18A). Until now, the function of Vasa's flanking domain was unknown because alleles within this domain did not previously exist. CRISPR was used to generate four additional alleles with mutations in the flanking domain, and all recapitulated the GLH-1::GFP dispersal phenotype (Figure 31 and Table 2). GLH-1-granule dispersal and expression intensity was quantified in 10 gonad arms under fixed

exposure conditions, as was the impact on embryonic lethality and fertility at permissive and restrictive temperatures (Figure 19 and Figure 31). At both permissive and restrictive temperatures, the parental GLH-1::GFP::3xFLAG fusion is fully wild-type, with perinuclear GLH-1 granules and no defects in fertility. For comparison, a complete *glh-1* deletion (Δ *glh-1*) that expresses only GFP::3xFLAG and a *glh-1* transcriptional reporter (GFP::3xFLAG separated from *glh-1* with an intercistronic rSL2 spacer, *glh-1* Txn GFP, Figure 18A) were generated from the parental strain. Interestingly, GFP expression in the deletion is almost three times as bright, suggesting that GLH-1 protein negatively autoregulates its own expression. Fertility defects at the restrictive

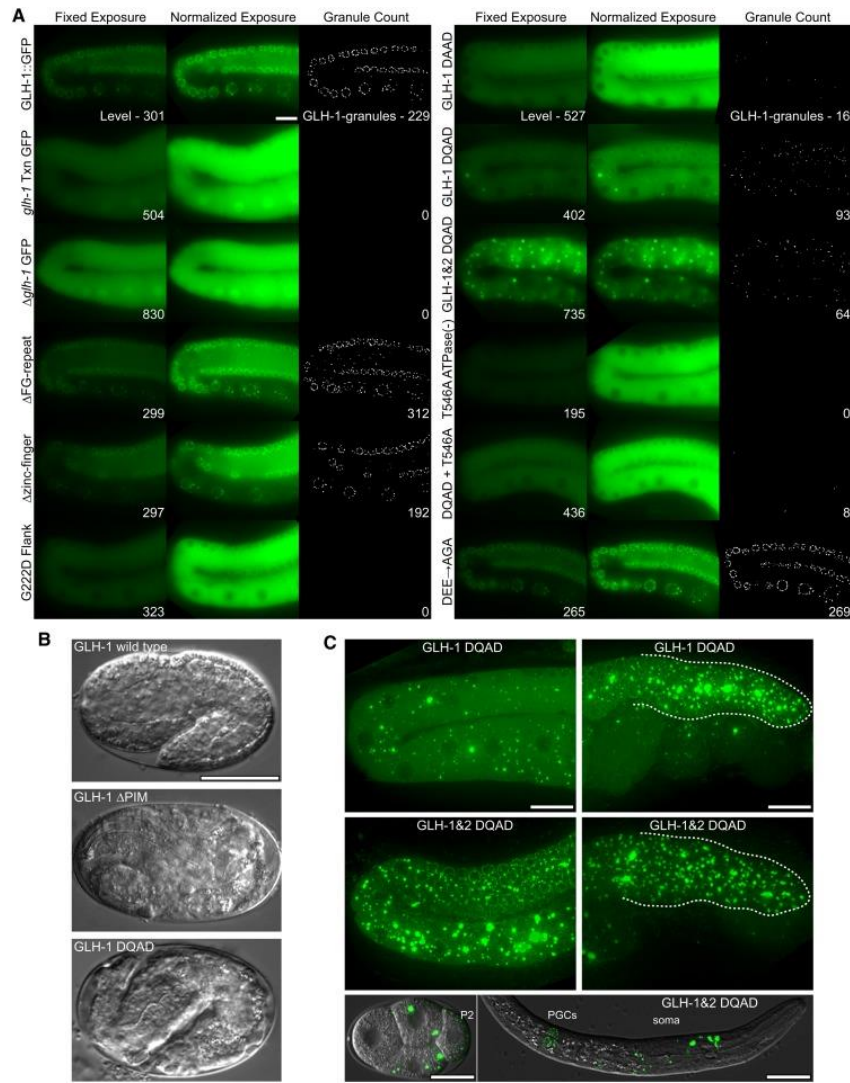


Figure 18: Level and distribution of mutant forms of GLH-1 in *C. elegans*.

(A) GLH-1::GFP::3xFLAG expression in the germline loop. Fixed exposures (left) were normalized (middle) to better view the distribution of fluorescence. GLH-1 granules were quantified using ImageJ (right). In Δ PIM and DQAD mutants, embryos arrest in the elongation phase. (C) GLH-1(DQAD)::GFP::3xFLAG accumulation in proximal (left) and distal (right) germlines is enhanced in GLH-2(DQAD). In double mutants, GLH-1(DQAD) aggregates persist in somatic blastomeres and the soma of hatched worms (bottom). Quantification was performed on images from 10 worms for each strain (see Figure 31). PGC, primordial germ cell.

temperature for flanking-domain mutations are comparable to the *glh-1* deletion, showing that these flanking-domain mutations reflect the phenotype of null alleles. To see if compromising GLH-1 helicase activity also caused its dispersal, 12 additional strains were created that replicated canonical *Drosophila* alleles of Vasa in endogenous GLH-1::GFP::3xFLAG or introduced changes in key conserved residues (Figure 1E) (Dehghani & Lasko, 2015, 2016; Sengoku et al., 2006). Attempts to generate a K→A mutation in the Walker I motif (Vasa position 295) to knock out helicase activity was unsuccessful but yielded three mutations (ΔL , ΔP , and ΔPIM) immediately to the right of the Walker I motif that all had the dispersed GLH-1::GFP phenotype (Figure 19 and Figure 31). Subsequently, a T→A mutation was generated just before motif V (Vasa position 546) that had previously been shown to abolish the ATPase activity of Vasa in vitro (Sengoku et al., 2006), and this allele dispersed GLH-1 and caused fertility defects at the restrictive temperature (Figure 18A and Figure 19). The DEAD-box in motif II is also essential for ATP hydrolysis (Pause & Sonenberg, 1992) so a deletion of the aspartic acid (D) residue from the DEAD-box ($_EAD$) was generated (Vasa position 399), as was an E to A (DAAD) substitution (Vasa position 400), both of which dispersed GLH-1 with ts-fertility defects (Figure 18A and Figure 19). When the $_EAD$ deletion and the DAAD substitution were put into both *glh-1* and *glh-2* to create double mutants, they resulted in fertility defects at both permissive and restrictive temperatures (Figure 19). At least some of these 17 mutations in the flanking and helicase domains affected the activities of adjacent domains. However, since most were point mutations, it would be unlikely for them all to have a structural impact. So, when taken together, these results suggest that (1) helicase activity is required for fertility, (2) GLH-1 associates with germ granules by its helicase activity and not through its structural

motifs, (3) that the flanking domain is integral to the helicase activity, and that (4) helicase activity is not required for GLH-1 to negatively autoregulate its expression.

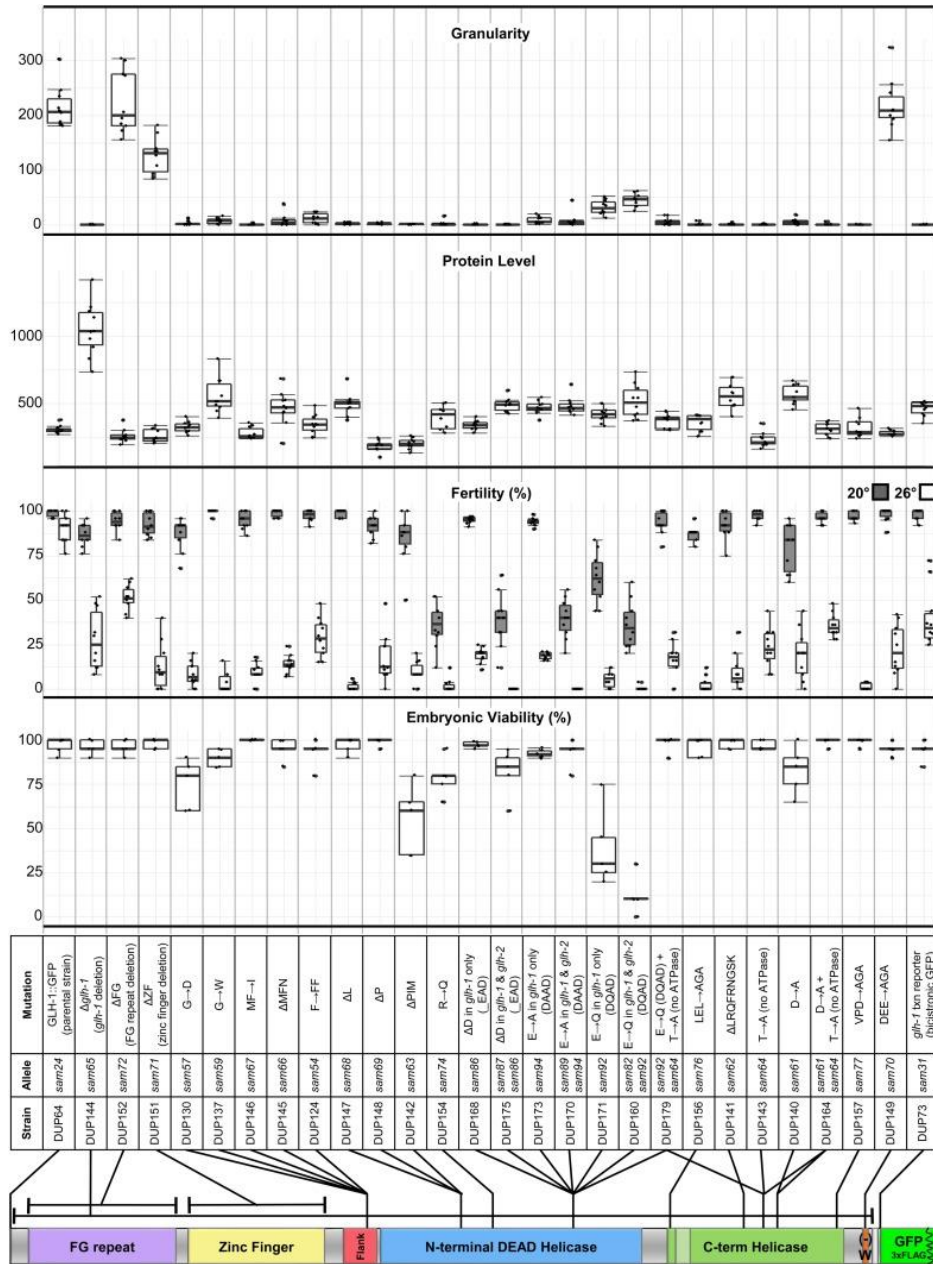


Figure 19: Consequences of GLH-1 mutant alleles.

From top to bottom: comparison of granularity (GLH-1 granules), GLH-1 protein level, fertility at permissive (20°) and restrictive (26°) temperatures, and embryonic viability in GLH-1 mutants.

Mutation details, strains, and allele names and their respective locations are indicated.

Replicates for each of the four assays are provided in the Materials and Methods. Box plots

represent quartiles above and below the median with whiskers extending 1 SD from the mean. See also Figure 31. C-term, C-terminal.

Vasa was identified as a component of a transient Amplifier complex that mediates piRNA amplification in the ping-pong loop (Wenda et al., 2017; Xiol et al., 2014). This association between Vasa and Argonaute proteins that mediates ping-pong amplification was detected using a Vasa DQAD mutation (position 400), which is thought to prevent the release of ATP hydrolysis products, facilitating the accumulation of larger Vasa-containing aggregates. While *C. elegans* use a ping-pong-independent method to amplify piRNA-mediated silencing, we sought to determine whether Argonaute proteins could be detected when DQAD substitutions were introduced into GLH-1, or both GLH-1 and GLH-2 (Figure 18A). Unlike EAD and DAAD, the DQAD substitution is more severe than the *glh-1* deletion, meaning that worms are less fertile at 20°, and most embryos arrest during elongation (Figure 18B and Figure 19). Also, instead of completely dispersed in the cytoplasm like EAD and DAAD, DQAD causes some GLH-1 to accumulate in large cytoplasmic aggregates, primarily in the shared cytoplasm of the distal germline (Figure 18C). Embryonic lethality and large aggregate formation of GLH-1(DQAD) become more pronounced when the DQAD substitution is also introduced into GLH-2. In the double GLH-1(DQAD) GLH-2(DQAD) mutant, large GLH-1::GFP(DQAD) aggregates are no longer cleared from somatic blastomeres, and some persist in various somatic cells during larval development (Figure 18C). These double mutants can be passaged for only a couple of generations and must be maintained over a balancer.

It should be noted that while these large aggregates have been ascribed as a specific transient state, their observation in DQAD, but not in EAD or DAAD, introduces the possibility

that DQAD creates a neomorphic allele prone to unspecific germline aggregate formation. The impact of the DQAD mutant has not been thoroughly characterized in vivo, and existing data from in vitro experiments are not enough to understand why $_EAD$ and DAAD disperses GLH-1 or Vasa, while DQAD causes them to aggregate. A prevailing and speculative assumption is that mutations like $_EAD$ and DAAD inhibit the binding of ATP and RNA substrates, while in DQAD these substrates are bound but not released. Further biochemical characterization of these mutations will be needed to confirm whether this is the case.

GLH-1 has been positioned upstream of PGL proteins in the embryonic P-granule assembly pathway, but in adult germlines the association is more mutualistic (Hanazawa et al., 2011; Kawasaki et al., 2004; Kuznicki et al., 2000a; Updike et al., 2011). Both PGL-1 and GLH-1 colocalize at all stages of development in wild-type animals, except for a brief resurgence of small somatic PGL-1 granules around the 30–50-cell stage of embryogenesis (Figure 20A). Even though PGL-1 is dispersed in early GLH-1(G222D) mutant embryos, it reassembles into P granules despite the dispersal of GLH-1(G222D) at the four-cell stage and largely stays associated with P granules in the adult germline (Figure 20B). A similar pattern is observed with mCherry-tagged PRG-1, the PIWI Argonaute in *C. elegans*, which maintains its association with P granules in the adult germline in $\Delta glh-1$ and GLH-1($_EAD$) mutants (Figure 20D). In contrast, large GLH-1(DQAD) aggregates contain both PGL-1 and PRG-1 (Figure 20, C, and D). Taken together, these results suggest that most It is possible that the proteins are primarily unaffected when GLH-1 is deleted or dispersed. In contrast, large GLH-1(DQAD) aggregates sequester or retain P-granule proteins, potentially impairing their normal function.

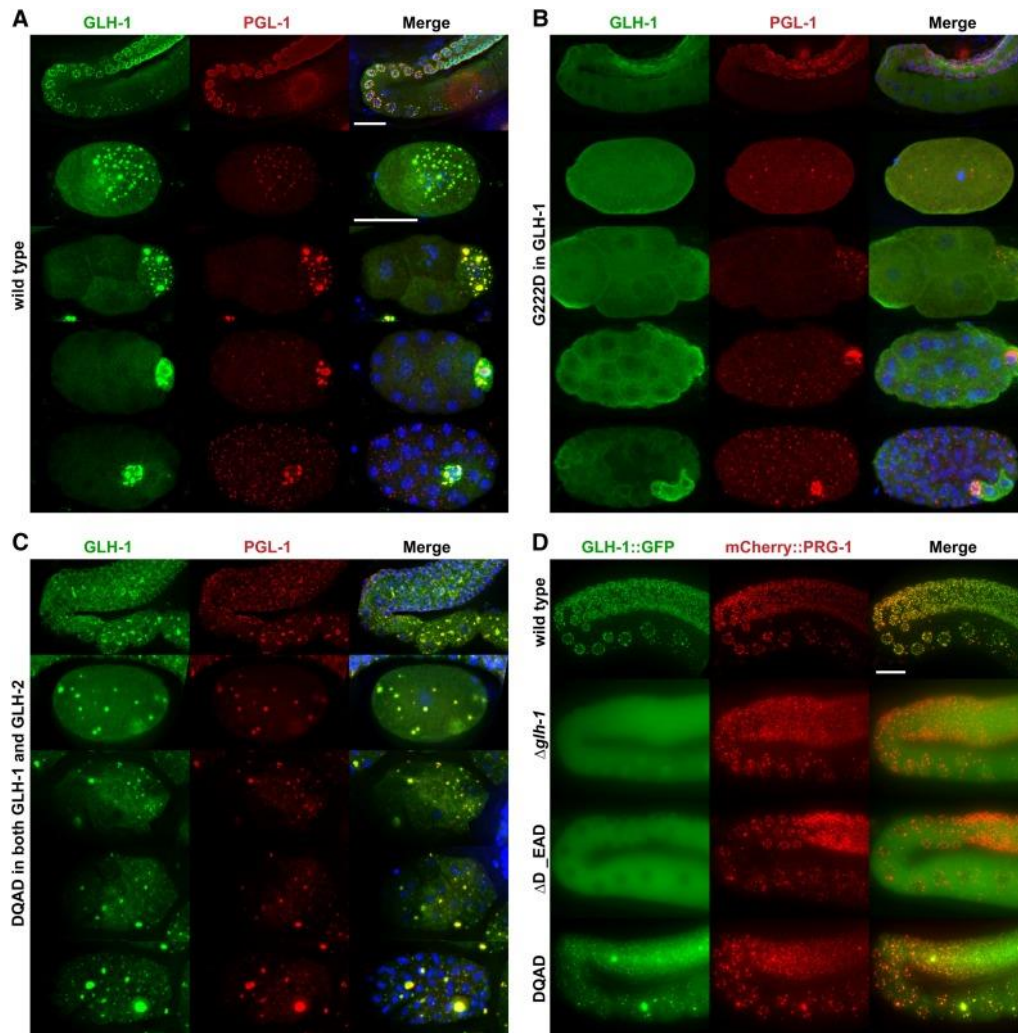


Figure 20: Colocalization of P-granule components in wild-type and GLH-1 mutants.

Colocalization of P-granule components in wild-type and GLH-1 mutants. (A–C) Immunostaining of GLH-1 (green) and PGL-1 (red) in fixed germlines, and 1-, 4-, 16-, and 32-cell embryos. (D) GLH-1::GFP and mCherry::PRG-1 in the germline of living worms. At least 10 worms were imaged for each indicated genotype.

It is possible that the GLH-1(DAAD) mutation inhibits ATP binding or hydrolysis, maintaining the N- and C-terminal domains in their open configuration, while the DQAD mutation remains bound to hydrolyzed ATP with N- and C-terminal domains closed, as has been proposed for Vasa. In that case, an indirect assessment would be to inhibit ATP hydrolysis to

see if it suppresses the embryonic lethality and fertility defects of DQAD. To assess this possibility, CRISPR was used to generate the (DQAD) + (T to A) (Vasa position 546) double mutant. This strain no longer exhibited large GLH-1 aggregates (Figure 18A), and the fertility defects and embryonic lethality were suppressed at the permissive temperature (Figure 19). These results support work in other systems that suggest DQAD aggregates are locked in a closed-conformation transient state (Dehghani & Lasko, 2016; Wenda et al., 2017; Xiol et al., 2014).

One Vasa mutation shown to uncouple ATP hydrolysis from its helicase activity in vitro is D to A (Vasa position 554), which lies at the interphase of Vasa's N- and C-terminal helicase domains (Sengoku et al., 2006). This mutation also has a mild dominant-negative phenotype in *C. elegans*, showing increased embryonic lethality and fertility defects (Figure 19). To determine if this could be caused by GLH-1 expending ATP but not coupling it with helicase activity, the analogous T546A was introduced to inhibit ATPase activity (Figure S2). This double mutant suppressed the embryonic and fertility defects of the D554A mutant (Figure 19). To further test this idea, an R to Q mutation (Vasa position 328) was engineered to disrupt helicase activity in the RNA-binding pocket with minimal impact on helicase structure, potentially uncoupling helicase activity from ATP hydrolysis. Like D554A, R328Q alleles also enhanced embryonic lethality and fertility defects (Figure 19). These alleles may suggest that expenditure of ATP uncoupled from helicase activity drives dominant Vasa and GLH-1 phenotypes. Two additional C-terminal helicase alleles were created to disrupt previously reported binding sites for KGB-1 (LEL→AGA) and eIF5b (VPD→AGA); however, both dispersed GLH-1 and looked like other helicase mutations (Figure 19).

Outside of the flanking and helicase domains, there are three Vasa-specific motifs: a glycine-rich FG repeat, a zinc-knuckle/finger, and a terminal tryptophan immediately preceded by three negatively charged amino acids. Unlike mutations in the flanking and helicase domains, deletions and substitutions in these motifs have little or no effect on GLH-1's association with P granules in the adult germline (Figure 18A); however, each show compromised fertility at the restrictive temperature (Figure 19). While this demonstrates that GLH-1 function can still be impaired despite showing proper P-granule localization, it was a surprise for the Δ FG-repeat strain since FG repeats were previously shown to facilitate contact with the nuclear periphery when ectopically expressed (Updike et al., 2011). Vasa proteins contain these glycine-rich repeats interspersed with either arginines or phenylalanines (Marnik & Updike, 2019). These are intrinsically disordered motifs, and in the case of the FG repeats of GLH, the interspersed phenylalanines form hydrophobic tethers with FG repeats in the nuclear pore complex (NPC) to maintain a wetting-like appearance on the nuclear periphery (Figure 21). Unlike the adult germline, deletion of the FG repeat in embryos caused larger GLH-1::GFP granules in primordial germ cells and their precursors and deleting the FG repeat of GLH-2 in this background further increased GLH-1::GFP granule size (Figure 21, A and B).

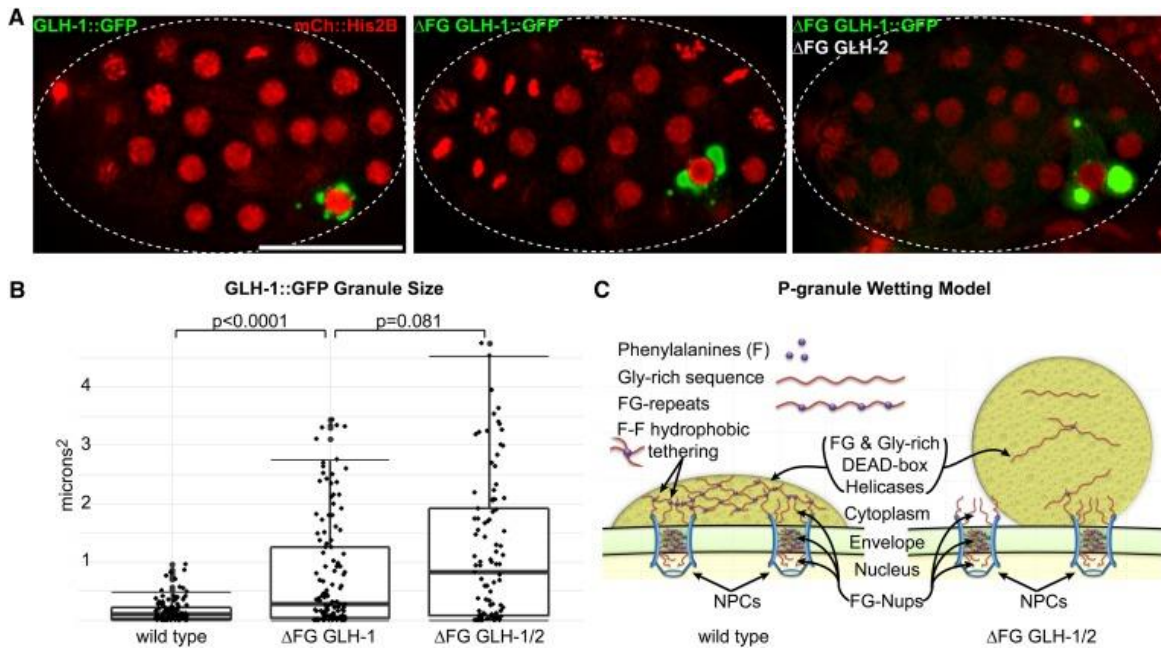


Figure 21: Glycine-rich FG repeats tether GLH-1 to the nuclear periphery.

(A) Distribution of GLH-1::GFP (green) in the germline blastomere P4 of a wild-type embryo (left), an embryo lacking FG repeats in GLH-1 (middle), and an embryo lacking FG repeats in both GLH-1 and GLH-2 (right). mCherry::H2B (red) marks chromatin. (B) GLH-1-granule sizes in the germline blastomere P4 quantified using ImageJ. (C) Model depicting the hydrophobic tethering of P-granule FG-repeat domains to FG-nucleoporins (Nups) at the nuclear periphery. For size assays, P granules were counted from ≥ 40 embryos for each strain. Box plots show median quartiles and 1 SD above the mean. NPC, nuclear pore complex.

Moreover, GLH-1 granules in these double mutants appeared more spherical, suggesting they had lost contacts that adhered them to the nuclear periphery. One potential role for FG-repeat tethering is to maximize coverage of NPCs so that nascent transcripts are captured by P granules as they exit the nucleus. Another might be to ensure the symmetric distribution of P granules as the P4 precursor divides into the two primordial germ cells. However, no evidence

supporting this was observed in the double mutant. It is also possible that the FG repeats found in GLH-4, RDE-12, and DDX-19 function redundantly to mask an asymmetric distribution phenotype when FG repeats are deleted from GLH-1 and GLH-2.

To get an idea of which proteins are loosely associated with GLH-1, and how these associations change when enzymatic activity is compromised in DQAD and DAAD mutants, GLH-1::GFP::3xFLAG was immunoprecipitated with anti-FLAG agarose beads and replicates were submitted for LC-MS/MS analysis (Figure 22 and Figure 32). Pairwise comparisons between the *glh-1* transcriptional reporter driving GFP::3xFLAG alone identified GLH-1-enriched proteins (Figure 31). As a proof of principle, NPC proteins and transport factors were identified among the 2505 proteins from the LC-MS/MS analysis (Figure 22, left column, blue and Figure 32). NPCs facilitate the interaction of P granules at the nuclear periphery and, when targeted by RNA interference (RNAi), several of them cause P granules to detach and distribute in the cytoplasm (Updike & Strome, 2009; Voronina et al., 2011). On average, NPCs are enriched in the GLH-1 IP, and this enrichment shows a significant decrease (left shift, DEAD to DAAD P-value = 0.0001 and DEAD to DQAD P-value = 0.0012) in both the DAAD and DQAD mutants, as would be expected with the dispersal of GLH-1 from the nuclear periphery in the mutants, confirming the robustness of the GLH-1 IP (Figure 22).

Gene ontology was examined in the enriched subsets (> 2.5-fold normalized increase, P-value < 0.05, Table S2), which identified most subunits of three evolutionarily conserved, multilobed scaffolding complexes collectively known as PCI complexes or zomes (Li et al., 2017). These include the COP9 signalosome, the regulatory Lid complex of the 26S proteasome, and the eIF3 translational initiation complex (Figure 22, left column, red; Table 2). One subunit of

the COP9 signalosome called CSN-5 was previously identified through a yeast two-hybrid screen with GLH-1 as bait, and the interaction was confirmed through pull-downs (Smith et al., 2002). Vasa-GST pull downs later confirmed that the direct interaction with CSN5 is protective and evolutionarily conserved (Orsborn et al., 2007). This LC-MS/MS analysis supports these previous observations with CSN5, and further suggests that it is the structural conservation of all three PCI complexes that facilitates the interaction with GLH-1. As these interactions are compromised in DAAD and DQAD mutants, they must be dependent upon GLH-1's enzymatic activity or P granule association.

Both the COP9 and Lid complexes modulate protein degradation by the 26S proteasome through deneddylation and deubiquitination, respectively (Meister et al., 2016). Interestingly, subunits of the 20S core of the 26S proteasome were depleted in the GLH-1 IP, and this depletion is dampened (right shift) as GLH-1 became dispersed in the cytoplasm of DAAD and DQAD mutants (Figure 22, middle column, blue). Whether GLH-1 is (1) sequestering these regulatory PCI complexes in P granules and away from the 20S proteasome core to antagonize protein degradation, (2) associating with the COP9 and Lid complexes prior to degradation in somatic blastomeres, or (3) facilitating the cycling of cullin-RING E3 ubiquitin ligase (CRL) activity still needs to be determined. Degradation of P granules in somatic blastomeres is mediated by CRL activity with the CCCH-finger-binding protein ZIF-1 acting as a receptor (DeRenzo et al., 2003; Oldenbroek et al., 2012). RNAi depletion of transcripts encoding multiple 20S core proteasome subunits, regulatory Lid subunits, and ubiquitins cause P-granule accumulation throughout the soma of arrested embryos (Updike & Strome, 2009). Interestingly, *Drosophila* Vasa is also regulated through CRL activity by two CRL specificity receptors (Gus and

Fsn) that compete for a single binding site on Vasa; the Gus receptor acts to stabilize Vasa and protect it from Fsn-mediated destabilization (Kugler et al., 2010). Gus and Fsn homologs were not enriched in our GLH-1 IP LC-MS/MS analysis, and the Gus-binding sites of Vasa do not appear conserved in GLHs; instead, in its place are ancestral CCHC zinc-knuckle motifs that have been independently lost in insects, tardigrades, vertebrates, and some sponges and flatworms (Figure 30C). While little is known about this motif in GLH-1, some evidence suggests that zinc knuckles may facilitate an interaction with an F-box containing a P-granule protein called PAN-1 (Gao et al., 2012). An intriguing possibility is that insects developed a convergent method using Gus and Fsn to protect Vasa from proteasome degradation, and that COP9 and Lid regulatory subunit sequestration by GLH-1 has a similar protective effect.

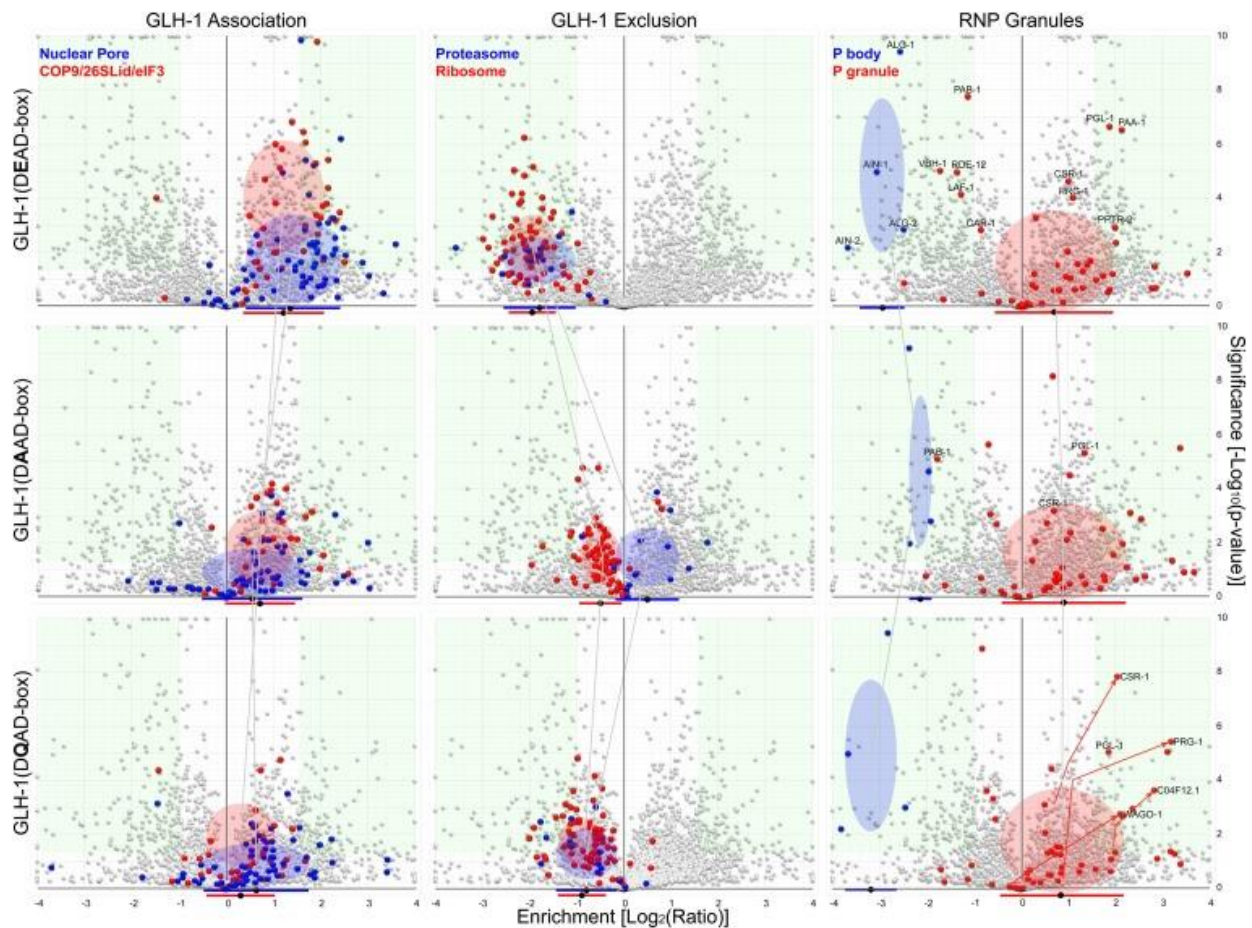


Figure 22: *GLH-1* protein associations.

Volcano plots show the significance and enrichment of proteins that immunoprecipitate with *GLH-1::GFP::3xFLAG* over the *glh-1* transcriptional reporter expressing *GFP::3xFLAG* alone, as identified by LC-MS/MS. Left column: protein families showing an enriched *GLH-1* association include nuclear pore proteins (blue) and subunits of PCI scaffolding complexes. These associations decrease in DAAD (middle row) and DQAD (bottom row) mutants. Red and blue bars under the x-axis indicate the median and 1 SD, and colored ovals do the same but also indicate the distribution of significance. Green boxes show normalized enrichment and exclusion > 2.5-fold, and a P-value < 0.05. Nuclear pore genes used in this analysis are indicated in Table S3. Middle column: protein families showing stronger enrichment for *GFP::3xFLAG*

alone include 20S core subunits of the 26S proteasome (blue) and subunits of the ribosome (red). Right column: proteins associated with RNP granules. P-body proteins (blue) and P-granule proteins (red). Data were obtained from two technical replicates for each indicated genotype. See also Table S3. LC, liquid chromatography; MS, mass spectrometry; PCI, 26S Proteasome Lid, COP9 Signalosome, and eIF3; RNP, ribonucleoproteins.

P granules may also act to exclude 40s and 60s ribosomes, whose proteins, like those of the 20S proteasome core, are depleted in the GLH-1 IP (Figure 22, middle column, red, Table 2). Again, this depletion is dampened (right shift) as GLH-1 becomes dispersed in the cytoplasm of DAAD and DQAD mutants, suggesting that there is nothing inherent to the GLH-1 protein that repels ribosomes, but that the bulk of the GLH-1 protein resides in a P-granule microenvironment devoid of assembled large and small ribosome subunits. To test whether P granules and ribosomal proteins occupy different domains in the *C. elegans* germline, GLH-1::GFP::3xFLAG germlines were costained with an antibody against RPL-7a and imaged through a single section (Figure 23A). While the RPL-7a signal was strongest in the rachis as opposed to the germline perimeter where P granules are more prevalent, this ribosomal protein is not excluded from P granules. It was previously shown that P granules extend the size exclusion properties within the nuclear pore out into the germline cytoplasm, and while fluorescent dextran molecules < 40 kDa in size diffuse freely through P granules, 70 and 155 kDa dextran molecules do not (Updike et al., 2011). The size of RPL-7a, estimated at 30 kDa, may allow the protein to diffuse through P granules and into the nucleus, where it can be assembled into the large ribosomal subunit. To get a better idea of whether assembled ribosomes are excluded from P granules, 18S rRNA probes were used as a proxy to visualize areas of the cytoplasm

occupied by 40S subunits. 18S rRNA undergoes rapid assembly with ribosomal proteins and is exported into the cytoplasm as the 40S subunit. Previous fluorescence detection of 5S, 5.8S, 18S, and 26S rRNA probes did not show any obvious concentration of rRNA in P granules (Schisa et al., 2001). Stellaris smFISH probes were designed for the 18S *rrn-1.1*. The vast abundance of this rRNA causes the probe to light up the dissected germlines, but voids in the cytoplasm are evident in areas occupied by GLH-1::GFP (Figure 23B). These results suggest that while some individual ribosomal proteins colocalize with P granules, assembled ribosomes do not, supporting a model where P granules partition the cytoplasm to create translationally silent microenvironments.

Finally, several established P-body (blue) and P-granule (red) components were examined in the context of GLH-1 association or exclusion (Figure 22, right column, Table S3). Generally, the average dispersal of P-granule components changes very little in the DAAD and DQAD mutants. The DQAD mutant has been utilized in other systems to capture factors that associate transiently in the piRNA amplifier complex (Wenda et al., 2017; Xiol et al., 2014). Proteomics data from the DQAD mutant were examined to see if any proteins increased in significance and association. Only four proteins showed this up-and-to-the-right shift from wild-type (DEAD) (red arrows), and they included the Argonaute proteins CSR-1, PRG-1, C04F12.1, and WAGO-1. This increased association between GLH-1 and Argonautes suggests that nematodes have a complex similar to the piRNA transient amplifying complex described in insects and vertebrates, albeit one that functions through RdRPs instead of ping-pong amplification.

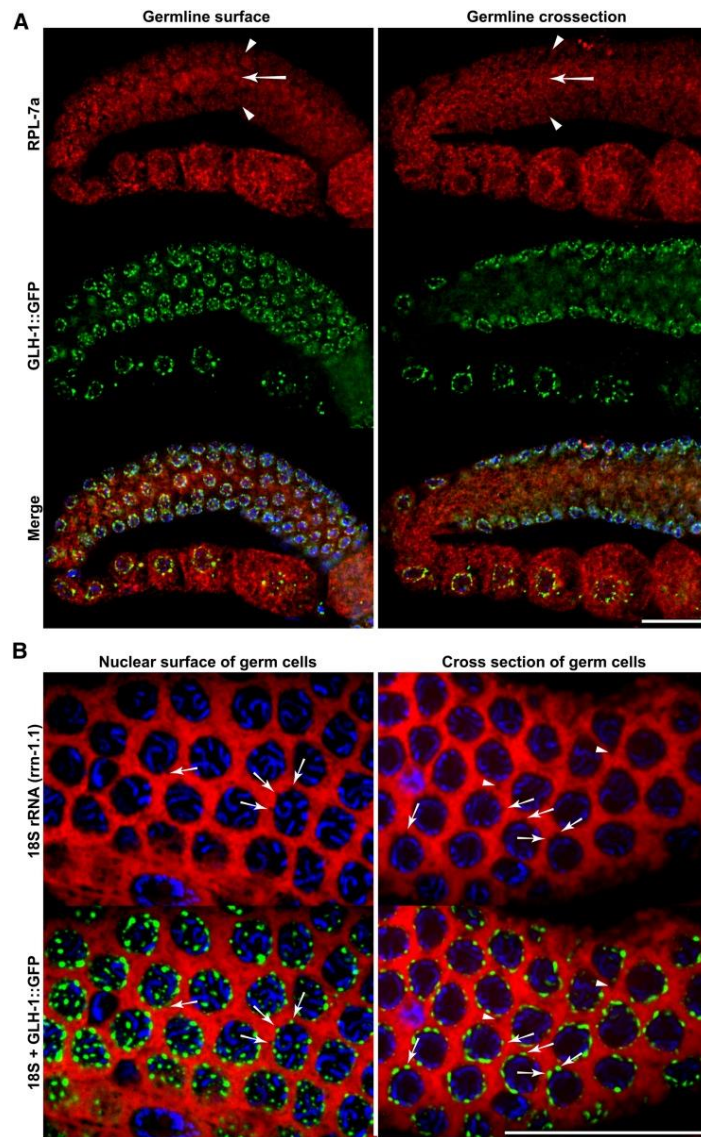


Figure 23: Ribosomes and the size exclusion properties of P granules.

(A) Immunostaining of RPL-7a (red) with GLH-1::GFP. RPL-7a is more concentrated in the shared cytoplasm of the rachis (arrows) than germ granule-rich areas at the perimeter (arrowheads), but it is not excluded from P granules. (B) 18S rRNA FISH signal (red) is saturated in the cytoplasm of germ cells where it associates with the 40S ribosomal subunit, but is excluded from GLH-1::GFP-marked P (arrows) and yolk granules (arrowheads).

4.4 Discussion

The role of germ granules in inducing or maintaining germ cell potency may come down to the molecular functions of their individual components. In this study, a comparative structure–function analysis was performed on the *C. elegans* Vasa homologs. These results show that GLH-1's helicase activity is necessary to maintain its tight association with P granules (Figure 24). Every edit of a conserved residue within the helicase domains caused GLH-1 to detach from P granules and disperse into the cytoplasm. Flanking domain mutations phenocopy this dispersal, suggesting that the flanking domain facilitates this helicase activity as it wraps between the N- and C-terminal RecA domains. Whether this means that GLH-1 localization is mediated through the continuous unwinding of RNA substrates or the continuous cycling of other protein interactions is unclear. However, GLH-1's P-granule association is not mediated by its glycine-rich intrinsically disordered region (IDR), zinc-knuckle, negatively charged C-terminus, or any inherent structural features on their own. Interestingly, while mutations in these domains do not disperse GLH-1 protein, they still exhibit close to the same degree of fertility defects at the restrictive temperature as the *glh-1* deletion, demonstrating one reason these Vasa-defining domains have been conserved throughout evolution. The specific contribution of each of these domains will need to be ascertained through complementary approaches that include: (1) generating similar edits and deletions in paralogs to observe additive effects, as was done with the FG-repeat deletion in GLH-1 and GLH-2.

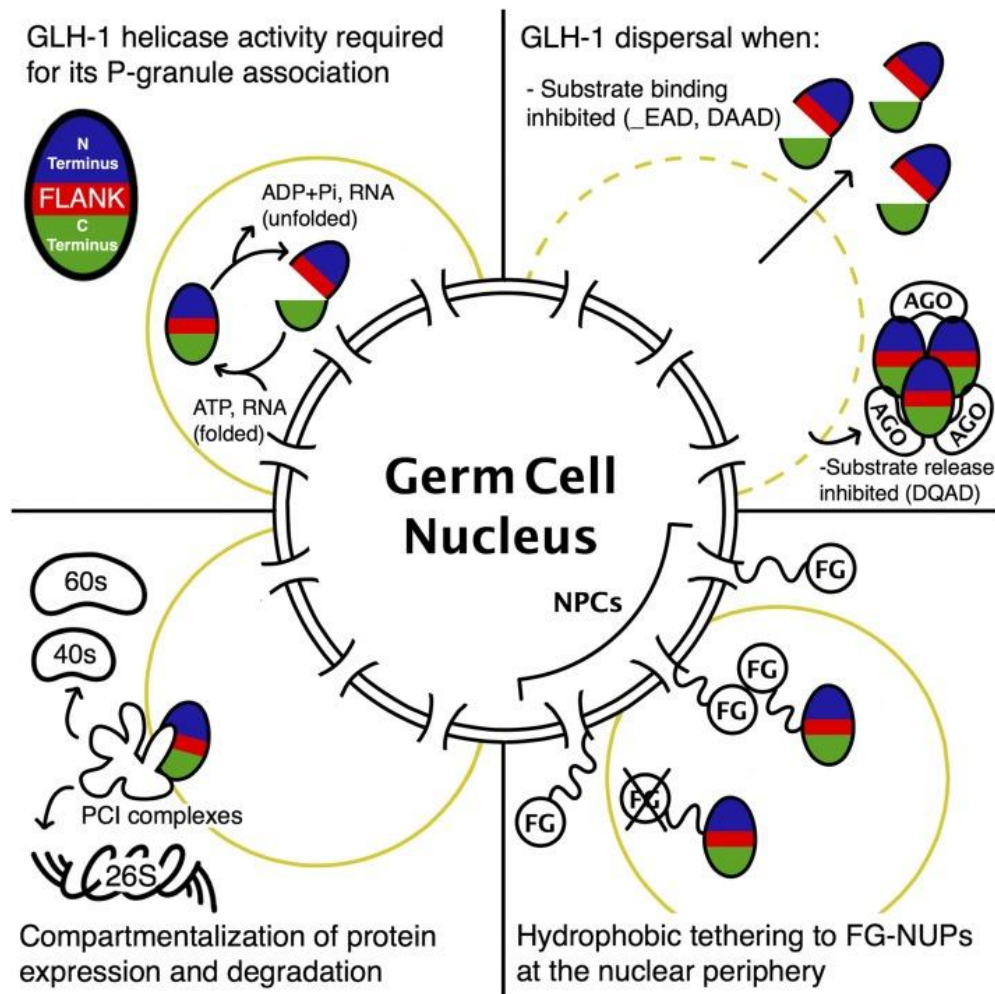


Figure 24: GLH-1 functionality summary.

Top left; GLH-1 represented as an oval with its N-terminal (blue), flanking (red), and C-terminal helicase domains. GLH-1's association in P granules (yellow outline) requires cycles of RNA and adenosine triphosphate (ATP) binding (closed) and release of adenosine diphosphate (ADP) and phosphate (Pi). Top right; GLH-1 is dispersed in mutants that inhibit substrate binding (_EAD, DAAD) or substrate release (DQAD), and in the latter case GLH-1(DQAD) forms aggregates with specific Argonaute (AGO) proteins. Bottom left; GLH-1 associates with the PCI complexes (26S Proteasome Lid, COP9, and eIF3) while excluding ribosomal subunits (60S and 40S) and the 26S

proteasome. Bottom right; The phenylalanine - glycine (FG) repeats of GLH-1 tether P granules to FG-nucleoporin proteins.

One outstanding question is whether GLH-1 and P granules demonstrate an affinity to specific germline-expressed transcripts. Multiple attempts to immunoprecipitate and sequence RNA substrates of GLH-1 and PGL-1 under varying conditions have been performed by our group; however, follow-up single-molecule FISH studies have yet to demonstrate consistent P-granule enrichment of these identified substrates. These negative results likely reflect the nonsequence-specific and transient manner in which core P-granule components—like PGL-1 and GLH-1—interact with RNA, and they add weight to the idea that GLH-1 and Vasa proteins simply function as mRNA solvents in phase-separated P granules (Nott et al., 2016). This may eventually be resolved as RNA immunoprecipitation (RIP), crosslinking immunoprecipitation (CLIP)-seq technologies improve, or the right P-granule target protein is found. However, the idea that P granules contain solvents to keep transcripts unfolded and accessible for sequence scanning by small RNA-bound Argonautes or other RNA-binding proteins is highly likely.

Dominant phenotypes were observed in R328Q and D554A mutations thought to uncouple ATP hydrolysis from RNA unwinding, which are possibly caused by increased energy expenditure that is not translated into enzymatic helicase activity. The DQAD mutation is also dominant, but the DAAD mutation is not. This E to Q change may induce sterility because it accumulates large aggregates that sequester components from their normal function within P granules, or because they fail to dissolve in the soma. Since these aggregates persist in somatic blastomeres, the extent to which they resemble P granules or retain normal P-granule function is unclear. Therefore, caution should be maintained when interpreting whether DQAD aggregates are

capturing a transient amplifying complex or a novel aggregate altogether. Given that these dominant alleles are suppressed with an intragenic T546A mutation, they are likely anti- or neomorphic alleles. Another unreported deletion of ER residues in motif V (Vasa position 550–551) caused a stronger dominant phenotype that could not be maintained beyond two generations, suggesting that some dominant *glh-1* alleles are too severe to recover with the current approach.

With the caveats of the GLH-1(DQAD) in mind, significant increases in association with this mutant were primarily restricted to Argonaute proteins. These included not only the piRNA Argonaute PRG-1, but also the Argonautes CSR-1, WAGO-1, and C04F12.1, which bind to other small RNA species. In this regard, GLH-1(DQAD) reflects the transient state of its insect and mammalian homologs that interact with piRNA-amplifying Argonaute proteins, but suggests that the *C. elegans* transient complex is not limited to interactions with piRNAs. It is worth noting that the GLH-1 enriched proteins showing the most significant decrease in association with DQAD are the PP2A subunits (PAA-1, PPTR-1, PPTR-2, and LET-92), whose phosphatase activities stabilize P granules in the early embryo (Gallo et al., 2010; Griffin et al., 2011; Updike & Strome, 2009). This suggests that the targets of this phosphatase activity are not enriched in these DQAD aggregates, and by extension may associate with GLH-1 in its open configuration but not this closed transient state.

Another exciting finding from this study is the enrichment of PCI complex zones in the GLH-1 IPs. While GLH-1's direct association with the COP9 signalosome component CSN5 had been previously established, finding an enrichment for almost every PCI protein strongly suggests that GLH-1 has an affinity for these multilobed and structurally conserved scaffolding

complexes. It will be imperative to understand how these scaffolds associate with GLH-1, the specific complex components that show direct interactions like CSN5, and whether there is a spatiotemporal element to these interactions during germline development. Interestingly, while CSN5 is found in the cytoplasm and nucleus, it exhibits no distinct P-granule enrichment (Pintard et al., 2003; Smith et al., 2002), nor have other PCI subunits to date. One model is that COP9 and the 26S Lid complex associate with GLH-1 in P granules. Another model is that, like ribosomes, assembled PCI complexes are also excluded from P granules, but facilitate the exchange of transcripts and proteins at the interface of the P-granule microenvironment to deliver them to assembled ribosomes or 26S proteasomes, respectively (Figure 24). Subsequent studies will need to determine where the interactions between PCI complex components and GLH-1 occur, whether the association between GLH-1 and the eIF3 complex mediates a positive or negative effect on translation, and the impact of GLHs on protein turnover and translational regulation.

4. CHAPTER V: GLH-1 PREVENTS EARLY SOMATIC REPROGRAMMING

The contents of this chapter are adapted from Rochester et al., *Developmental Biology*, doi: 10.1016/j.ydbio.2022.10.003, Published 21 October 2022.

Author Contributions:

Catherine Sharp and Jesse Rochester performed strain creation and validation. Jesse Rochester developed a liquid culture protocol generating samples for RNA-seq and polysome profiling performed by Jesse Rochester with assistance from Jarod Rollins. Joel Graber headed the primary analysis of RNA-seq data sets, aided by Nathaniel Maki, Dustin Updike, and Jesse D. Rochester. Primary investigation by Jesse Rochester and Hyemin Min. Hyemin Min performed sperm motility and activation assays. Writing, review, and editing by Jesse D. Rochester, Hyemin Min, Brett Keiper, and Dustin L. Updike. Supervision, administration, and funding by Dustin L. Updike.

5.1 Chapter Summary

Germ granules harbor processes that maintain germline integrity and germline stem cell capacity. Depleting core germ granule components in *C. elegans* leads to the reprogramming of germ cells, causing them to express markers of somatic differentiation in day-two adults. Somatic reprogramming is associated with complete sterility at this stage. The resulting germ cell atrophy and other pleiotropic defects complicate our understanding of the initiation of reprogramming and how processes within germ granules safeguard the totipotency and immortal potential of germline stem cells. To better understand the initial events of somatic reprogramming, we examined total mRNA (transcriptome) and polysome-associated mRNA (translatome) changes in a precision full-length deletion of *glh-1*, which encodes a homolog of

the germline-specific Vasa/DDX4 DEAD-box RNA helicase. Fertile animals at a permissive temperature were analyzed as young adults, a stage that precedes by 24 h the previously determined onset of somatic reporter-gene expression in the germline. Two significant changes are observed at this early stage. First, the majority of neuropeptide-encoding transcripts increase in both the total and polysomal mRNA fractions, suggesting that GLH-1 or its effectors suppress this expression. Second, there is a significant decrease in Major Sperm Protein (MSP)-domain mRNAs when *glh-1* is deleted. We find that the presence of GLH-1 helps repress spermatogenic expression during oogenesis, but boosts MSP expression to drive spermiogenesis and sperm motility. These insights define an early role for GLH-1 in repressing somatic reprogramming to maintain germline integrity.

Graphical Summary:

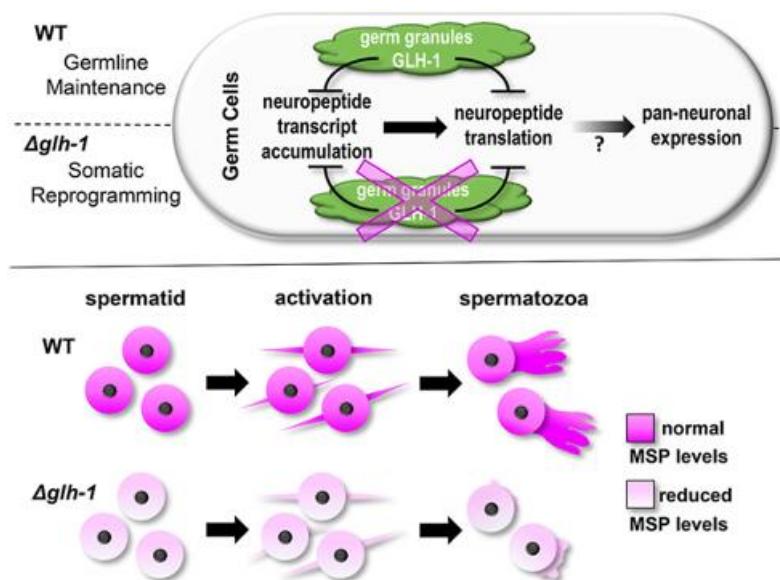


Figure 25: GLH-1 RNA-seq graphical summary.

Top) GLH-1 repression of neuropeptide expression to prevent early somatic reprogramming of the germline. Bottom) GLH-1 promotes the expression of MSPs to drive spermiogenesis.

5.2 Introduction

Cytoplasmic, germline-specific ribonucleoproteins called germ granules are hubs of small RNA biogenesis and amplification (Phillips & Updike, 2022). In *C. elegans*, processes within germ granules confer a transgenerational memory of gene expression and ensure robust fertility and cellular potency through environmental challenges. Coincident depletion of four core germ-granule components (*pgl-1*, *pgl-3*, *glh-1*, *glh-4*) by RNAi feeding (germ-granule RNAi) prevents germ-granule assembly in the progeny, and consequently, germ cells lose potency and express markers of somatic differentiation (Updike et al., 2014). Early events that trigger somatic reprogramming following germ granule depletion are difficult to ascertain as somatic reporters are not expressed in germ-granule depleted animals until the second day of adulthood, coincident with atrophied germlines and other pleiotropic defects. Transcriptional profiling of dissected germlines during the early events of somatic reprogramming reveals a slight decrease in oogenic mRNAs, higher levels of spermatogenic mRNAs, and evidence of an incomplete sperm-to-oocyte switch, but no overall increase in soma-enriched transcripts (Campbell & Updike, 2015). A follow-up study profiled mRNAs from the fourth larval stage to the second day of adulthood following germ-granule RNAi depletion (A. K. Knutson et al., 2017b). Here, evidence was found for increased somatic mRNA accumulation in the germline, but again, not until the second day of adulthood. None of these three studies completely uncoupled the accumulation of somatic mRNAs from germline atrophy and sterility. These approaches were unable to delineate the early events of somatic reprogramming or fully resolve whether processes within intact germ granules antagonize somatic expression through mRNA accumulation, mRNA translation, or a combination of both.

Importantly, Knutson et al. demonstrated that the germline expression of GFP-tagged somatic transgenes could be recapitulated in strains carrying a *glh-1* loss-of-function allele. At 24 °C, the efficiency of somatic reprogramming in this *glh-1* mutant was nearly three times higher than with germ-granule RNAi or in *pgl-1* or *pgl-1; pgl-3* mutant strains at the same temperature (A. K. Knutson et al., 2017b). At restrictive temperatures of 26 °C, this loss-of-function allele is sterile, with spermatheca nearly devoid of sperm (Spike et al., 2008b). This finding suggested that early and initial somatic reprogramming events can be uncoupled from sterility and other germline defects if profiled in healthy *glh-1* loss-of-function mutants prior to somatic reporter expression. Here we have taken that approach, profiling both the transcriptome and translome of a precise *glh-1* full coding region deletion strain in synchronized one-day-old adults grown at the permissive temperature of 20 °C – conditions optimized to preserve germline development and minimize the occurrence of pleiotropic defects.

GLH-1 is a homolog of Vasa/DDX4, a non-sequence-specific DEAD-box RNA helicase expressed in the germ cells of animals. In *C. elegans*, there are four GLH proteins, GLH-1, GLH-2, GLH-3, and GLH-4 (Kuznicki et al., 2000c). Both GLH-1 and GLH-4 are found in other nematode species, while GLH-1 gave rise to GLH-2 and GLH-3 through a more recent duplication in *C. elegans* (Bezares-Calderón et al., 2010; Spike et al., 2008b). Of the four GLH proteins, only GLH-1 and GLH-2 contain all the signature domains that distinguish Vasa from other DEAD-box helicases (Marnik et al., 2019). GLH-1 is the most prominent of the four GLHs in expression, germ-granule dispersion, and germline phenotypes, but null alleles retain fertility at the

permissive temperature of 20 °C due to partial redundancy with GLH-2 and GLH-4 (Kuznicki et al., 2000c; Spike et al., 2008b). This redundancy provides the opportunity to survey subtleties in germline development caused by the loss of GLH-1.

Models for Vasa/DDX4 function emphasize its association with Argonaute proteins to stimulate piRNA amplification in the germline (S. Dai et al., 2022; Dehghani & Lasko, 2015; Kuramochi-Miyagawa et al., 2010; Malone et al., 2009; Megosh et al., 2006; Wenda et al., 2017). While *C. elegans* *glh-1* mutants do not show exogenous RNAi defects (Spike et al., 2008b), germline RNAi inheritance is compromised (Spracklin et al., 2017). GLH-1 has also been shown to bind specific microRNAs to facilitate translational silencing (Dallaire et al., 2018). Multiple studies have demonstrated an affinity between GLH-1 and the Argonautes PRG-1 and WAGO-1 (Chen et al., 2020, 2022; S. Dai et al., 2022; Marnik & Updike, 2019; Price et al., 2021). In addition, the depletion of germ-granule components phenocopies *prg-1* mutant sterility and increased spermatogenic transcripts (Campbell & Updike, 2015; Cornes et al., 2022; Spichal et al., 2021). Currently, evidence directly implicating small RNA regulation to somatic reprogramming in *glh-1* mutants is sparse and potentially point to functions of GLH-1 that are piRNA-independent.

One likely function for Vasa/DDX4 homologs like GLH-1 during germ cell development is translational regulation (Mercer et al., 2021) or, more specifically, the hand-off from germ-granule-mediated mRNA surveillance prior to translation initiation. As such, the impact of GLH-1 on expression would be better assessed by profiling the translation efficiency of individual mRNAs along with changes in their abundance. Vasa/DDX4 resembles eukaryotic initiation factor-4A (eIF4A) (P. F. Lasko & Ashburner, 1988). In *Drosophila*, Vasa activates the translation

of nanos in the pole plasm of the embryo in conjunction with the translation initiation factor eIF5B (Carrera et al., 2000; Gavis & Lehmann, 1994; Johnstone & Lasko, 2004). Vasa also mediates translational repression through interactions with RNA-binding proteins Bruno and the eIF4E interacting protein, Cup (Ottone et al., 2012). GLH-1 exhibits an affinity for the eIF3 complex in *C. elegans* (Marnik et al., 2019). In *Drosophila*, piRNA regulation via the PIWI protein Aubergine recruits eIF3 to activate translation in the germlasm (Ramat et al., 2020). In mammals, a MIWI/piRNA/eIF3 complex binds a subset of spermiogenic mRNAs to activate their translation (P. Dai et al., 2019). Therefore, Vasa/DDX-4/GLH proteins likely play dynamic roles in transitioning from RBP-, microRNA-, or piRNA-mediated translational repression to initiation complex assembly and mRNA translational activation. *C. elegans* germ granules are known assembly sites of eIF4E:4EIP complexes that have been shown to exert translational repression as messenger ribonucleoproteins (mRNPs) (Huggins et al., 2020; Huggins & Keiper, 2020); however, the extent to which germ-granule components interface with translation initiation complexes has not thoroughly been explored.

Here an alternative approach is used to decipher the impact of GLH-1 on germline development. Rather than evaluating mRNA regulation in severe terminal phenotypes, we examine more subtle impacts on the transcriptome and translome when germ-granule assembly, in otherwise healthy one-day-old adults, is compromised by *glh-1* loss. We find that most changes in mRNA accumulation correlate with its fraction being translated; however, increases of spermatogenic mRNAs are largely offset to wild-type levels in their translation. Two smaller gene classes stand out in their regulation by GLH-1. First, the abundance of MSP-domain-encoding mRNAs decreases in both total and translated fractions in the absence of

GLH-1, in contrast to most other spermatogenic mRNAs that accumulate when germ granules are compromised. This decrease in MSP expression impacts spermiogenesis, specifically pseudopod extension, and suggests that GLH-1 drives MSP expression and spermiogenesis under wild-type conditions. Second, mRNAs encoding neuropeptides accumulate and become translated upon germ-granule depletion or *glh-1* loss. These increases suggest that processes within germ granules initially antagonize neuronal reprogramming, not by blocking the expression of neuronal transcription factors but by quelling the expression of neuropeptides. A critical next step will be determining the GLH-1-dependent processes through which MSP and neuropeptide mRNAs are recognized and regulated.

5.3 Results

To examine the impact of GLH-1 on translational efficiency in *C. elegans*, mRNA-seq was performed on polysome and total mRNA fractions from three biological replicates of synchronized young adult populations from wild-type (WT) and *glh-1* deletion (Δ *glh-1*) strains (Figure 26A). Our traditional approach of profiling gene expression in dissected germlines yields insufficient starting material for polysome gradients, so lysates for these studies were prepared from whole worms, which are half-comprised of germ cells. The WT and Δ *glh-1* strains have been previously described (Marnik & Updike, 2019). Briefly, the WT-designated strain was generated using CRISPR/Cas9 to place a GFP:3xFLAG tag just before the stop codon of the endogenous *glh-1* gene. The Δ *glh-1* strain was generated from this WT-designated strain using CRISPR/Cas9 to make a precision deletion of *glh-1*, leaving GFP:3xFLAG expressed from the endogenous *glh-1* promoter and 3' end sequences. Libraries were created by placing unique adapters on the three replicates of WT and Δ *glh-1* from total and polysome fractions (12

samples) and sequenced together. Differential expression between WT and Δ glh-1 replicates was determined using DESeq2 (Love et al., 2014) for both total mRNA (transcriptome) and polysomal mRNA (translatome), and the $\text{Log}_2(\text{Fold Change})$ plotted on the x and y axis, respectively (Figure 26B, Supplemental Table 3). mRNAs deviating from the correlation between transcriptome and translatome are identified by the difference in the fold change ($\Delta \text{Log}_2\text{FC}$). Transcripts with a $\Delta \text{Log}_2\text{FC}$ greater than 1 or less than -1 are shown in red (Figure 26B). In principle, a high $\Delta \text{Log}_2\text{FC}$ would indicate mRNAs whose translation efficiency decreases with GLH-1 (107 transcripts >1), whereas a low $\Delta \text{Log}_2\text{FC}$ would indicate mRNAs whose translation efficiency increases with GLH-1 (81 transcripts < -1).

The 107 mRNAs whose translation efficiency is decreased by the presence of GLH-1 were run through the STRING database (v11.5) to look for network clustering (Supplemental Table 1, (Szklarczyk et al., 2021)). Patterns were not observed for most of these mRNAs. Enrichment of a subset of replication-dependent histones was observed (false discovery rate = $3.07\text{e-}08$), which could point to proliferative defects in Δ glh-1 mutants (see Figure 28D). Four out of six hsp-16 mRNAs were also observed in these 107 mRNAs (false discovery rate = $2.81\text{e-}05$), which point to Δ glh-1 mutants exhibiting increased cellular stress. On the other end of the spectrum, most mRNAs whose translation efficiency is increased by GLH-1 are co-expressed and form one large network cluster (Supplemental Table 1). Components of this cluster contain major sperm protein (MSP) domains and protein kinases that are primarily co-expressed during spermatogenesis.

Spermatogenic genes in *C. elegans* are not thoroughly annotated in current gene ontology databases. One available dataset (Ortiz et al., 2014) uses the ratio of fem-3(q96gf)

(male) to *fog-2(q71)* (female) expression in dissected germlines to define oogenic, gender-neutral, and spermatogenic subsets. We further separated the defined spermatogenic mRNAs in this dataset into those with high (>5) and low (<5) *fem-3::fog-2* ratios based on a natural, bimodal distribution (Supplemental Figure 26A). Compared to all genes in our analysis, a significant increase in the translational efficiency (positive ΔLog2FC) of oogenic genes is observed in $\Delta\text{glh-1}$ mutants, which partially compensates for the decreased accumulation of oogenic mRNAs (Figure 26C–E). While there was little change in the ΔLog2FC of gender-neutral or spermatogenic (low) mRNAs, the translational efficiency of spermatogenic (high) genes drops in $\Delta\text{glh-1}$ mutants, partially compensating for the increased accumulation of spermatogenic (high) mRNAs (Figure 26C–E). It was previously demonstrated that simultaneous depletion of four core germ-granule components (PGL-1, PGL-3, GLH-1, and GLH-4) by RNAi induces spermatogenic gene expression in one-day-old adult germlines, and then soma-specific and neuronal genes in two-day-old adult germlines (Campbell & Updike, 2015; A. K. Knutson et al., 2017b; Updike et al., 2014). Therefore, we also looked at transcriptional and translational changes in soma-specific and neuronal subsets in our one-day-old adult $\Delta\text{glh-1}$ mutants, again observing only subtle changes at this early stage (Figure 26C–E, Supplemental Figure 33B). Taken together, GLH-1 loss leads to an average decrease in oogenic mRNAs and an average increase in spermatogenic (high) mRNAs in one-day-old adults, reflecting our previous observations with germ-granule RNAi. But here, we find that these changes in mRNA accumulation are compensated by altered translational efficiency, thereby reducing their impact on the germline.

mRNAs encoding MSP-domain proteins are one exception to compensatory feedback we see with the expression of oogenic and spermatogenic (high) gene sets. Because MSP-domain proteins were enriched in the 81 mRNAs with a $\Delta \text{Log}_2\text{FC} < -1$, we profiled the expression of all 72 annotated MSP-domain-containing proteins in our sequencing analysis. Unlike the increased accumulation of spermatogenic (high) mRNAs in $\Delta\text{glh-1}$ mutants, MSP mRNA abundance is decreased (Figure 26D), and this was accompanied by a further reduction in MSP mRNA translation (Figure 26E) and translation efficiency (Figure 26C, Supplemental Figure 33B). The genome browser expression profile of *msp-142* from total mRNA and polysome-associated fractions is an example showing a more substantial decrease in polysome-associated mRNAs in $\Delta\text{glh-1}$ mutants (Supplemental Figure 33C). This pattern is reflected with another spermatogenic (high) mRNA, *ssq-1*, which does not encode an MSP domain (Supplemental Figure 33D). As expected, both *msp-142* and *ssq-1* transcripts are increased in a male-enriched *him-5* background, but to a lesser extent in $\Delta\text{glh-1}; \text{him-5}$ nematodes, showing the presence of GLH-1 further increases the accumulation of these mRNAs (Supplemental Figure 33E).

Another exception to compensatory feedback models can be observed in subsets of neuronal genes in $\Delta\text{glh-1}$ mutants. Modest increases in soma-specific and neuronal genes were observed in the transcriptome and translome of these animals. But, neuropeptides were the most significantly enriched (false discovery rate = $1.05\text{e-}10$) in the translome of $\Delta\text{glh-1}$ mutants. Therefore, we profiled the expression of other neuronal subsets as defined by the CeNGEN gene expression map of the *C. elegans* nervous system (Taylor et al., 2021). $\Delta\text{glh-1}$ mutants increased the accumulation of mRNAs encoding ion-channels and neuropeptides, and

this was accompanied by enrichment of these mRNAs in the translated polysome fraction (Figure 26C–E, Supplemental Figure 33B). To see if the enrichment was evident but missed in previous expression profiling experiments of dissected germlines following germ-granule RNAi, we re-examined neuropeptide mRNA accumulation in these published datasets (Figure 26F). In each case, the accumulation of neuropeptide mRNAs was significantly higher in dissected germlines from day one adults following germ-granule RNAi (Campbell & Updike, 2015; A. K. Knutson et al., 2017b). Moreover, the neuropeptide mRNAs progressively increased in dissected germlines from the fourth larval stage (no change) to two-day-old adults, and further increased when germ cells expressed a pan-neuronal *unc-119:GFP* reporter (A. K. Knutson et al., 2017b dataset). Significant increases were also observed when the neuropeptide subset was plotted against expression profiles of dissected germlines from *glh-1* and *pgl-1* mutants (Figure 26F) (A. K. Knutson et al., 2017b). These findings are consistent and show, for the first time, that neuropeptides become ectopically expressed during the early phase of somatic reprogramming that ensues after germ granules are compromised. The mechanisms behind the reduced accumulation and translation of MSP-domain encoding mRNAs or the increased accumulation and translation of the specified neuronal subsets in Δ *glh-1* mutants are currently unknown.

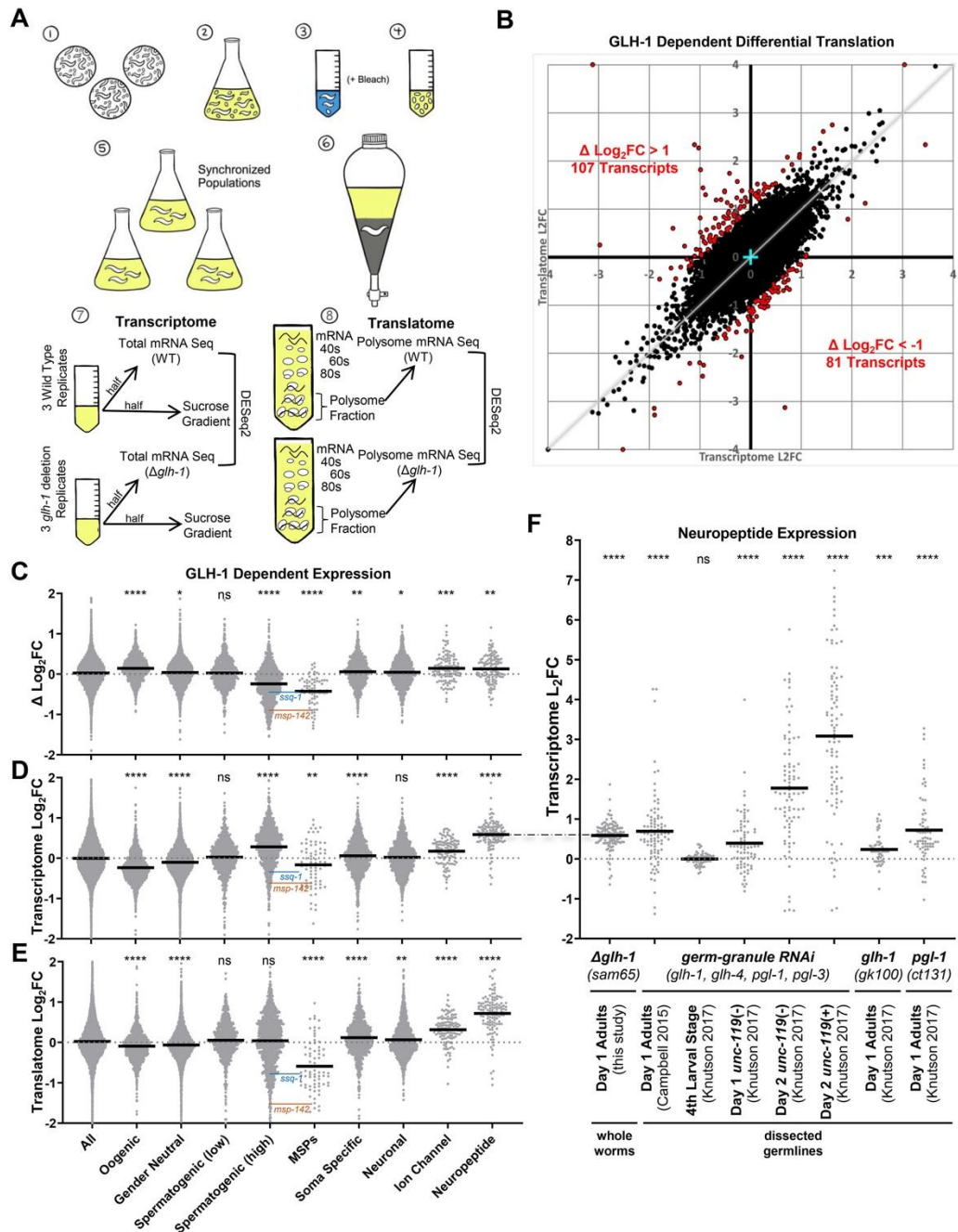


Figure 26: GLH-1 impact on the transcriptome and translatome.

A) Schematic of expression profiling experiments. Starved plates (1) were used to inactivate S-media cultures containing freeze-dried OP50 (2). Following incubation at 20 °C, gravid adults were bleach treated (3) to harvest embryos (4). Embryos were hatched overnight on unseeded

plates to obtain a synchronized population and used to inoculate new S-media cultures containing freeze-dried OP50 (5). Following incubation at 20 °C, young adults were precipitated, washed, and flash-frozen (6). Lysates were prepared from the synchronized WT and Δ glh-1 mutants. Half of the lysate was used for total mRNA isolation (7), while the other half was placed in a sucrose gradient for polysome fractionation (8). B) $\text{Log}_2(\text{Fold Change})$ from total mRNA-seq (transcriptome, X-axis) plotted against the $\text{Log}_2(\text{Fold Change})$ from polysome mRNA-seq (translatome, Y-axis). Red points indicate differentially translated transcripts where the $\Delta\text{Log}_2\text{FC}$ (difference between transcriptome and translatome) was >1 (107 transcripts) or < -1 (81 transcripts). Four data points fell outside the boundaries of the graph and are shown on edge. Cyan cross marks 0,0. Grey diagonal indicates a 1 to 1 correlation between the transcriptome and translatome. Violin plots showing $\text{Log}_2(\text{Fold Change})$ in C) translation efficiency (difference between transcriptome and translatome), D) transcriptome, and E) translatome in Δ glh-1 mutants compared to WT. F) Violin plots showing $\text{Log}_2(\text{Fold Change})$ of neuropeptide mRNA accumulation in this and other datasets. For C–F, bold horizontal line = mean, and significance from “all” shown as ****p < 0.0001, ***p < 0.001, **p < 0.01, *p < 0.05, ns p > 0.05. ssq-1 (blue) and msp-142 (orange) levels are indicated in the Spermatogenic (high) and MSP datasets. The dash-dot line connecting D to F indicates a duplication of the same Day 1 Adult data in both panels.

The redundancy of GLH-1 with its paralogs (GLH-2 and GLH-4) makes the analysis of Δ glh-1 advantageous because the germline remains healthy, minimizing the opportunity for secondary effects to cause expression changes. Given the observed impact of GLH-1 on MSP-domain encoding mRNAs, we performed an in-depth analysis of germline phenotypes in Δ glh-1

animals. We previously reported a 14% reduction ($p < 0.0001$) in the fertility of $\Delta glh-1$ compared to WT at permissive temperature (Marnik et al., 2019). Further analysis revealed that brood differences occur within the first two days of egg-laying (Figure 27A). Part of the reduction can be accounted for by a 2.3-fold decrease in PH3-positive (proliferating) germ cells in $\Delta glh-1$ mutants (Figure 27B). Differences in total and polysome-associated mRNA profiles suggested that reduced broods may also reflect defects in spermatogenesis. In fact, $glh-1$ loss-of-function mutants grown at the restrictive temperature of 26 °C often do not have sperm (Spike et al., 2008). To investigate this at the permissive temperature of 20 °C, we counted the number of sperm in the spermatheca of young adult worms and found no difference between WT and $\Delta glh-1$ mutants. These results suggest that at 20 °C, the absence of GLH-1 does not impact spermatogenesis (Figure 27C).

An mCherry:V5 tag was placed on endogenous MSP-142 in WT and $\Delta glh-1$ worms to visualize differences in MSP expression. This translational reporter begins expressing during spermatogenesis in L4-staged hermaphrodites (Figure 27D). It is later observed in the cytoplasm of spermatids, in the pseudopod ends of activated sperm, and in secreted filaments surrounding the most proximal oocytes, reflecting MSP expression patterns previously reported (Roberts et al., 1986). In L4-staged animals, MSP-142:mCherry germline expression expands more distally into developing oocytes (Figure 27E). This reflects the expansion of MSP transcripts into oocytes

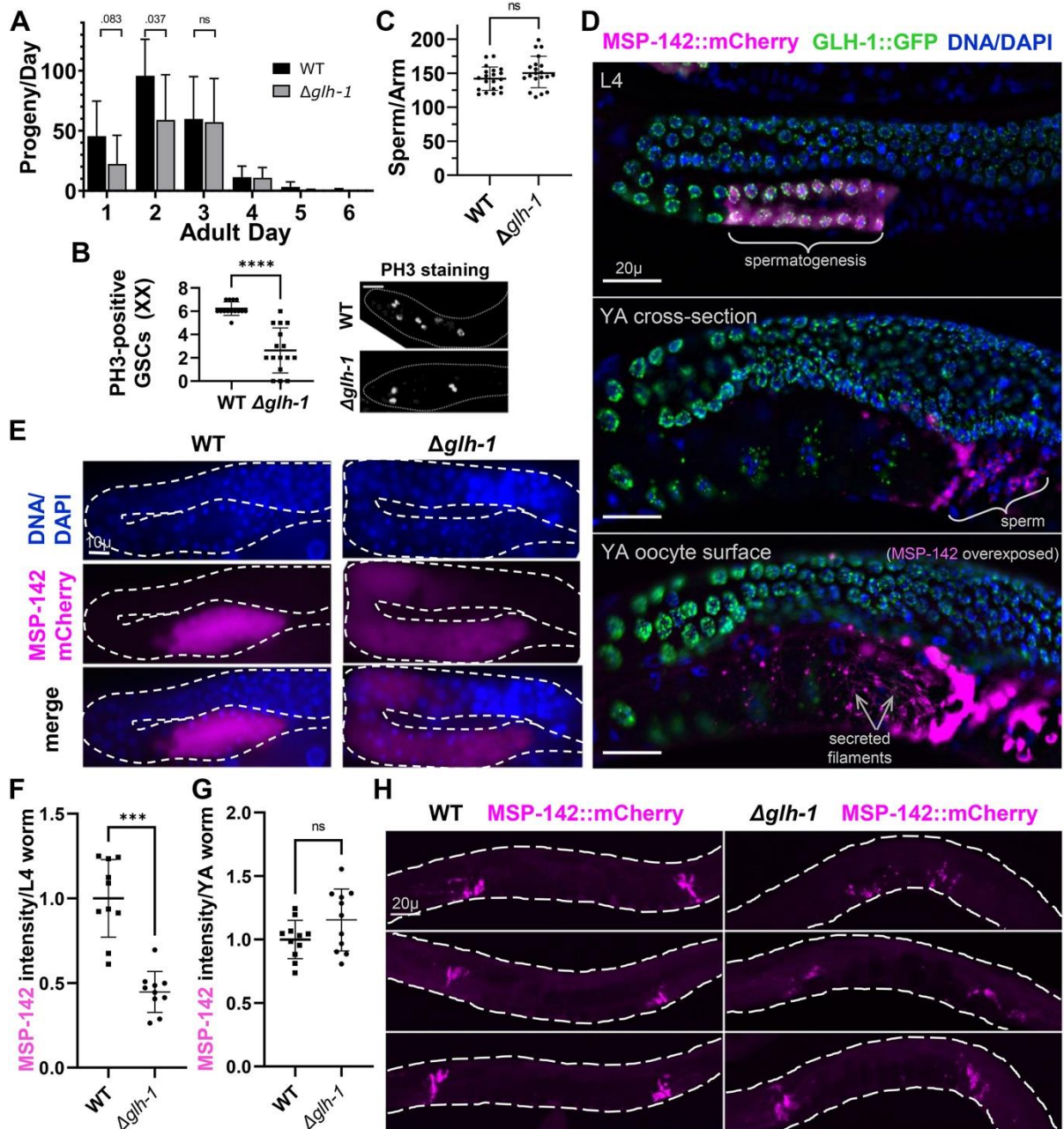


Figure 27: *GLH-1* impact on fertility and *MSP-142* expression.

A) Self-fertility of hermaphrodites in WT and $\Delta glh-1$ mutants during adulthood. B) Quantification of PH3-positive germ cells in distal gonadal ends in WT (n = 14) and $\Delta glh-1$ mutant (n = 16) hermaphrodite gonads. Fluorescence images of distal gonadal ends in WT and

Δ glh-1 mutant gonads immunostained with the anti-PH3 antibody. Representative images are shown. The dashed lines indicate the shape of gonad arms: scale bar, 20 μ m. C) Quantification of the number of DAPI-stained sperm in WT Δ glh-1 mutant hermaphrodites. D) GLH-1:GFP and MSP-142:mCherry expression in L4-stage and young adult (YA) stage animals. Expression of MSP-142 at the YA stage. Gonads were fixed and counter-stained with DAPI (blue): scale bars, 20 μ m. E) MSP-142:mCherry expression in L4 stage WT and Δ glh-1 mutant animals. Gonads were fixed and counter-stained with DAPI (blue): scale bar, 10 μ m. F and G) Quantification of MSP-142:mCherry intensity in WT (n = 10 for F, n = 11 for G) and Δ glh-1 mutant (n = 10 for F, n = 11 for G) L4 and YA stage animals. H) Representative images of MSP-142:mCherry in WT and Δ glh-1 mutant young adults: scale bar, 20 μ m. Error bars indicate s.d., ****p < 0.0001, ***p < 0.001, ns p > 0.05.

previously detected by in situ hybridization following germ-granule RNAi (Campbell & Updike, 2015). However, the expression intensity of MSP-142:mCherry is lower in Δ glh-1 worms, reflecting the decrease of msp-142 mRNA observed in the polysome fraction (Figure 27E and F). This difference in MSP-142:mCherry expression between WT and Δ glh-1 mutants is no longer evident in young adult hermaphrodites (Figure 27G and H), where individual spermatids are condensed in the spermatheca and harder to visualize individually.

To better visualize expression differences at the cellular level, spermatids were dissected from WT and Δ glh-1 males, and MSP-142:mCherry expression intensity was quantified. While sperm from both WT and Δ glh-1 males express MSP-142:mCherry, expression is lower when glh-1 is deleted (Figure 28A). All developmental zones of mitosis and meiosis were comparable between WT and Δ glh-1 mutant males, as visualized in DAPI-stained

morphologies in each germline (Figure 28B). Moreover, co-immunostaining with anti-pH3 and anti- α -tubulin antibodies revealed the presence of karyosomes, diakinesis, metaphase, anaphase, spermatid budding, and mature spermatids in both WT and Δ glh-1 mutant males (Figure 28C) (Shakes et al., 2009). Anti-pH3 staining was also examined in the distal end of male germlines to estimate the rate of mitosis in germline stem cells. As observed in hermaphrodites, a significant but variable mitotic decrease was confirmed in Δ glh-1 males (Figure 28D). While all developmental zones of male and hermaphrodite germlines are present in the absence of GLH-1, germline stem cell proliferation and MSP-142:mCherry expression are reduced, the latter reflecting the decreased expression of MSPs in the transcriptome and translome of Δ glh-1 mutants.

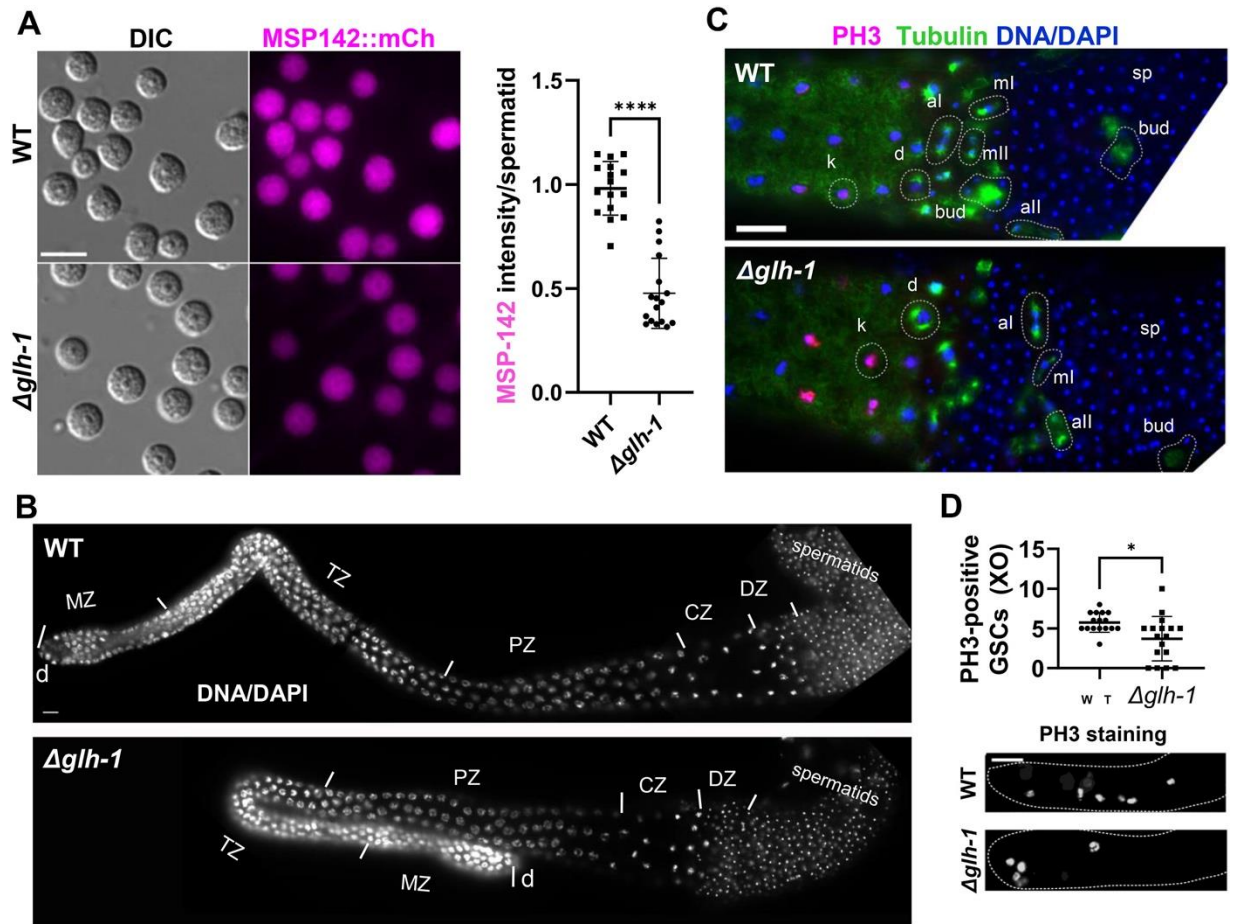


Figure 28: Male germline dependence on GLH-1.

A) Fluorescence live images of spermatids dissected from MSP-142:mCherry males in WT and $\Delta glh-1$ mutants: scale bar, 8 μ m. The plot shows the MSP-142:mCh fluorescence intensity in spermatids from WT and $\Delta glh-1$ mutant males. n = 16 for WT, n = 17 for $\Delta glh-1$. Error bars indicate s.d. ****, p < 0.0001. B) DAPI-stained YA male dissected gonads labeled by the following developmental stages: d, distal end. MZ, mitotic zone. TZ, transition zone. PZ, pachytene zone. CZ, condensation zone. DZ, division zone: scale bar, 10 μ m. C) Spermatogenesis stages are similar in WT and $\Delta glh-1$ mutant males. Meiosis I and II were observed in dissected WT (n = 20) and $\Delta glh-1$ mutant (n = 20) male gonads after co-

immunostaining with anti-PH3 (magenta), anti- α -tubulin (green), and DAPI (blue). k, karyosome. d, diakinesis. ml, metaphase I. al, anaphase I. mII, metaphase II. all, anaphase II. bud, budding spermatid. sp, spermatid: scale bar, 10 μ m. D) Quantification of PH3-positive germ cells in distal gonadal ends in WT (n = 16) and Δ glh-1 mutant (n = 17) male gonads. Error bars indicate s.d. *, p < 0.05. Representative images are shown. Dashed lines indicate the shape of gonad arms: scale bar, 20 μ m.

We next asked how the decrease in MSP expression in Δ glh-1 mutants impacts membranous organelle (MO) fusion and sperm activation. Sperm activating factors, such as Proteinase K (ProK) and ZnCl₂, transition the morphology of round spermatids to adopt a spikey and irregular shape as an intermediate phase before spermatozoa extend pseudopods and become motile (Figure 29A) (Singaravelu et al., 2011). Upon exposure to ProK and ZnCl₂, fewer spermatids were fully activated in Δ glh-1 mutants, and many failed to progress through the spikey and irregular-shaped intermediate phases (Figure 29B and C). The membrane probe FM1-43 fluoresces when MOs fuse to the plasma membrane during spermiogenesis (Washington & Ward, 2006). Staining shows that MO fusion is normal in both WT and Δ glh-1 animals. Although activation does initiate in Δ glh-1 spermatids, there is a defect that coincides with pseudopod extension (Figure 29D). It is known that MSPs migrate asymmetrically to polymerize and drive pseudopod extension, so we examined the distribution of MSP-142:mCherry in WT and Δ glh-1 sperm following activation (Figure 29E). MSP-142 is distributed into the pseudopod but to a lesser extent in Δ glh-1 sperm (Figure 29F). To determine if this redistribution defect was observed in a spermatogenic (high) non-MSP reporter, an N-terminal V5:mCherry tag was placed in-frame and upstream of endogenous *ssq-1* in both WT and Δ glh-1

backgrounds. The distribution of mCherry:SSQ-1 also showed that asymmetric distribution was impacted (Figure 29G). These results suggest that sperm initiate activation, but pseudopod functionality in Δ glh-1 animals is compromised.

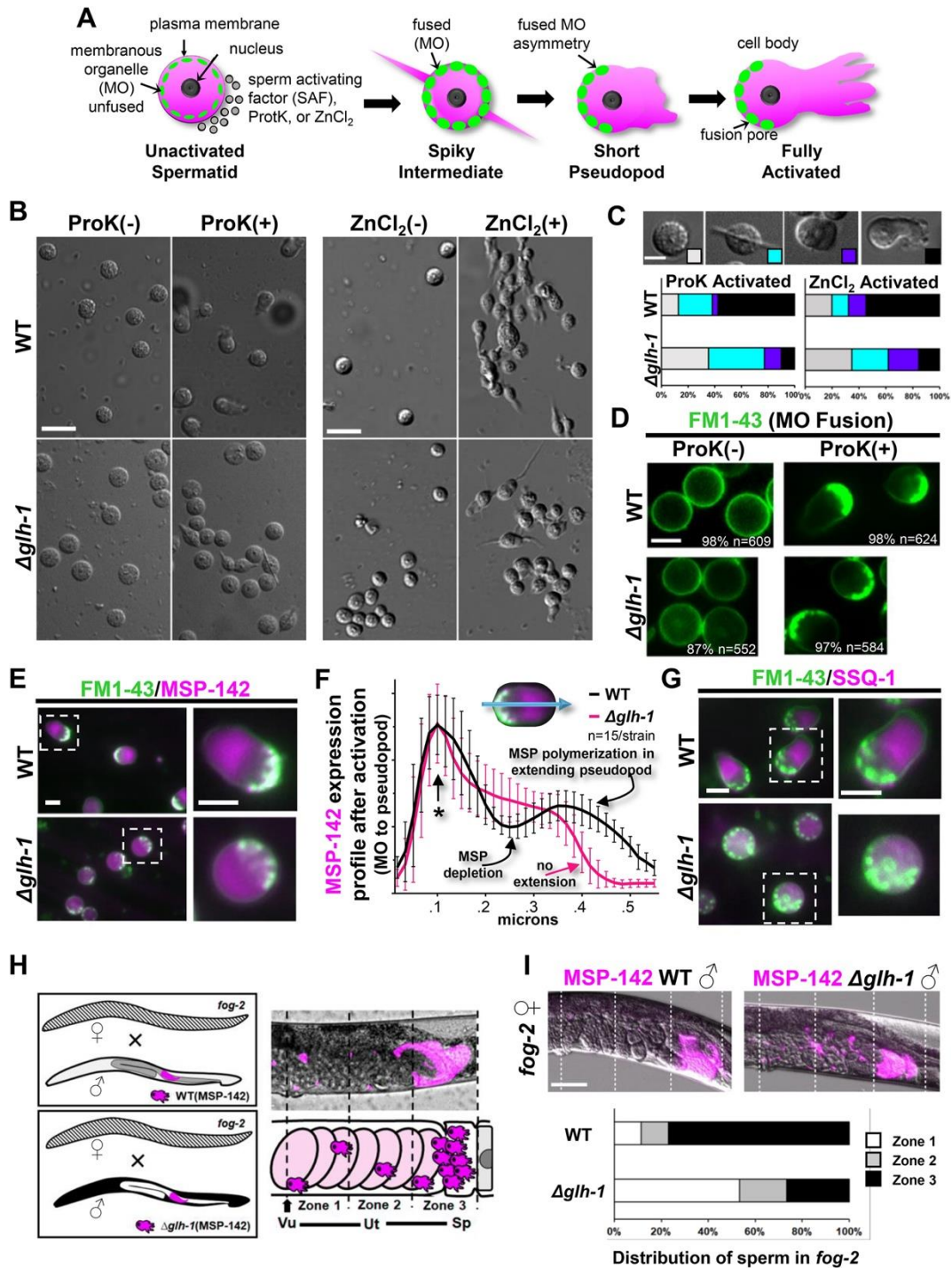


Figure 29: GLH-1 impact on sperm activation.

A) Activation of spermatozoa during *C. elegans* spermiogenesis. Treatment of *C. elegans* spermatids with spermatid-activating factors (SAFs) stimulates the round spermatids to extend pseudopods, transforming them into motile spermatozoa. Membranous organelles (MOs) fuse

with the plasma membrane to release contents into the extracellular space. B) Live images of sperm after in vitro activation by Proteinase K (ProK) or ZnCl₂ treatment from WT and Δ glh-1 mutant males. Representative images are shown: scale bar, 8 μ m. C) Categorized morphologies of sperm after in vitro activation by ProK or ZnCl₂. Stages were defined by the morphology of sperm and its pseudopod extension observed by DIC microscope: scale bar, 4 μ m.

Quantification of sperm of WT (n = 118 for ProK activation, n = 146 for ZnCl₂ activation) and Δ glh-1 mutant (n = 198 for ProK activation, n = 199 for ZnCl₂ activation). D) Live fluorescent images of sperm from WT and Δ glh-1 mutant males stained with FM1-43 to observe MOs after in vitro activation by ProK. Representative images are shown, with the percent and number of sperm with the pictured FM1-43 distribution: scale bar, 4 μ m. E) Live fluorescent images of sperm from WT and Δ glh-1 mutant males stained with FM1-43 after in vitro activation by ProK treatment: scale bar, 4 μ m. F) Average expression intensity profiles (ImageJ) of MSP-142:mCherry in sperm stained with FM1-43 following in vitro activation by ProK. Error bars indicate s.d. An asterisk marks the FM1-43 stained end of activated sperm, where plot profiles were aligned: scale bar, 4 μ m. G) Live fluorescent images of sperm stained with FM1-43 after in vitro activation by ProK treatment on SSQ-1:mCherry from WT and Δ glh-1 mutant males: scale bar, 4 μ m. H) Scheme of sperm migration assay. WT and Δ glh-1 mutant MSP-142:mCherry expressing males were crossed to fog-2 females. The uterus was divided into 3 zones from the vulva (zone 1, arrow) to the spermatheca (zone 3). Vu, vulva. Ut, uterus. Sp, spermatheca. I) Quantification of WT and Δ glh-1 mutant male sperm migration in fog-2 females (n = 26 for WT male, n = 30 for Δ glh-1 mutant male). The fluorescent intensity of each zone was measured and

calculated proportionally against the total fluorescent intensity of all three zones: scale bar, 50 μm .

Spermatozoa are swept into the uterus during ovulation and use their pseudopods to crawl to the spermatheca for further opportunities to fertilize eggs (Ellis & Stanfield, 2014). In male/hermaphrodite matings, pseudopods also allow male sperm to crawl from the vulva through the uterus into the spermatheca. To test whether pseudopod functionality is compromised in $\Delta\text{glh-1}$ animals, *fog-2* females were crossed with MSP-142:mCh expressing males from WT and $\Delta\text{glh-1}$ worms (Figure 29H). MSP-142:mCh expression was examined in three equal-sized zones from the vulva to the distal end of the spermatheca. Sperm expressing wild-type GLH-1 crawl to the spermatheca, while a more significant proportion of $\Delta\text{glh-1}$ mutants have sperm near the vulva (Figure 29I). These results suggest that increased accumulation of MSP-encoding transcripts in the presence of GLH-1 ensures the mobility of activated sperm and may explain the absence of sperm in *glh-1* mutants grown at 26 °C if non-motile sperm purged during ovulation and unable to crawl back.

5.4 Discussion

The somatic reprogramming previously reported with germ-granule RNAi most consistently induced pan-neuronal reporter expression and neurite-like extensions in germ cells (A. K. A. A. Knutson et al., 2016; Updike et al., 2014). Nearly one-third of somatic cells in *C. elegans* are neurons, which may make neuronal differentiation a logical default. A default model for neural induction has been well-established for stem cells and animal development (reviewed in Cao, 2022). Moreover, unsolicited induction of neuronal fates in the *C. elegans* germline can be observed in *mex-3 glh-1* (R. Ciosk et al., 2006), *spr-5 let-418* (Käser-Pébernard

et al., 2014), and *wdr-5.1* (Robert et al., 2014) backgrounds (reviewed in Marchal & Tursun, 2021). Our data suggest that an initial step in somatic reprogramming when core germ-granule components are compromised includes a global increase in neuropeptide expression. The increase is modest but nearly universal among neuropeptide mRNAs in the total and polysome fractions of Δ glh-1 mutants (Figure 26C–E) and also consistent when examined in previously published datasets from isolated germlines following germ-granule depletion (Figure 26F) (Campbell & Updike, 2015; Strome & Updike, 2015). It is unclear how neuropeptides might drive somatic reprogramming in Δ glh-1 mutants, as they are markers of terminal neuron specification. One model is that neuropeptide expression introduces noise, or stochastic variations in gene expression, to prime germ cells for somatic reprogramming. Transcriptional noise may increase responsiveness to fate-determining stimuli and has been shown to potentiate cell fate transitions in stem cells (Desai et al., 2021). Given the low and basal levels of neuropeptide transcripts in wild-type germlines, an alternative model is that the change in neuropeptide expression is simply the easiest readout to detect when default neuronal differentiation is induced and does not necessarily represent a functional step in somatic reprogramming. Unfortunately, the observed increase following germ-granule depletion is not likely sufficient to detect with fluorescent reporters of neuropeptide expression – unless it represents stochastic expression in individual germ cells. It will be interesting to see whether that is the case and if the increase in neuropeptide expression is specific to the loss of core germ granule proteins like GLH-1 or shared in other genetic perturbations that induce somatic reprogramming of the *C. elegans* germline.

Loss of GLH-1 had a very different effect on the expression of MSPs. Decreased expression of MSP-142:mCherry in Δ glh-1 mutants is uniformly observed in developing germ cells and in spermatids. While the presence of GLH-1 suppresses the accumulation of spermatogenic transcripts during oocyte differentiation, it selectively promotes the accumulation and translation of MSP-domain-encoding mRNAs during spermatogenesis. The mechanisms behind the selectivity of GLH-1 for these transcripts merit further investigation. The helicase activity of GLH-1 could linearize conserved structural motifs in MSP-domain-encoding transcripts, making them accessible to translation machinery or small RNA processing. Vasa helicases are thought to exhibit non-sequence-specific RNA binding, but GLH CLIP assays suggest mRNA target specificity is conferred, at least in part, through GLH-associated Argonaute pathways (S. Dai et al., 2022). The selective silencing of spermatogenic genes is known to be mediated through piRNA pathways that interact with GLH-1 (Cornes et al., 2022). Translational silencing by GLH-1-bound microRNAs has also been demonstrated and could be a mechanism for selectivity (Dallaire et al., 2018). Precursory attempts to identify moieties (correlative small RNA and microRNA binding sites, sequence conservation, structural features) capable of distinguishing MSP-domain encoding mRNAs from other germline-expressed or spermatogenic mRNAs showed no strong correlations, but do not exclude the possibility that these moieties exist. Here, we show that lower levels of MSP expression impact pseudopod extension following sperm activation in Δ glh-1 mutants, leading to subtle reductions in fertility even at the permissive temperature. Therefore, one of the primary impacts of loss or depletion of GLH-1 can be observed on sperm motility and function.

Our approach aimed to identify early events during somatic reprogramming of the germline that could be separated from other pleiotropic defects, such as atrophied germlines and germ cell loss. By looking for changes in polysomal-associated mRNAs, we also sought to uncover defects in Δ glh-1 mutants that were masked (or caused) by changes in translational efficiency. We found that early reprogramming events include enhanced expression of neuropeptides and a decrease in MSP expression. The bulk of these changes are correlative at the level of transcription and translation. In fact, Δ glh-1 mutants showed surprisingly little evidence to support a general role for GLH-1 in the selective activation or repression of translation that was independent of mRNA accumulation. Therefore, the functional relevance of GLH-1's association with translation initiation components requires further exploration. What we did observe is that changes in oogenic and spermatogenic (high) mRNA levels from total mRNA sequencing are dampened in the polysome fraction, showing the capacity of systems to reduce or compensate for fluctuations in mRNA abundance of some gene subsets at the level of their translation. This compensation was not observed for changes in MSP- and neuropeptide-encoding transcripts. The reason for discrimination among mRNA types remains unclear but may depend on how GLH-1 interfaces with translation initiation components as mRNAs pass from germ granules and into the cytoplasm for translation.

5. CHAPTER VI: CONCLUDING DISCUSSION AND FUTURE DIRECTIONS

6.1 Chapter Summary

This thesis presents a comprehensive study of the PQN-75 protein, establishing its functions that were previously undefined. Additionally, a protocol for mass collection of synchronized *C. elegans* and a "genetic toolkit" was developed to explore and characterize functional motifs of GLH-1. RNA-seq data sets were analyzed to gain insights into GLH-1's early role in the adult *C. elegans* germline. The analysis revealed that GLH-1 suppresses nearly all neuropeptides 24 hours before previously reported, potentially indicating a marker of early somatic development. GLH-1 also promotes MSP and sperm-associated transcripts, driving spermatogenesis, sperm motility and preserving fertility rates. This work contributes to understanding GLH-1's role in *C. elegans* germline development and provides a platform for future research.

Highlighted findings:

- All gland cells of the *C. elegans* pharynx express PQN-75, which is secreted into the mussel of the pharynx and likely the pharyngeal lumen.
- PQN-75 aids in thermotolerance and innate immunity but is dispensable for germline development.
- Developed a liquid culture protocol for mass collection of synchronized *C. elegans*.
- Created a "genetic tool kit" to define all functional motifs of GLH-1.
- GLH-1 Helicase activity is required to retain an association with P granules.
- Glycine-rich repeats of GLH-1 promote P granules' contact with NPCs.
- Neuropeptides may be an indicator of early somatic development, suppressed by GLH-1
- GLH-1 preferentially up-regulates MSP transcripts, promoting sperm motility.

6.2 Concluding Discussions

6.2.1 PQN-75

The focus of my thesis project was to unravel the intricate mechanisms underlying germ granule function in the *C. elegans* germline, with focuses on GLH-1s role the *C. elegans* germline protein. As previously described in Chapter IV GLH-1 contains a FG repeat domain that plays a critical role in maintaining the microenvironments of these granules. However, our research took an unexpected turn when a mutagenesis screen uncovered the PQN-75 protein, which also contains an FG repeat domain whose functional role had yet to be characterized, thus presenting a potentially novel candidate involved in P granule association.

Our initial analysis, however, revealed that PQN-75 was not dispensable for germline development. As the observed phenotype in our EMS mutant were likely associated with another germline protein. Instead, was expressed exclusively in the gland cells of the *C. elegans* pharynx, where it is likely secreted into the pharyngeal lumen suggested by its presence in all pharyngeal gland cells and ducts. While our initial observations seemed to contradict this conclusion, as we found no expression of PQN-75 outside of gland cells, it is possible that the use of a GFP marker reliant on a C-terminal GFP::3xFLAG tag, may not be expressed in the event of protein proteolysis, offering a potential explanation for this discrepancy. In support of this, it is worth noting that human salivary proline-rich-proteins (PRPs), which make up 20%-30% of all salivary proteins, many of which are excreted proteins that are subject to secondary processing prior to excretion. Moreover, PQN-75 and PRB2, both found exclusively in the gland cells of the upper digestive tract, share a similarity in there sequence particularly in the FG repeat domains.

Recent studies in mammals have demonstrated two primary functionalities of PRPs. First, as essential adhesion antigens, PRPs can initiate an immunological response that attaches to bacteria, such as *Streptococcus*, preventing plaque buildup on tooth enamel and potentially preventing caries (Nobbs et al., 2011). Our findings suggest that PQN-75 may serve a similar role, as demonstrated by the innate immunity results of Chapter III. Specifically, our data implies that PQN-75 may provide lubrication within the pharynx, which could help impede bacterial buildup and maintain optimal feeding behavior, particularly when pathogenic bacteria are present. For example, the introduction of *X. nematophila*, a parasitic bacterium of *C. elegans*, led to an increased buildup of bacteria in the pharyngeal lumen in pqn-75 deletion mutants, supporting the notion that PQN-75 may provide vital lubrication for the pharyngeal lumen and potentially grinder and cuticle integrity demonstrated by our thermotolerance results. Nevertheless, further studies are required to support this hypothesis fully.

Secondly, recent studies have suggested that PRPs, particularly PRB2, play a supporting role in digestion. For example, a study conducted on boars demonstrated that increased consumption of hydrolysable tannins resulted in parotid gland enlargement, along with significant increases in PRB2 expression levels (Mavri et al., 2022). This adaptation enables boars to avoid the anti-nutritive effects of tannins. By secreting high amounts of proline-rich proteins, such as PRB2, in saliva, tannins can bind to these proteins, thereby preventing their interaction with other enzymes and proteins of the digestive tract. Based on our results and presence in the upper digestive tract is plausible that PQN-75 secretion could serve a similar function for *C. elegans* in their natural environment (Schulenburg & Félix, 2017).

6.2.1.1 Future Directions

Our research delved deeply into potential roles of PQN-75 in the *C. elegans*, investigating its potential involvement in processes such as pharyngeal function, gland cell activity, cuticle integrity, and feeding behavior. We established PQN-75 is dispensable for germline development and provided compelling evidence regarding its secretion into the pharyngeal lumen however, further exploration is needed to confirm our predictions. To this end, we propose the use of CRISPR to introduce an N-terminal fluorescent tag on *pqn-75*, enabling visualization of its *in vivo* expression patterns. This approach is likely to reveal differential patterns of excretion distinct from those previously observed through use of a C-terminal GFP::3xFLAG tag. Since secreted proteins often undergo secondary processing, the new tag may enable visualization of PQN-75 expression not only in the pharynx, but also in the lumen of the digestive tract. Additionally, further investigation into the innate immunity potential of PQN-75 is necessary to bolster our findings. The introduction of additional pathogenic bacteria may provide additional supportive evidence, and if the N-terminal GFP tag is present in the lumen, up-regulation of PQN-75 could be observed in response to stressors such as pathogenic bacteria, which could be quantified through quantitative polymerase chain reaction (qPCR).

Finally, since we did not observe continuous excretions of PQN-75 into the pharyngeal lumen, we did not focus extensively on PQN-75 potential effects on the digestive tract. Nonetheless, new data on bores indicates the upregulation of PRB2 in saliva upon exposure to a diet containing increased tannins. The study also demonstrated PRB2s ability to bind to and neutralize tannins, preventing the molecules from interacting with proteins and enzymes of the

digestive track. This finding may point to an overlooked role of PQN-75 in our study. Given that *C. elegans* inhabits the duff and topsoil where organic matter and tannins are present, and that tannins are water-soluble. It is likely that *C. elegans* has an innate immunity to neutralize the effects of tannins of the digestive track's pH levels, like bores. This role of PQN-75 may be masked in a laboratory setting. However, the effects could be observed by increasing the levels of tannins in agar plates and quantifying the expression levels of PQN-75 using qPCR in both deletion mutants and wild-type worms. In conclusion, the upregulation of PRB2 in bores upon exposure to increased tannins may indicate an overlooked role of PQN-75 in the digestive tract of *C. elegans* that will further define the proteins' role in a natural setting. All strains used in this study are available upon request.

6.2.2 GLH-1

Since our initial focus for this thesis was on germline stem cell development, we turned our attention to GLH-1, a protein crucial to the germline of *C. elegans*. Like PQN-75, several germ granule proteins in the *C. elegans* germline possess disordered glycine-rich domains interspersed with phenylalanine repeats (FG- or RG-repeats), including GLH-1. As an ATP-dependent DEAD-box helicase, GLH-1 plays a critical role in specifying and safeguarding the germline of *C. elegans*. Our work in Chapter IV provides further evidence for its involvement in the regulation of translation, amplification of piwi-interacting RNAs (piRNAs), and functioning as an RNA chaperone. This includes the development of a "genetic toolkit" by utilizing advancements in CRISPR/Cas9 genetic engineering systems to create 28 endogenous mutant alleles targeting the functional motifs of GLH-1.

Our findings contribute to a deeper understanding of GLH-1's functional domains and indicate that its helicase activity is essential for association with P granules and NPCs, which compartmentalize the cytoplasm to exclude large protein assemblies. This effectively creates a secondary microenvironment outside the nucleus, shielding transcripts from translation initiation factors. Furthermore, this study uncovers an affinity between GLH-1 and three structurally conserved PCI (26S Proteasome Lid, COP9, and eIF3) complexes, or "zomes," which likely aid in selective translational processes initiated by GLH-1, as discussed in Chapter V. These findings warrant further investigation into the precise interactions between GLH-1 and its binding partners.

6.2.2.1 Future Directions

The eIF3 complex is of particular interest since nearly all its subunits were found to interact with GLH-1 in Chapter IV's IP data sets, including the ribosomal 40S subunit eIF3 interacts with. Dr. Dustin Updike's current, unpublished results from a yeast two-hybrid screen with full-length GLH-1 revealed six high-confidence interactions, including eIF3g. This finding is particularly interesting since eIF3g is not part of the multi-protein core of the eIF3 scaffold (Figure 30); instead, eIF3g is part of eIF3s RNA-binding periphery. Tagging eIF3g with RFP has demonstrated its presence throughout the germline cytoplasm and within P granules themselves (Figure 30). When a core scaffold element of the eIF3 complex, such as eIF3a, is tagged with RFP, it reveals the eIF3 complex to be in close association with P granules but only localizing near the size exclusion barrier. Our current hypothesis is that eIF3 anchors to granules' periphery through the interaction between eIF3g and GLH-1. Super-resolution

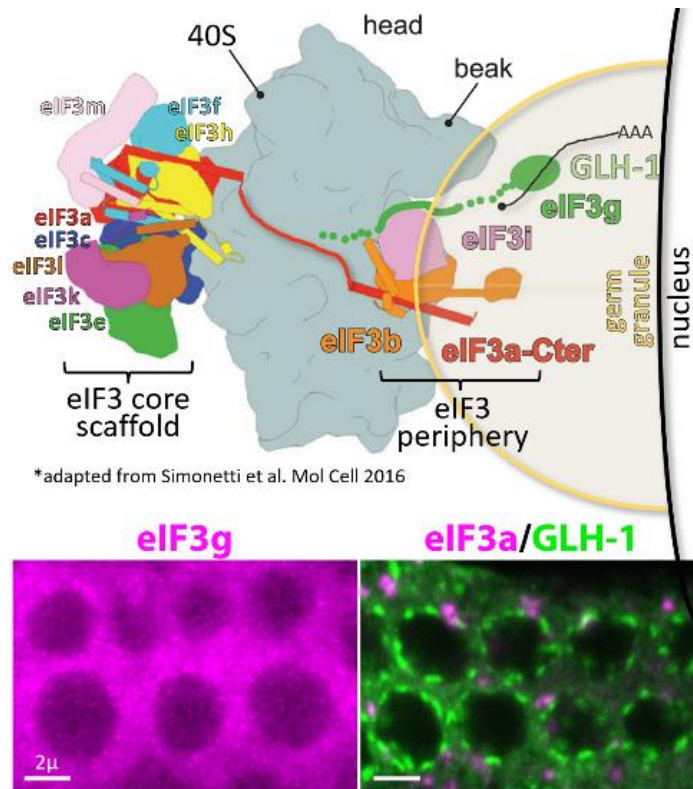


Figure 30: eIF3 interaction with *P* granules nuclear periphery.

Top - Model for eIF3 assembly at the germ-granule periphery. Bottom left Live (non-SR) imaging of eIF3g in the cytoplasm, and Bottom right eIF3a in foci that dock with germ granules.

microscopy will be used to determine this possibility in conjunction with the tagging of other eIF3 subunits to reconfirm observations with eIF3a.

Given our demonstrated results in Chapter V that GLH-1 selectively promotes sperm-associated transcripts while suppressing nearly all neuropeptides, one current hypothesis is that the observed interaction between GLH-1 and eIF3g could be used to ferry germline-licensed transcripts to be selectively translated in the germline cytoplasm. To confirm this, smFISH could be used to tag the various transcripts GLH-1 interacts with, using our data sets in Chapter V to determine where the most transcript accumulation occurs and its proximity to

ribosome-rich regions of the germline cytoplasm. These results will help further our understanding of the roles of eIF3 and GLH-1 and potentially reveal how integrations with each other preserve GSC through selective promotion or suppression of mRNA transcripts. That could not be defined through sequence similarity in our RNA-seq data sets.

6.2.3 Somatic Reprogramming

Germ granules have been shown to play a crucial role in maintaining the functionality of germline stem cells and preserving germ line integrity (Updike et al., 2014). Depletion of core P granule components in *C. elegans* has been demonstrated to result in increased sterility rates and markers for somatic development. In this study, we build on previous work by analyzing GLH-1 RNA-seq data sets to uncover the earliest signs of germ cell reprogramming events in the *C. elegans* germline.

To collect highly synchronized worms for analysis, we developed a liquid culture protocol, enabling the examination of the transcriptome and translome of healthy wild-type and *glh-1* deletion mutants a full day before previous reports. Our analysis revealed two significant discoveries. First, GLH-1 was found to increase the translational efficiency of nearly all MSP-encoding mRNA, promoting sperm mobility by aiding the MSP chain elongation process within sperm pseudopods. However, the reason for the discrimination among mRNA types remains unclear and may depend on how GLH-1 interfaces with translation initiation components such as eIF3. Second, we observed an accumulation of nearly all neuropeptide-encoding mRNA during early somatic reprogramming in the germline of *glh-1* deletion mutants. These findings align with the default model of neural induction established for stem cells and animal development (Cao, 2022). However, it was surprising that neuropeptide expression

occurs before known neuron-expressed transcription and specification factors since neuropeptides are typical markers of terminal neuron specifications. This observation suggests that neuropeptide expression is a functional step to direct GSCs towards somatic reprogramming, introducing noise or stochastic variations in gene expression, and potentially priming GSCs for neuronal induction.

To confirm these findings in living animals (discussed below), future steps will aim to determine whether the increase in neuropeptide expression is specific to the loss of core germ granule proteins like GLH-1 or whether it is a shared trait in other granule components that induce somatic reprogramming in the *C. elegans* germline.

6.2.3.1 Future Directions

The results of our study demonstrate that GLH-1 has the ability to suppress the global signal of neuropeptide expression in the *C. elegans* germline while selectively driving sperm-associated transcripts, with a particular affinity to MSP transcripts. However, the use of whole worms in our RNA-seq study prevents us from definitively determining if these changes represent a global increase of neuropeptide expression in all germ cells or a stochastic variation where initial expression of one germ cell potentiates a response to neighboring cells. To determine this single-cell sequencing approaches are often used for this purpose, however, these methods were not considered for our RNA-seq study due to their unsuitability for analyzing germ cells housed in a cytoplasmic syncytium. The profiling of single nuclei would likely miss effects conferred through the shared cytoplasm and the germ granules dispersed throughout the distal germline's shared cytoplasm, resulting in a misrepresentation of the distal

germ cells microenvironment. Furthermore, single-cell sequencing is also unlikely to detect the low expression levels of *C. elegans* 119 neuropeptide encoding transcripts.

A more practical solution for quantifying neuropeptide transcripts while providing a clear spatial mRNA expression reference, including neuropeptide precursor translation, would be to use single-molecule fluorescence in situ hybridization (smFISH). This method has been shown to work well in the *C. elegans* germline and can detect low-level expression of neuropeptide-encoding transcripts. The use of smFISH will provide further clarification if increases in neuropeptide signals are increased globally or stochastically within the *C. elegans* germline.

Our next steps will involve identifying potential candidates of interest amongst the 119 neuropeptides expressed in the *C. elegans*, using smFISH to provide further support to our total RNA-seq findings. Additionally, we will select and tag specific neuropeptide proteins with RFP tags using CRISPR to support our translation data sets. For instance, RFamide (Processed FLP neuropeptides) *npl-75* or *nlp-39* were both upregulated in our total and translational RNA-seq data sets in the GLH-1 deletion mutants (DUP144). By adding an RFP marker in both our WT (DUP64) and DUP144 lines, we will be able to visualize and quantify whether observable differences can be found in protein levels of various neuropeptides using expression intensity protocols described in (Marnik et al., 2019).

Our data also suggests that neuropeptides may be an indicator of the early events of a shift to somatic development. However, GLH-1 mutant backgrounds are not the only ones where a shift to somatic development within the *C. elegans* germline can be observed. Similar traits can be found in the mutant backgrounds of *mex-3*, *gld-1*, *spr-5*, *let-418*, and *wdr-5.1*. To

determine if a similar effect of neuropeptides can be observed in these mutant lines, the previously mentioned neuropeptide lines could be crossed into these backgrounds to observe if global or stochastic increases of neuropeptides can be seen in the translation of mRNA and at the protein level. These experiments can be used to further support our findings' suggestions that increases in neuropeptides are an early event of somatic development, increase its significance, or determine if these effects are specific to GLH-1.

6.3 Concluding Remarks

The significance of the findings in this thesis are not limited to germ granules' influence on gene expression regulation within the *C. elegans* germline. Rather, our results offer novel insights into the intricate regulatory mechanisms acting to govern neuropeptide expression during the earliest stages of neurogenesis in stem cells. The insights gained from our research have the potential to advise and advance our understanding of gene expression control within the stem cells cytoplasm that may help direct stem cells specification, providing insights into the fields of regenerative medicine and neuroscience.

REFERENCES

1. Albertson, D. G., & Thomson, J. N. (1976). The pharynx of *Caenorhabditis elegans*. *Philosophical Transactions of the Royal Society of London. Series B, Biological Sciences*, 275(938), 299–325. <https://doi.org/10.1098/RSTB.1976.0085>
2. Andralojc, K. M., Campbell, A. C., Kelly, A. L., Terrey, M., Tanner, P. C., Gans, I. M., Senter-Zapata, M. J., Khokhar, E. S., & Updike, D. L. (2017). ELLI-1, a novel germline protein, modulates RNAi activity and P-granule accumulation in *Caenorhabditis elegans*. *PLOS Genetics*, 13(2), e1006611. <https://doi.org/10.1371/JOURNAL.PGEN.1006611>
3. Antonov, S. A., & Novosadova, E. v. (2021). Current State-of-the-Art and Unresolved Problems in Using Human Induced Pluripotent Stem Cell-Derived Dopamine Neurons for Parkinson's Disease Drug Development. *International Journal of Molecular Sciences* 2021, Vol. 22, Page 3381, 22(7), 3381. <https://doi.org/10.3390/IJMS22073381>
4. Aoki, S. T., Kershner, A. M., Bingman, C. A., Wickens, M., & Kimble, J. (2016). PGL germ granule assembly protein is a base-specific, single-stranded RNase. *Proceedings of the National Academy of Sciences of the United States of America*, 113(5), 1279–1284. https://doi.org/10.1073/PNAS.1524400113/SUPPL_FILE/PNAS.201524400SI.PDF
5. Assinck, P., Duncan, G. J., Hilton, B. J., Plemel, J. R., & Tetzlaff, W. (2017). Cell transplantation therapy for spinal cord injury. *Nature Neuroscience* 2017 20:5, 20(5), 637–647. <https://doi.org/10.1038/nn.4541>
6. Baker, A. M. E., Roberts, T. M., & Stewart, M. (2002). 2.6 Å resolution crystal structure of helices of the motile major sperm protein (MSP) of *Caenorhabditis elegans*. *Journal of Molecular Biology*, 319(2), 491–499. [https://doi.org/10.1016/S0022-2836\(02\)00294-2](https://doi.org/10.1016/S0022-2836(02)00294-2)
7. Baugh, L. R., DeModena, J., & Sternberg, P. W. (2009). RNA Pol II accumulates at promoters of growth genes during developmental arrest. *Science*, 324(5923), 92–94. https://doi.org/10.1126/SCIENCE.1169628/SUPPL_FILE/BAUGH.SOM.PDF
8. Beck, M., & Hurt, E. (2017). The nuclear pore complex: understanding its function through structural insight. *Nature Reviews. Molecular Cell Biology*, 18(2), 73–89. <https://doi.org/10.1038/NRM.2016.147>
9. Bezares-Calderón, L. A., Becerra, A., Salinas, L. S., Maldonado, E., & Navarro, R. E. (2010). Bioinformatic analysis of P granule-related proteins: Insights into germ granule evolution in nematodes. *Development Genes and Evolution*, 220(1–2), 41–52. <https://doi.org/10.1007/S00427-010-0327-3/METRICS>
10. Bourgeois, C. F., Mortreux, F., & Auboeuf, D. (2016a). The multiple functions of RNA helicases as drivers and regulators of gene expression. *Nature Reviews Molecular Cell Biology* 2016 17:7, 17(7), 426–438. <https://doi.org/10.1038/nrm.2016.50>

11. Bourgeois, C. F., Mortreux, F., & Auboeuf, D. (2016b). The multiple functions of RNA helicases as drivers and regulators of gene expression. *Nature Reviews Molecular Cell Biology*, 17(7), 426–439. <https://doi.org/10.1038/NRM.2016.50>
12. Boveri, T. (1892). *Über die Entstehung des Gegensatzes zwischen den Geschlechtszellen und den somatischen Zellen bei Ascaris megalocephala*. *Sitzungsk. Ges. Morphol. Physiol.* <https://www.scopus.com/record/display.uri?eid=2-s2.0-0006971888&origin=inward&txGid=a03bed826ff645e228d678d211305465>
13. Brangwynne, C. P., Eckmann, C. R., Courson, D. S., Rybarska, A., Hoege, C., Gharakhani, J., Jülicher, F., & Hyman, A. A. (2009). Germline P granules are liquid droplets that localize by controlled dissolution/condensation. *Science*, 324(5935), 1729–1732. https://doi.org/10.1126/SCIENCE.1172046/SUPPL_FILE/BRANGWYNNE.SOM.PDF
14. Brenner, S. (1974). THE GENETICS OF CAENORHABDITIS ELEGANS. *Genetics*, 77(1), 71–94. <https://doi.org/10.1093/GENETICS/77.1.71>
15. Bullock, T. L., Roberts, T. M., & Stewart, M. (1996). 2.5 A resolution crystal structure of the motile major sperm protein (MSP) of *Ascaris suum*. *Journal of Molecular Biology*, 263(2), 284–296. <https://doi.org/10.1006/JMBI.1996.0575>
16. Burke, D. J., & Ward, S. (1983). Identification of a large multigene family encoding the major sperm protein of *Caenorhabditis elegans*. *Journal of Molecular Biology*, 171(1), 1–29. [https://doi.org/10.1016/S0022-2836\(83\)80312-X](https://doi.org/10.1016/S0022-2836(83)80312-X)
17. Cabras, T., Pisano, E., Mastinu, A., Denotti, G., Pusceddu, P. P., Inzitari, R., Fanali, C., Nemolato, S., Castagnola, M., & Messana, I. (2010). Alterations of the salivary secretory peptidome profile in children affected by type 1 diabetes. *Molecular and Cellular Proteomics*, 9(10), 2099–2108. <https://doi.org/10.1074/mcp.M110.001057>
18. Campbell, A. C., & Updike, D. L. (2015). CSR-1 and P granules suppress sperm-specific transcription in the *C. elegans* germline. *Development (Cambridge)*, 142(10), 1745–1755. <https://doi.org/10.1242/DEV.121434/-/DC1>
19. Cao, Y. (2022). Neural is Fundamental: Neural Stemness as the Ground State of Cell Tumorigenicity and Differentiation Potential. *Stem Cell Reviews and Reports*, 18(1), 37–55. <https://doi.org/10.1007/S12015-021-10275-Y>
20. Carrera, P., Johnstone, O., Nakamura, A., Casanova, J., Jäckle, H., & Lasko, P. (2000). VASA Mediates Translation through Interaction with a *Drosophila* yIF2 Homolog. *Molecular Cell*, 5(1), 181–187. [https://doi.org/10.1016/S1097-2765\(00\)80414-1](https://doi.org/10.1016/S1097-2765(00)80414-1)

21. Castrillon, D. H., Quade, B. J., Wang, T. Y., Quigley, C., & Crum, C. P. (2000). The human VASA gene is specifically expressed in the germ cell lineage. *Proceedings of the National Academy of Sciences*, 97(17), 9585–9590. <https://doi.org/10.1073/PNAS.160274797>
22. Cheloufi, S., & Hochedlinger, K. (2017a). Emerging roles of the histone chaperone CAF-1 in cellular plasticity. *Current Opinion in Genetics & Development*, 46, 83–94. <https://doi.org/10.1016/J.GDE.2017.06.004>
23. Cheloufi, S., & Hochedlinger, K. (2017b). Emerging roles of the histone chaperone CAF-1 in cellular plasticity. *Current Opinion in Genetics & Development*, 46, 83–94. <https://doi.org/10.1016/J.GDE.2017.06.004>
24. Chen, W., Brown, J. S., He, T., Wu, W. S., Tu, S., Weng, Z., Zhang, D., & Lee, H. C. (2022). GLH/VASA helicases promote germ granule formation to ensure the fidelity of piRNA-mediated transcriptome surveillance. *Nature Communications* 2022 13:1, 13(1), 1–14. <https://doi.org/10.1038/s41467-022-32880-2>
25. Chen, W., Hu, Y., Lang, C. F., Brown, J. S., Schwabach, S., Song, X., Zhang, Y., Munro, E., Bennett, K., Zhang, D., & Lee, H. C. (2020). The Dynamics of P Granule Liquid Droplets Are Regulated by the *Caenorhabditis elegans* Germline RNA Helicase GLH-1 via Its ATP Hydrolysis Cycle. *Genetics*, 215(2), 421–434. <https://doi.org/10.1534/GENETICS.120.303052>
26. Cohen, D. E., & Melton, D. (2011). Turning straw into gold: directing cell fate for regenerative medicine. *Nature Reviews Genetics* 2011 12:4, 12(4), 243–252. <https://doi.org/10.1038/nrg2938>
27. Consortium*, T. C. *elegans* S. (1998). Genome sequence of the nematode *C. elegans*: A platform for investigating biology. *Science*, 282(5396), 2012–2018. https://doi.org/10.1126/SCIENCE.282.5396.2012/SUPPL_FILE/C-ELEGANS.XHTML
28. Cordin, O., Banroques, J., Tanner, K., Linder, P., & Tanner, N. K. (2006). *The DEAD-box protein family of RNA helicases*. <https://doi.org/10.1016/j.gene.2005.10.019>
29. Cornes, E., Bourdon, L., Singh, M., Mueller, F., Quarato, P., Wernersson, E., Bienko, M., Li, B., & Cecere, G. (2022). piRNAs initiate transcriptional silencing of spermatogenic genes during *C. elegans* germline development. *Developmental Cell*, 57(2), 180–196.e7. <https://doi.org/10.1016/J.DEVCEL.2021.11.025>
30. Couillault, C., & Ewbank, J. J. (2002). Diverse bacteria are pathogens of *Caenorhabditis elegans*. *Infection and Immunity*, 70(8), 4705–4707. <https://doi.org/10.1128/IAI.70.8.4705-4707.2002/ASSET/04861020-D131-49E0-AAD7-634DA85C6840/ASSETS/GRAPHIC/II0820042002.JPEG>

31. Cruciat, C. M., Dolde, C., De Groot, R. E. A., Ohkawara, B., Reinhard, C., Korswagen, H. C., & Niehrs, C. (2013). RNA helicase DDX3 is a regulatory subunit of casein kinase 1 in Wnt- β -catenin signaling. *Science*, 339(6126), 1436–1441. https://doi.org/10.1126/SCIENCE.1231499/SUPPL_FILE/CRUCIAT.SM.PDF
32. Dai, P., Wang, X., Gou, L. T., Li, Z. T., Wen, Z., Chen, Z. G., Hua, M. M., Zhong, A., Wang, L., Su, H., Wan, H., Qian, K., Liao, L., Li, J., Tian, B., Li, D., Fu, X. D., Shi, H. J., Zhou, Y., & Liu, M. F. (2019). A Translation-Activating Function of MIWI/piRNA during Mouse Spermiogenesis. *Cell*, 179(7), 1566–1581.e16. <https://doi.org/10.1016/J.CELL.2019.11.022>
33. Dai, S., Tang, X., Li, L., Ishidate, T., Ozturk, A. R., Chen, H., Dude, A. L., Yan, Y. H., Dong, M. Q., Shen, E. Z., & Mello, C. C. (2022). A family of *C. elegans* VASA homologs control Argonaute pathway specificity and promote transgenerational silencing. *Cell Reports*, 40(10), 111265. <https://doi.org/10.1016/J.CELREP.2022.111265>
34. Dallaire, A., Frédérick, P. M., & Simard, M. J. (2018). Somatic and Germline MicroRNAs Form Distinct Silencing Complexes to Regulate Their Target mRNAs Differently. *Developmental Cell*, 47(2), 239–247.e4. <https://doi.org/10.1016/J.DEVCEL.2018.08.022>
35. de Luca, M., Aiuti, A., Cossu, G., Parmar, M., Pellegrini, G., & Robey, P. G. (2019). Advances in stem cell research and therapeutic development. *Nature Cell Biology* 2019 21:7, 21(7), 801–811. <https://doi.org/10.1038/s41556-019-0344-z>
36. Dehghani, M., & Lasko, P. (2015). In vivo mapping of the functional regions of the DEAD-box helicase Vasa. *Biology Open*, 4(4), 450–462. <https://doi.org/10.1242/BIO.201410579>
37. Dehghani, M., & Lasko, P. (2016). C-terminal residues specific to Vasa among DEAD-box helicases are required for its functions in piRNA biogenesis and embryonic patterning. *Development Genes and Evolution*, 226(6), 401–412. <https://doi.org/10.1007/S00427-016-0560-5/FIGURES/8>
38. Delemarre, E. M., van den Broek, T., Mijnheer, G., Meerding, J., Wehrens, E. J., Olek, S., Boes, M., van Herwijnen, M. J. C., Broere, F., van Royen, A. v., Wulffraat, N. M., Prakken, B. J., Spierings, E., & van Wijk, F. (2016). Autologous stem cell transplantation aids autoimmune patients by functional renewal and TCR diversification of regulatory T cells. *Blood*, 127(1), 91–101. <https://doi.org/10.1182/BLOOD-2015-06-649145>
39. DeRenzo, C., Reese, K. J., & Seydoux, G. (2003). Exclusion of germ plasm proteins from somatic lineages by cullin-dependent degradation. *Nature* 2003 424:6949, 424(6949), 685–689. <https://doi.org/10.1038/nature01887>
40. Desai, R. V., Chen, X., Martin, B., Chaturvedi, S., Hwang, D. W., Li, W., Yu, C., Ding, S., Thomson, M., Singer, R. H., Coleman, R. A., Hansen, M. M. K., & Weinberger, L. S. (2021). A DNA repair pathway can regulate transcriptional noise to promote cell fate transitions.

Science, 373(6557).

https://doi.org/10.1126/SCIENCE.ABC6506/SUPPL_FILE/SCIENCE.ABC6506_TABLES_S1_TO_S8.ZIP

41. Detwiler, M. R., Reuben, M., Li, X., Rogers, E., & Lin, R. (2001). Two Zinc Finger Proteins, OMA-1 and OMA-2, Are Redundantly Required for Oocyte Maturation in *C. elegans*. *Developmental Cell*, 1(2), 187–199. [https://doi.org/10.1016/S1534-5807\(01\)00026-0](https://doi.org/10.1016/S1534-5807(01)00026-0)
42. Dor, Y., Brown, J., Martinez, O. I., & Melton, D. A. (2004). Adult pancreatic β -cells are formed by self-duplication rather than stem-cell differentiation. *Nature* 2004 429:6987, 429(6987), 41–46. <https://doi.org/10.1038/nature02520>
43. Draper, B. W., Mello, C. C., Bowerman, B., Hardin, J., & Priess, J. R. (1996). MEX-3 Is a KH Domain Protein That Regulates Blastomere Identity in Early *C. elegans* Embryos. *Cell*, 87(2), 205–216. [https://doi.org/10.1016/S0092-8674\(00\)81339-2](https://doi.org/10.1016/S0092-8674(00)81339-2)
44. Eckmann, C. R., Kraemer, B., Wickens, M., & Kimble, J. (2002). GLD-3, a Bicaudal-C Homolog that Inhibits FBF to Control Germline Sex Determination in *C. elegans*. *Developmental Cell*, 3(5), 697–710. [https://doi.org/10.1016/S1534-5807\(02\)00322-2](https://doi.org/10.1016/S1534-5807(02)00322-2)
45. Eguchi, A., Lee, G. O., Wan, F., Erwin, G. S., & Ansari, A. Z. (2014). Controlling gene networks and cell fate with precision-targeted DNA-binding proteins and small-molecule-based genome readers. *The Biochemical Journal*, 462(3), 397–413. <https://doi.org/10.1042/BJ20140400>
46. Ellis, R. E., & Stanfield, G. M. (2014). The regulation of spermatogenesis and sperm function in nematodes. *Seminars in Cell & Developmental Biology*, 29, 17–30. <https://doi.org/10.1016/J.SEMCDB.2014.04.005>
47. Engelmann, I., Griffon, A., Tichit, L., Montañana-Sanchis, F., Wang, G., Reinke, V., Waterston, R. H., Hillier, L. D. W., & Ewbank, J. J. (2011). A Comprehensive Analysis of Gene Expression Changes Provoked by Bacterial and Fungal Infection in *C. elegans*. *PLOS ONE*, 6(5), e19055. <https://doi.org/10.1371/JOURNAL.PONE.0019055>
48. Ewen-Campen, B., Schwager, E. E., & Extavour, C. G. M. (2010). The molecular machinery of germ line specification. *Molecular Reproduction and Development*, 77(1), 3–18. <https://doi.org/10.1002/MRD.21091>
49. Fang, Y., Gao, T., Zhang, B., & Pu, J. (2018). Recent Advances: Decoding Alzheimer's Disease With Stem Cells. *Frontiers in Aging Neuroscience*, 10, 77. <https://doi.org/10.3389/FNAGI.2018.00077>
50. Ferizi, L., Dragidella, F., Spahiu, L., Begzati, A., & Kotori, V. (2018). The Influence of Type 1 Diabetes Mellitus on Dental Caries and Salivary Composition. *International Journal of Dentistry*, 2018. <https://doi.org/10.1155/2018/5780916>

51. Fire, A., Xu, S., Montgomery, M. K., Kostas, S. A., Driver, S. E., & Mello, C. C. (1998). Potent and specific genetic interference by double-stranded RNA in *Caenorhabditis elegans*. *Nature*, *391*(6669), 806–811. <https://doi.org/10.1038/35888>
52. Flibotte, S., Edgley, M. L., Chaudhry, I., Taylor, J., Neil, S. E., Rogula, A., Zapf, R., Hirst, M., Butterfield, Y., Jones, S. J., Marra, M. A., Barstead, R. J., & Moerman, D. G. (2010). Whole-Genome Profiling of Mutagenesis in *Caenorhabditis elegans*. *Genetics*, *185*(2), 431–441. <https://doi.org/10.1534/GENETICS.110.116616>
53. Fujita, M., Takasaki, T., Nakajima, N., Kawano, T., Shimura, Y., & Sakamoto, H. (2002). MRG-1, a mortality factor-related chromodomain protein, is required maternally for primordial germ cells to initiate mitotic proliferation in *C. elegans*. *Mechanisms of Development*, *114*(1–2), 61–69. [https://doi.org/10.1016/S0925-4773\(02\)00058-8](https://doi.org/10.1016/S0925-4773(02)00058-8)
54. Fujiwara, T., Dunn, N. R., & Hogan, B. L. M. (2001). Bone morphogenetic protein 4 in the extraembryonic mesoderm is required for allantois development and the localization and survival of primordial germ cells in the mouse. *Proceedings of the National Academy of Sciences of the United States of America*, *98*(24), 13739–13744. <https://doi.org/10.1073/PNAS.241508898>
55. Fujiwara, Y., Komiya, T., Kawabata, H., Sato, M., Fujimoto, H., Furusawa, M., & Noce, T. (1994). Isolation of a DEAD-family protein gene that encodes a murine homolog of *Drosophila vasa* and its specific expression in germ cell lineage. *Proceedings of the National Academy of Sciences*, *91*(25), 12258–12262. <https://doi.org/10.1073/PNAS.91.25.12258>
56. Gallo, C. M., Wang, J. T., Motegi, F., & Seydoux, G. (2010). Cytoplasmic partitioning of P granule components is not required to specify the germline in *C. elegans*. *Science*, *330*(6011), 1685–1689. https://doi.org/10.1126/SCIENCE.1193697/SUPPL_FILE/GALLO_SOM.PDF
57. Gao, G., Deeb, F., Mercurio, J. M., Parfenova, A., Smith, P. A., & Bennett, K. L. (2012). PAN-1, a P-granule component important for *C. elegans* fertility, has dual roles in the germline and soma. *Developmental Biology*, *364*(2), 202–213. <https://doi.org/10.1016/J.YDBIO.2012.02.006>
58. Gaudet, J., & Mango, S. E. (2002). Regulation of organogenesis by the *Caenorhabditis elegans* FoxA protein PHA-4. *Science*, *295*(5556), 821–825. https://doi.org/10.1126/SCIENCE.1065175/SUPPL_FILE/GUADETTABLE3.PDF
59. Gavis, E. R., & Lehmann, R. (1994). Translational regulation of nanos by RNA localization. *Nature* *1994* *369*:6478, *369*(6478), 315–318. <https://doi.org/10.1038/369315a0>

60. George-Raizen, J. B., Shockley, K. R., Trojanowski, N. F., Lamb, A. L., & Raizen, D. M. (2014). Dynamically-expressed prion-like proteins form a cuticle in the pharynx of *Caenorhabditis elegans*. *Biology Open*, *3*(11), 1139–1149. <https://doi.org/10.1242/BIO.20147500>
61. Griffin, E. E., Odde, D. J., & Seydoux, G. (2011). Regulation of the MEX-5 Gradient by a Spatially Segregated Kinase/Phosphatase Cycle. *Cell*, *146*(6), 955–968. <https://doi.org/10.1016/J.CELL.2011.08.012>
62. Gruidl, M. E., Smith, P. A., Kuznicki, K. A., McCrone, J. S., Kirchner, J., Rousell, D. L., Strome, S., & Bennett, K. L. (1996). Multiple potential germ-line helicases are components of the germ-line-specific P granules of *Caenorhabditis elegans*. *Proceedings of the National Academy of Sciences*, *93*(24), 13837–13842. <https://doi.org/10.1073/PNAS.93.24.13837>
63. Guedes, S., & Priess, J. R. (1997). The *C. elegans* MEX-1 protein is present in germline blastomeres and is a P granule component. *Development*, *124*(3), 731–739. <https://doi.org/10.1242/DEV.124.3.731>
64. Gupta, P., Leahul, L., Wang, X., Wang, C., Bakos, B., Jasper, K., & Hansen, D. (2015). Proteasome regulation of the chromodomain protein MRG-1 controls the balance between proliferative fate and differentiation in the *C. elegans* germ line. *Development*, *142*(2), 291–302. <https://doi.org/10.1242/DEV.115147>
65. Gustafson, E. A., & Wessel, G. M. (2010). Vasa genes: Emerging roles in the germ line and in multipotent cells. *BioEssays*, *32*(7), 626–637. <https://doi.org/10.1002/BIES.201000001>
66. Häcker, V. (1892). *Archiv für mikroskopische Anatomie*. <https://www.scopus.com/record/display.uri?eid=2-s2.0-0004675858&origin=inward&txGid=ed455ad589e4cfbec218bc68e8f06c9a>
67. Haeckel, E. (1868). *Natürliche Schöpfungsgeschichte*. George Reimer, Berlin. <https://books.google.com/books?hl=en&lr=&id=Kh4fdEy0OWYC&oi=fnd&pg=PA1&ots=hRmzSUjIjy&sig=WIh5Vkh3ki3-gkboMIzNIXy6d1w#v=onepage&q&f=false>
68. Hajduskova, M., Baytek, G., Kolundzic, E., Godschan, A., Kazmierczak, M., Ofenbauer, A., del Rosal, M. L. B., Herzog, S., Ul Fatima, N., Mertins, P., Seelk-Müthel, S., & Tursun, B. (2019). MRG-1/MRG15 Is a Barrier for Germ Cell to Neuron Reprogramming in *Caenorhabditis elegans*. *Genetics*, *211*(1), 121–139. <https://doi.org/10.1534/GENETICS.118.301674>

69. Hall, D. H., & Hedgecock, E. M. (1991). Kinesin-related gene *unc-104* is required for axonal transport of synaptic vesicles in *C. elegans*. *Cell*, *65*(5), 837–847. [https://doi.org/10.1016/0092-8674\(91\)90391-B](https://doi.org/10.1016/0092-8674(91)90391-B)
70. Hall, D. H., Winfrey, V. P., Blaeuer, G., Hoffman, L. H., Furuta, T., Rose, K. L., Hobert, O., & Greenstein, D. (1999). Ultrastructural Features of the Adult Hermaphrodite Gonad of *Caenorhabditis elegans*: Relations between the Germ Line and Soma. *Developmental Biology*, *212*(1), 101–123. <https://doi.org/10.1006/DBIO.1999.9356>
71. Hanazawa, M., Yonetani, M., & Sugimoto, A. (2011). PGL proteins self associate and bind RNPs to mediate germ granule assembly in *C. elegans*. *The Journal of Cell Biology*, *192*(6), 929. <https://doi.org/10.1083/JCB.201010106>
72. Hartman, P. S., Barry, J., Finstad, W., Khan, N., Tanaka, M., Yasuda, K., & Ishii, N. (2014). Ethyl methanesulfonate induces mutations in *Caenorhabditis elegans* embryos at a high frequency. *Mutation Research/Fundamental and Molecular Mechanisms of Mutagenesis*, *766–767*, 44–48. <https://doi.org/10.1016/J.MRFMMM.2014.05.011>
73. Hay, B., Ackerman, L., Barbel, S., Jan, L. Y., & Jan, Y. N. (1988). Identification of a component of *Drosophila* polar granules. *Development*, *103*(4), 625–640. <https://doi.org/10.1242/DEV.103.4.625>
74. Heestand, B. N., Shen, Y., Liu, W., Magner, D. B., Storm, N., Meharg, C., Habermann, B., & Antebi, A. (2013). Dietary Restriction Induced Longevity Is Mediated by Nuclear Receptor NHR-62 in *Caenorhabditis elegans*. *PLoS Genetics*, *9*(7), e1003651. <https://doi.org/10.1371/JOURNAL.PGEN.1003651>
75. Hegner, R. W. (1908). EFFECTS OF REMOVING THE GERM-CELL DE TERMINANTS FROM THE EGGS OF SOME CHRYSOMELID BEETLES. PRELIMINARY REPORT. *Biol Bull*, *16*, 19–26.
76. Hikichi, T., Matoba, R., Ikeda, T., Watanabe, A., Yamamoto, T., Yoshitake, S., Tamura-Nakano, M., Kimura, T., Kamon, M., Shimura, M., Kawakami, K., Okuda, A., Okochi, H., Inoue, T., Suzuki, A., & Masui, S. (2013). Transcription factors interfering with dedifferentiation induce cell type-specific transcriptional profiles. *Proceedings of the National Academy of Sciences of the United States of America*, *110*(16), 6412–6417. <https://doi.org/10.1073/PNAS.1220200110/-/DCSUPPLEMENTAL/PNAS.201220200SI.PDF>
77. Hirsh, D., Oppenheim, D., & Klass, M. (1976). Development of the reproductive system of *Caenorhabditis elegans*. *Developmental Biology*, *49*(1), 200–219. [https://doi.org/10.1016/0012-1606\(76\)90267-0](https://doi.org/10.1016/0012-1606(76)90267-0)

78. Hoang, H. D., Prasain, J. K., Dorand, D., & Miller, M. A. (2013). A Heterogeneous Mixture of F-Series Prostaglandins Promotes Sperm Guidance in the *Caenorhabditis elegans* Reproductive Tract. *PLOS Genetics*, *9*(1), e1003271. <https://doi.org/10.1371/JOURNAL.PGEN.1003271>
79. Hobert, O. (2010). Neurogenesis in the nematode *Caenorhabditis elegans*. *Wormbook*, 1. <https://doi.org/10.1895/WORMBOOK.1.12.2>
80. Howard, A. C., Mir, D., Snow, S., Horrocks, J., Sayed, H., Ma, Z., & Rogers, A. N. (2021). Anabolic Function Downstream of TOR Controls Trade-offs Between Longevity and Reproduction at the Level of Specific Tissues in *C. elegans*. *Frontiers in Aging*, *2*. <https://doi.org/10.3389/FRAGI.2021.725068>
81. Hubert, A., & Anderson, P. (2009). The *C. elegans* sex determination gene *laf-1* encodes a putative DEAD-box RNA helicase. *Developmental Biology*, *330*(2), 358–367. <https://doi.org/10.1016/J.YDBIO.2009.04.003>
82. Huggins, H. P., & Keiper, B. D. (2020). Regulation of Germ Cell mRNPs by eIF4E:4EIP Complexes: Multiple Mechanisms, One Goal. *Frontiers in Cell and Developmental Biology*, *8*, 562. <https://doi.org/10.3389/FCELL.2020.00562/BIBTEX>
83. Huggins, H. P., Subash, J. S., Stoffel, H., Henderson, M. A., Hoffman, J. L., Buckner, D. S., Sengupta, M. S., Boag, P. R., Lee, M. H., & Keiper, B. D. (2020). Distinct roles of two eIF4E isoforms in the germline of *Caenorhabditis elegans*. *Journal of Cell Science*, *133*(6). <https://doi.org/10.1242/JCS.237990/266302/AM/DISTINCT-ROLES-OF-TWO-EIF4E-ISOFORMS-IN-THE>
84. Itakura, G., Kawabata, S., Ando, M., Nishiyama, Y., Sugai, K., Ozaki, M., Iida, T., Ookubo, T., Kojima, K., Kashiwagi, R., Yasutake, K., Nakauchi, H., Miyoshi, H., Nagoshi, N., Kohyama, J., Iwanami, A., Matsumoto, M., Nakamura, M., & Okano, H. (2017). Fail-Safe System against Potential Tumorigenicity after Transplantation of iPSC Derivatives. *Stem Cell Reports*, *8*(3), 673–684. <https://doi.org/10.1016/J.STEMCR.2017.02.003>
85. Ivics, Z. (2015). Self-Destruct Genetic Switch to Safeguard iPS Cells. *Molecular Therapy*, *23*(9), 1417. <https://doi.org/10.1038/MT.2015.139>
86. Jeske, M., Bordi, M., Glatt, S., Müller, S., Rybin, V., Müller, C. W., & Ephrussi, A. (2015). The Crystal Structure of the *Drosophila* Germline Inducer Oskar Identifies Two Domains with Distinct Vasa Helicase- and RNA-Binding Activities. *Cell Reports*, *12*(4), 587–598. <https://doi.org/10.1016/J.CELREP.2015.06.055>
87. Jinek, M., Chylinski, K., Fonfara, I., Hauer, M., Doudna, J. A., & Charpentier, E. (2012). A programmable dual-RNA-guided DNA endonuclease in adaptive bacterial immunity.

Science, 337(6096), 816–821.

https://doi.org/10.1126/SCIENCE.1225829/SUPPL_FILE/JINEK.SM.PDF

88. Johnstone, O., & Lasko, P. (2004). Interaction with eIF5B is essential for Vasa function during development. *Development*, 131(17), 4167–4178.
<https://doi.org/10.1242/DEV.01286>
89. Jones, A. R., Francis, R., & Schedl, T. (1996). GLD-1, a Cytoplasmic Protein Essential for Oocyte Differentiation, Shows Stage- and Sex-Specific Expression during *Caenorhabditis elegans* Germline Development. *Developmental Biology*, 180(1), 165–183.
<https://doi.org/10.1006/DBIO.1996.0293>
90. Käser-Pébernard, S., Müller, F., & Wicky, C. (2014). LET-418/Mi2 and SPR-5/LSD1 Cooperatively Prevent Somatic Reprogramming of *C. elegans* Germline Stem Cells. *Stem Cell Reports*, 2(4), 547–559. <https://doi.org/10.1016/J.STEMCR.2014.02.007>
91. Kawasaki, I., Amiri, A., Fan, Y., Meyer, N., Dunkelbarger, S., Motohashi, T., Karashima, T., Bossinger, O., & Strome, S. (2004). The PGL Family Proteins Associate With Germ Granules and Function Redundantly in *Caenorhabditis elegans* Germline Development. *Genetics*, 167(2), 645–661. <https://doi.org/10.1534/GENETICS.103.023093>
92. Kawasaki, I., Jeong, M. H., & Shim, Y. H. (2011). Regulation of sperm-specific proteins by IFE-1, a germline-specific homolog of eIF4E, in *C. elegans*. *Molecules and Cells*, 31(2), 191–197. <https://doi.org/10.1007/S10059-011-0021-Y>
93. Kawasaki, I., Shim, Y.-H., Kirchner, J., Kaminker, J., Wood, W. B., & Strome, S. (1998). PGL-1, a Predicted RNA-Binding Component of Germ Granules, Is Essential for Fertility in *C. elegans*. *Cell*, 94(5), 635–645. [https://doi.org/10.1016/S0092-8674\(00\)81605-0](https://doi.org/10.1016/S0092-8674(00)81605-0)
94. Kazmierczak, M., Díaz, C. F. i, Ofenbauer, A., & Tursun, B. (2020). The CONDOR pipeline for simultaneous knockdown of multiple genes identifies RBBP-5 as a germ cell reprogramming barrier in *C. elegans*. *BioRxiv*, 2020.09.01.276972.
<https://doi.org/10.1101/2020.09.01.276972>
95. Kershner, A. M., Shin, H., Hansen, T. J., & Kimble, J. (2014). Discovery of two GLP-1/Notch target genes that account for the role of GLP-1/Notch signaling in stem cell maintenance. *Proceedings of the National Academy of Sciences of the United States of America*, 111(10), 3739–3744.
https://doi.org/10.1073/PNAS.1401861111/SUPPL_FILE/PNAS.201401861SI.PDF
96. Kikuchi, T., Morizane, A., Doi, D., Magotani, H., Onoe, H., Hayashi, T., Mizuma, H., Takara, S., Takahashi, R., Inoue, H., Morita, S., Yamamoto, M., Okita, K., Nakagawa, M., Parmar, M., & Takahashi, J. (2017). Human iPS cell-derived dopaminergic neurons

function in a primate Parkinson's disease model. *Nature* 2017 548:7669, 548(7669), 592–596. <https://doi.org/10.1038/nature23664>

97. Kim, K. P., Han, D. W., Kim, J., & Schöler, H. R. (2021). Biological importance of OCT transcription factors in reprogramming and development. *Experimental & Molecular Medicine* 2021 53:6, 53(6), 1018–1028. <https://doi.org/10.1038/s12276-021-00637-4>
98. Kim, W., Underwood, R. S., Greenwald, I., & Shaye, D. D. (2018). OrthoList 2: A New Comparative Genomic Analysis of Human and *Caenorhabditis elegans* Genes. *Genetics*, 210(2), 445. <https://doi.org/10.1534/GENETICS.118.301307>
99. Kimble, J., & Hirsh, D. (1979). The postembryonic cell lineages of the hermaphrodite and male gonads in *Caenorhabditis elegans*. *Developmental Biology*, 70(2), 396–417. [https://doi.org/10.1016/0012-1606\(79\)90035-6](https://doi.org/10.1016/0012-1606(79)90035-6)
100. Kimble, J., & Sharrock, W. J. (1983). Tissue-specific synthesis of yolk proteins in *Caenorhabditis elegans*. *Developmental Biology*, 96(1), 189–196. [https://doi.org/10.1016/0012-1606\(83\)90322-6](https://doi.org/10.1016/0012-1606(83)90322-6)
101. King, K. L., Essig, J., Roberts, T. M., & Moerland, T. S. (1994). Regulation of the *Ascaris* major sperm protein (MSP) cytoskeleton by intracellular pH. *Cell Motility and the Cytoskeleton*, 27(3), 193–205. <https://doi.org/10.1002/CM.970270302>
102. King, K. L., Stewart, M., Roberts, T. M., & Seavy, M. (1992). Structure and macromolecular assembly of two isoforms of the major sperm protein (MSP) from the amoeboid sperm of the nematode, *Ascaris suum*. *Journal of Cell Science*, 101(4), 847–857. <https://doi.org/10.1242/JCS.101.4.847>
103. Knaut, H., Pelegri, F., Bohmann, K., Schwarz, H., & Nüsslein-Volhard, C. (2000). Zebrafish vasa RNA but Not Its Protein Is a Component of the Germ Plasm and Segregates Asymmetrically before Germline Specification. *Journal of Cell Biology*, 149(4), 875–888. <https://doi.org/10.1083/JCB.149.4.875>
104. Knutson, A. K. A. A., Rechtsteiner, A., & Strome, S. (2016). Reevaluation of whether a soma-to-germ-line transformation extends lifespan in *Caenorhabditis elegans*. *Proceedings of the National Academy of Sciences of the United States of America*, 113(13), 3591–3596. https://doi.org/10.1073/PNAS.1523402113/SUPPL_FILE/PNAS.1523402113.SD02.XLSX
105. Knutson, A. K., Egelhofer, T., Rechtsteiner, A., & Strome, S. (2017a). Germ granules prevent accumulation of somatic transcripts in the adult *Caenorhabditis elegans* germline. *Genetics*, 206(1), 163–178. <https://doi.org/10.1534/GENETICS.116.198549/-/DC1>

106. Knutson, A. K., Egelhofer, T., Rechtsteiner, A., & Strome, S. (2017b). Germ granules prevent accumulation of somatic transcripts in the adult *Caenorhabditis elegans* germline. *Genetics*, *206*(1), 163–178. <https://doi.org/10.1534/GENETICS.116.198549/-/DC1>
107. Koen Braat, A., Zandbergen, T., de Water, S. van, Goos, H. J. T., & Zivkovic, D. (n.d.). *Characterization of Zebrafish Primordial Germ Cells: Morphology and Early Distribution of vasa RNA*. [https://doi.org/10.1002/\(SICI\)1097-0177\(199910\)216:2](https://doi.org/10.1002/(SICI)1097-0177(199910)216:2)
108. Kolundzic, E., Ofenbauer, A., Bulut, S. I., Uyar, B., Baytek, G., Sommermeier, A., Seelk, S., He, M., Hirsekorn, A., Vucicevic, D., Akalin, A., Diecke, S., Lacadie, S. A., & Tursun, B. (2018a). FACT Sets a Barrier for Cell Fate Reprogramming in *Caenorhabditis elegans* and Human Cells. *Developmental Cell*, *46*(5), 611-626.e12. <https://doi.org/10.1016/J.DEVCEL.2018.07.006>
109. Kolundzic, E., Ofenbauer, A., Bulut, S. I., Uyar, B., Baytek, G., Sommermeier, A., Seelk, S., He, M., Hirsekorn, A., Vucicevic, D., Akalin, A., Diecke, S., Lacadie, S. A., & Tursun, B. (2018b). FACT Sets a Barrier for Cell Fate Reprogramming in *Caenorhabditis elegans* and Human Cells. *Developmental Cell*, *46*(5), 611-626.e12. <https://doi.org/10.1016/J.DEVCEL.2018.07.006>
110. Kriks, S., Shim, J. W., Piao, J., Ganat, Y. M., Wakeman, D. R., Xie, Z., Carrillo-Reid, L., Auyeung, G., Antonacci, C., Buch, A., Yang, L., Beal, M. F., Surmeier, D. J., Kordower, J. H., Tabar, V., & Studer, L. (2011). Dopamine neurons derived from human ES cells efficiently engraft in animal models of Parkinson's disease. *Nature* *2011* *480*:7378, *480*(7378), 547–551. <https://doi.org/10.1038/nature10648>
111. Kubagawa, H. M., Watts, J. L., Corrigan, C., Edmonds, J. W., Sztul, E., Browse, J., & Miller, M. A. (2006a). Oocyte signals derived from polyunsaturated fatty acids control sperm recruitment in vivo. *Nature Cell Biology* *2006* *8*:10, *8*(10), 1143–1148. <https://doi.org/10.1038/ncb1476>
112. Kubagawa, H. M., Watts, J. L., Corrigan, C., Edmonds, J. W., Sztul, E., Browse, J., & Miller, M. A. (2006b). Oocyte signals derived from polyunsaturated fatty acids control sperm recruitment in vivo. *Nature Cell Biology*, *8*(10), 1143–1148. <https://doi.org/10.1038/NCB1476>
113. Kugler, J.-M., Woo, J.-S., Oh, B.-H., & Lasko, P. (2010). Regulation of *Drosophila* Vasa In Vivo through Paralogous Cullin-RING E3 Ligase Specificity Receptors. *Molecular and Cellular Biology*, *30*(7), 1769–1782. https://doi.org/10.1128/MCB.01100-09/SUPPL_FILE/SUPPL_FIG_2_LR.PDF
114. Kulkarni, A., & Extavour, C. G. (2017). Convergent evolution of germ granule nucleators: A hypothesis. *Stem Cell Research*, *24*, 188–194. <https://doi.org/10.1016/J.SCR.2017.07.018>

115. Kumar, R., Dimenna, L., Schrode, N., Liu, T. C., Franck, P., Muñoz-Descalzo, S., Hadjantonakis, A. K., Zarrin, A. A., Chaudhuri, J., Elemento, O., & Evans, T. (2013). AID stabilizes stem cell phenotype by removing epigenetic memory of pluripotency genes. *Nature*, *500*(7460), 89. <https://doi.org/10.1038/NATURE12299>
116. Kuramochi-Miyagawa, S., Watanabe, T., Gotoh, K., Takamatsu, K., Chuma, S., Kojima-Kita, K., Shiromoto, Y., Asada, N., Toyoda, A., Fujiyama, A., Totoki, Y., Shibata, T., Kimura, T., Nakatsuji, N., Noce, T., Sasaki, H., & Nakano, T. (2010). MVH in piRNA processing and gene silencing of retrotransposons. *Genes & Development*, *24*(9), 887–892. <https://doi.org/10.1101/GAD.1902110>
117. Kuznicki, K. A., Smith, P. A., Leung-Chiu, W. M. A., Estevez, A. O., Scott, H. C., & Bennett, K. L. (2000a). Combinatorial RNA interference indicates GLH-4 can compensate for GLH-1; these two P granule components are critical for fertility in *C. elegans*. *Development*, *127*(13), 2907–2916. <https://doi.org/10.1242/DEV.127.13.2907>
118. Kuznicki, K. A., Smith, P. A., Leung-Chiu, W. M. A., Estevez, A. O., Scott, H. C., & Bennett, K. L. (2000b). Combinatorial RNA interference indicates GLH-4 can compensate for GLH-1; these two P granule components are critical for fertility in *C. elegans*. *Development*, *127*(13), 2907–2916. <https://doi.org/10.1242/DEV.127.13.2907>
119. Kuznicki, K. A., Smith, P. A., Leung-Chiu, W. M. A., Estevez, A. O., Scott, H. C., & Bennett, K. L. (2000c). Combinatorial RNA interference indicates GLH-4 can compensate for GLH-1; these two P granule components are critical for fertility in *C. elegans*. *Development*, *127*(13), 2907–2916. <https://doi.org/10.1242/DEV.127.13.2907>
120. Kwak, J. E., Wang, L., Ballantyne, S., Kimble, J., & Wickens, M. (2004). Mammalian GLD-2 homologs are poly(A) polymerases. *Proceedings of the National Academy of Sciences of the United States of America*, *101*(13), 4407. <https://doi.org/10.1073/PNAS.0400779101>
121. LaMunyon, C. W., & Ward, S. (1998). Larger sperm outcompete smaller sperm in the nematode *Caenorhabditis elegans*. *Proceedings of the Royal Society B: Biological Sciences*, *265*(1409), 1997. <https://doi.org/10.1098/RSPB.1998.0531>
122. Lasko, P. (2013). The DEAD-box helicase Vasa: Evidence for a multiplicity of functions in RNA processes and developmental biology. *Biochimica et Biophysica Acta (BBA) - Gene Regulatory Mechanisms*, *1829*(8), 810–816. <https://doi.org/10.1016/J.BBAGRM.2013.04.005>
123. Lasko, P. F., & Ashburner, M. (1988). The product of the *Drosophila* gene *vasa* is very similar to eukaryotic initiation factor-4A. *Nature* *1988* *335*:6191, *335*(6191), 611–617. <https://doi.org/10.1038/335611a0>

124. Laws, K. M., & Drummond-Barbosa, D. (2017). Control of germline stem cell lineages by diet and physiology. *Results and Problems in Cell Differentiation*, 59, 67. https://doi.org/10.1007/978-3-319-44820-6_3
125. Lawson, K. A., Dunn, N. R., Roelen, B. A. J., Zeinstra, L. M., Davis, A. M., Wright, C. V. E., Korving, J. P. W. F. M., & Hogan, B. L. M. (1999). *Bmp4 is required for the generation of primordial germ cells in the mouse embryo*. www.genesdev.org
126. Lee, C. H., Sorensen, E. B., Lynch, T. R., & Kimble, J. (2016). *C. elegans* GLP-1/Notch activates transcription in a probability gradient across the germline stem cell pool. *ELife*, 5(OCTOBER2016). <https://doi.org/10.7554/ELIFE.18370>
127. Lee, J. H., Lee, J. B., Shapovalova, Z., Fiebig-Comyn, A., Mitchell, R. R., Laronde, S., Szabo, E., Benoit, Y. D., & Bhatia, M. (2014). Somatic transcriptome priming gates lineage-specific differentiation potential of human-induced pluripotent stem cell states. *Nature Communications* 2014 5:1, 5(1), 1–13. <https://doi.org/10.1038/ncomms6605>
128. Li, P., Xie, L., Gu, Y., Li, J., & Xie, J. (2017). Roles of Multifunctional COP9 Signalosome Complex in Cell Fate and Implications for Drug Discovery. *Journal of Cellular Physiology*, 232(6), 1246–1253. <https://doi.org/10.1002/JCP.25696>
129. Linder, P., & Jankowsky, E. (2011). From unwinding to clamping - the DEAD box RNA helicase family. *Nature Reviews. Molecular Cell Biology*, 12(8), 505–516. <https://doi.org/10.1038/NRM3154>
130. Liu, N., Han, H., & Lasko, P. (2009). Vasa promotes *Drosophila* germline stem cell differentiation by activating mei-P26 translation by directly interacting with a (U)-rich motif in its 3' UTR. *Genes & Development*, 23(23), 2742–2752. <https://doi.org/10.1101/GAD.1820709>
131. Lo, T. W., Pickle, C. S., Lin, S., Ralston, E. J., Gurling, M., Schartner, C. M., Bian, Q., Doudna, J. A., & Meyer, B. J. (2013). Precise and heritable genome editing in evolutionarily diverse nematodes using TALENs and CRISPR/Cas9 to engineer insertions and deletions. *Genetics*, 195(2), 331–348. <https://doi.org/10.1534/GENETICS.113.155382/-/DC1>
132. Love, M. I., Huber, W., & Anders, S. (2014). Moderated estimation of fold change and dispersion for RNA-seq data with DESeq2. *Genome Biology*, 15(12), 1–21. <https://doi.org/10.1186/S13059-014-0550-8/FIGURES/9>
133. Lytle, N. K., Barber, A. G., & Reya, T. (2018). Stem cell fate in cancer growth, progression and therapy resistance. *Nature Reviews Cancer* 2018 18:11, 18(11), 669–680. <https://doi.org/10.1038/s41568-018-0056-x>

134. Malone, C. D., Brennecke, J., Dus, M., Stark, A., McCombie, W. R., Sachidanandam, R., & Hannon, G. J. (2009). Specialized piRNA Pathways Act in Germline and Somatic Tissues of the *Drosophila* Ovary. *Cell*, *137*(3), 522–535.
<https://doi.org/10.1016/J.CELL.2009.03.040>
135. Manconi, B., Castagnola, M., Cabras, T., Olianias, A., Vitali, A., Desiderio, C., Sanna, M. T., & Messana, I. (2016). The intriguing heterogeneity of human salivary proline-rich proteins: Short title: Salivary proline-rich protein species. *Journal of Proteomics*, *134*, 47–56. <https://doi.org/10.1016/J.JPROT.2015.09.009>
136. Marchal, I., & Tursun, B. (2021). Induced Neurons From Germ Cells in *Caenorhabditis elegans*. *Frontiers in Neuroscience*, *15*, 1627.
<https://doi.org/10.3389/FNINS.2021.771687/BIBTEX>
137. Marnik, E. A., Fuqua, J. H., Sharp, C. S., Rochester, J. D., Xu, E. L., Holbrook, S. E., & Updike, D. L. (2019). Germline maintenance through the multifaceted activities of GLH/Vasa in *Caenorhabditis elegans* P Granules. *Genetics*, *213*(3), 923–939.
<https://doi.org/10.1534/genetics.119.302670>
138. Marnik, E. A., & Updike, D. L. (2019). Membraneless organelles: P granules in *Caenorhabditis elegans*. *Traffic (Copenhagen, Denmark)*, *20*(6), 373.
<https://doi.org/10.1111/TRA.12644>
139. Martin, G. R. (1981). Isolation of a pluripotent cell line from early mouse embryos cultured in medium conditioned by teratocarcinoma stem cells. *Proceedings of the National Academy of Sciences*, *78*(12), 7634–7638.
<https://doi.org/10.1073/PNAS.78.12.7634>
140. Maupas, E. (1899). La mue et l'enkystement chez les nématodes. *Arch. Zool. Exp. Gen.* *7*, 563–628.
141. Maupas, E. (1900). Modes et formes de reproduction des nématodes. *Archives de Zoologie Expérimentale et Générale*, 463–624.
142. Mavri, M., Čandek-Potokar, M., Fazarinc, G., Škrlep, M., Rutland, C. S., Potočnik, B., Batorek-Lukač, N., & Kubale, V. (2022). Salivary Gland Adaptation to Dietary Inclusion of Hydrolysable Tannins in Boars. *Animals 2022, Vol. 12, Page 2171*, *12*(17), 2171.
<https://doi.org/10.3390/ANI12172171>
143. Mazzini, L., Ferrari, D., Andjus, P. R., Buzanska, L., Cantello, R., de Marchi, F., Gelati, M., Giniatullin, R., Glover, J. C., Grilli, M., Kozlova, E. N., Maioli, M., Mitrečić, D., Pivoriunas, A., Sanchez-Pernaute, R., Sarnowska, A., & Vescovi, A. L. (2018). Advances in stem cell therapy for amyotrophic lateral sclerosis. *Https://Doi.Org/10.1080/14712598.2018.1503248*, *18*(8), 865–881.
<https://doi.org/10.1080/14712598.2018.1503248>

144. Megosh, H. B., Cox, D. N., Campbell, C., & Lin, H. (2006). The Role of PIWI and the miRNA Machinery in *Drosophila* Germline Determination. *Current Biology*, *16*(19), 1884–1894. <https://doi.org/10.1016/J.CUB.2006.08.051>
145. Meister, C., Kolog Gulko, M., Köhler, A. M., & Braus, G. H. (2016). The devil is in the details: comparison between COP9 signalosome (CSN) and the LID of the 26S proteasome. *Current Genetics*, *62*(1), 129–136. <https://doi.org/10.1007/S00294-015-0525-7/METRICS>
146. Meneely, P. M., Dahlberg, C. L., & Rose, J. K. (2019). Working with Worms: *Caenorhabditis elegans* as a Model Organism. *Current Protocols Essential Laboratory Techniques*, *19*(1), e35. <https://doi.org/10.1002/CPET.35>
147. Mercer, M., Jang, S., Ni, C., & Buszczak, M. (2021). The Dynamic Regulation of mRNA Translation and Ribosome Biogenesis During Germ Cell Development and Reproductive Aging. *Frontiers in Cell and Developmental Biology*, *9*, 3023. <https://doi.org/10.3389/FCELL.2021.710186/BIBTEX>
148. Michelitsch, M. D., & Weissman, J. S. (2000). A census of glutamine/asparagine-rich regions: Implications for their conserved function and the prediction of novel prions. *Proceedings of the National Academy of Sciences of the United States of America*, *97*(22), 11910–11915. https://doi.org/10.1073/PNAS.97.22.11910/SUPPL_FILE/2543SUPPLDATA.HTML
149. Mi-Mi, L., Votra, S. B., Kempfues, K., Bretscher, A., & Pruyne, D. (2012). Z-line formins promote contractile lattice growth and maintenance in striated muscles of *C. elegans*. *Journal of Cell Biology*, *198*(1), 87–102. <https://doi.org/10.1083/JCB.201202053>
150. Mojica, F. J. M., Díez-Villaseñor, C., García-Martínez, J., & Soria, E. (2005). Intervening sequences of regularly spaced prokaryotic repeats derive from foreign genetic elements. *Journal of Molecular Evolution*, *60*(2), 174–182. <https://doi.org/10.1007/S00239-004-0046-3/METRICS>
151. Moronetti Mazzeo, L. E., Dersh, D., Boccitto, M., Kalb, R. G., & Lamitina, T. (2012). Stress and aging induce distinct polyQ protein aggregation states. *Proceedings of the National Academy of Sciences of the United States of America*, *109*(26), 10587–10592. https://doi.org/10.1073/PNAS.1108766109/SUPPL_FILE/SM01.AVI
152. Morton, J., Davis, M. W., Jorgensen, E. M., & Carroll, D. (2006). Induction and repair of zinc-finger nuclease-targeted double-strand breaks in *Caenorhabditis elegans* somatic cells. *Proceedings of the National Academy of Sciences of the United States of America*, *103*(44), 16370–16375. https://doi.org/10.1073/PNAS.0605633103/SUPPL_FILE/05633TABLE7.PDF

153. Mounsey, A., Bauer, P., & Hope, I. A. (2002). Evidence Suggesting That a Fifth of Annotated *Caenorhabditis elegans* Genes May Be Pseudogenes. *Genome Research*, *12*(5), 770–775. <https://doi.org/10.1101/GR208802>
154. Mueller, M. M., Castells-Roca, L., Babu, V., Ermolaeva, M. A., Müller, R. U., Frommolt, P., Williams, A. B., Greiss, S., Schneider, J. I., Benzing, T., Schermer, B., & Schumacher, B. (2014). DAF-16/FOXO and EGL-27/GATA promote developmental growth in response to persistent somatic DNA damage. *Nature Cell Biology* *2014 16:12*, *16*(12), 1168–1179. <https://doi.org/10.1038/ncb3071>
155. Nelson, G. A., Roberts, T. M., & Ward, S. (1982). *Caenorhabditis elegans* spermatozoan locomotion: amoeboid movement with almost no actin. *Journal of Cell Biology*, *92*(1), 121–131. <https://doi.org/10.1083/JCB.92.1.121>
156. Nobbs, A. H., Jenkinson, H. F., & Jakubovics, N. S. (2011). Stick to Your Gums: Mechanisms of Oral Microbial Adherence. *Journal of Dental Research*, *90*(11), 1271. <https://doi.org/10.1177/0022034511399096>
157. Nolbrant, S., Heuer, A., Parmar, M., & Kirkeby, A. (2017). Generation of high-purity human ventral midbrain dopaminergic progenitors for in vitro maturation and intracerebral transplantation. *Nature Protocols*, *12*(9), 1962–1979. <https://doi.org/10.1038/NPROT.2017.078>
158. Nott, T. J., Craggs, T. D., & Baldwin, A. J. (2016). Membraneless organelles can melt nucleic acid duplexes and act as biomolecular filters. *Nature Chemistry* *2016 8:6*, *8*(6), 569–575. <https://doi.org/10.1038/nchem.2519>
159. Nott, T. J., Petsalaki, E., Farber, P., Jervis, D., Fussner, E., Plochowitz, A., Craggs, T. D., Bazett-Jones, D. P., Pawson, T., Forman-Kay, J. D., & Baldwin, A. J. (2015). Phase Transition of a Disordered Nuage Protein Generates Environmentally Responsive Membraneless Organelles. *Molecular Cell*, *57*(5), 936–947. <https://doi.org/10.1016/J.MOLCEL.2015.01.013>
160. Novotna, M., Podzimek, S., Broukal, Z., Lencova, E., & Duskova, J. (2015). Periodontal Diseases and Dental Caries in Children with Type 1 Diabetes Mellitus. *Mediators of Inflammation*, *2015*. <https://doi.org/10.1155/2015/379626>
161. Ogura, K. I., Kishimoto, N., Mitani, S., Gengyo-Ando, K., & Kohara, Y. (2003). Translational control of maternal glp-1 mRNA by POS-1 and its interacting protein SPN-4 in *Caenorhabditis elegans*. *Development*, *130*(11), 2495–2503. <https://doi.org/10.1242/DEV.00469>

162. Okita, K., Ichisaka, T., & Yamanaka, S. (2007). Generation of germline-competent induced pluripotent stem cells. *Nature*, *448*(7151), 313–317. <https://doi.org/10.1038/NATURE05934>
163. Oldenbroek, M., Robertson, S. M., Guven-Ozkan, T., Gore, S., Nishi, Y., & Lin, R. (2012). Multiple RNA-binding proteins function combinatorially to control the soma-restricted expression pattern of the E3 ligase subunit ZIF-1. *Developmental Biology*, *363*(2), 388–398. <https://doi.org/10.1016/J.YDBIO.2012.01.002>
164. Orsborn, A. M., Li, W., McEwen, T. J., Mizuno, T., Kuzmin, E., Matsumoto, K., & Bennett, K. L. (2007). GLH-1, the *C. elegans* P granule protein, is controlled by the JNK KGB-1 and by the COP9 subunit CSN-5. *Development*, *134*(18), 3383–3392. <https://doi.org/10.1242/DEV.005181>
165. Ottone, C., Gigliotti, S., Giangrande, A., Graziani, F., & di Pianella, A. V. (2012). The translational repressor cup is required for germ cell development in *Drosophila*. *Journal of Cell Science*, *125*(13), 3114–3123. <https://doi.org/10.1242/JCS.095208/258110/AM/THE-TRANSLATIONAL-REPRESSOR-CUP-IS-REQUIRED-FOR>
166. P Linder, PF Lasko, M Ashburner, P Leroy, & PJ Nielsen. (1989). Birth of the D-E-A-D box. *Nature*, *337*.
167. Pachonski, M., Jarosz-Chobot, P., Koczor-Rozmus, A., Łanowy, P., & Mocny-Pachonska, K. (2020). Dental caries and periodontal status in children with type 1 diabetes mellitus. *Pediatric Endocrinology Diabetes and Metabolism*, *26*(1), 39–44. <https://doi.org/10.5114/PEDM.2020.93249>
168. Pappa, E., Vougas, K., Zoidakis, J., Papaioannou, W., Rahiotis, C., & Vastardis, H. (2021). Downregulation of salivary proteins, protective against dental caries, in type 1 diabetes. *Proteomes*, *9*(3), 33. <https://doi.org/10.3390/PROTEOMES9030033/S1>
169. Pause, A., & Sonenberg, N. (1992). Mutational analysis of a DEAD box RNA helicase: the mammalian translation initiation factor eIF-4A. *The EMBO Journal*, *11*(7), 2643–2654. <https://doi.org/10.1002/J.1460-2075.1992.TB05330.X>
170. Petersen, C., Dirksen, P., & Schulenburg, H. (2015). Why we need more ecology for genetic models such as *C. elegans*. *Trends in Genetics*, *31*(3), 120–127. <https://doi.org/10.1016/J.TIG.2014.12.001>
171. Phillips, C. M., & Updike, D. L. (2022). Germ granules and gene regulation in the *Caenorhabditis elegans* germline. *Genetics*, *220*(3). <https://doi.org/10.1093/GENETICS/IYAB195>

172. Pintard, L., Kurz, T., Glasser, S., Willis, J. H., Peter, M., & Bowerman, B. (2003). Neddylation and Deneddylation of CUL-3 Is Required to Target MEI-1/Katanin for Degradation at the Meiosis-to-Mitosis Transition in *C. elegans*. *Current Biology*, *13*(11), 911–921. [https://doi.org/10.1016/S0960-9822\(03\)00336-1](https://doi.org/10.1016/S0960-9822(03)00336-1)
173. Pitt, J. N., Schisa, J. A., & Priess, J. R. (2000). P granules in the germ cells of *Caenorhabditis elegans* adults are associated with clusters of nuclear pores and contain RNA. *Developmental Biology*, *219*(2), 315–333. <https://doi.org/10.1006/DBIO.2000.9607>
174. Polo, J. M., Liu, S., Figueroa, M. E., Kulal, W., Eminli, S., Tan, K. Y., Apostolou, E., Stadtfeld, M., Li, Y., Shioda, T., Natesan, S., Wagers, A. J., Melnick, A., Evans, T., & Hochedlinger, K. (2010). Cell type of origin influences the molecular and functional properties of mouse induced pluripotent stem cells. *Nature Biotechnology*, *28*(8), 848. <https://doi.org/10.1038/NBT.1667>
175. Poon, J., Wessel, G. M., & Yajima, M. (2016). An unregulated regulator: Vasa expression in the development of somatic cells and in tumorigenesis. *Developmental Biology*, *415*(1), 24–32. <https://doi.org/10.1016/J.YDBIO.2016.05.012>
176. Price, I. F., Hertz, H. L., Pastore, B., Wagner, J., & Tang, W. (2021). Proximity labeling identifies lotus domain proteins that promote the formation of perinuclear germ granules in *C. elegans*. *ELife*, *10*. <https://doi.org/10.7554/ELIFE.72276>
177. R. Ciosk, M. DePalma, & J.R. Priess. (2006). Translational regulators maintain totipotency in the *Caenorhabditis elegans* germline. *Science*, *311*, 851–853.
178. Raabe, F. J., Stephan, M., Waldeck, J. B., Huber, V., Demetriou, D., Kannaiyan, N., Galinski, S., Glaser, L. v., Wehr, M. C., Ziller, M. J., Schmitt, A., Falkai, P., & Rossner, M. J. (2022). Expression of Lineage Transcription Factors Identifies Differences in Transition States of Induced Human Oligodendrocyte Differentiation. *Cells*, *11*(2), 241. <https://doi.org/10.3390/CELLS11020241/S1>
179. Raharjo, I., & Gaudet, J. (2007). Gland-specific expression of *C. elegans* hlh-6 requires the combinatorial action of three distinct promoter elements. *Developmental Biology*, *302*(1), 295–308. <https://doi.org/10.1016/J.YDBIO.2006.09.036>
180. Ramat, A., Garcia-Silva, M. R., Jahan, C., Naït-Saïdi, R., Dufourt, J., Garret, C., Chartier, A., Cremaschi, J., Patel, V., Decourcelle, M., Bastide, A., Juge, F., & Simonelig, M. (2020). The PIWI protein Aubergine recruits eIF3 to activate translation in the germ plasm. *Cell Research* *2020 30:5*, *30*(5), 421–435. <https://doi.org/10.1038/s41422-020-0294-9>
181. Raz, E. (2000). The function and regulation of vasa-like genes in germ-cell development. *Genome Biology* *2000 1:3*, *1*(3), 1–6. <https://doi.org/10.1186/GB-2000-1-3-REVIEWS1017>

182. Robert, V. J., Mercier, M. G., Bedet, C., Janczarski, S., Merlet, J., Garvis, S., Ciosk, R., & Palladino, F. (2014). The SET-2/SET1 Histone H3K4 Methyltransferase Maintains Pluripotency in the *Caenorhabditis elegans* Germline. *Cell Reports*, *9*(2), 443–450. <https://doi.org/10.1016/J.CELREP.2014.09.018>
183. Roberts, T. M., Pavalko, F. M., & Ward, S. (1986). Membrane and cytoplasmic proteins are transported in the same organelle complex during nematode spermatogenesis. *The Journal of Cell Biology*, *102*(5), 1787–1796. <https://doi.org/10.1083/JCB.102.5.1787>
184. Rochester, J. D., Min, H., Gajjar, G. A., Sharp, C. S., Maki, N. J., Rollins, J. A., Keiper, B. D., Graber, J. H., & Updike, D. L. (2022). GLH-1/Vasa represses neuropeptide expression and drives spermiogenesis in the *C. elegans* germline. *Developmental Biology*, *492*, 200–211. <https://doi.org/10.1016/j.ydbio.2022.10.003>
185. Rochester, J. D., Tanner, P. C., Sharp, C. S., Andralojc, K. M., & Updike, D. L. (2017). PQN-75 is expressed in the pharyngeal gland cells of *Caenorhabditis elegans* and is dispensable for germline development. *Biology Open*, *6*(9), 1355. <https://doi.org/10.1242/BIO.027987>
186. Schisa, J. A., Pitt, J. N., & Priess, J. R. (2001). Analysis of RNA associated with P granules in germ cells of *C. elegans* adults. *Development*, *128*(8), 1287–1298. <https://doi.org/10.1242/DEV.128.8.1287>
187. Schönichen, A., & Geyer, M. (2010). Fifteen formins for an actin filament: A molecular view on the regulation of human formins. *Biochimica et Biophysica Acta (BBA) - Molecular Cell Research*, *1803*(2), 152–163. <https://doi.org/10.1016/J.BBAMCR.2010.01.014>
188. Schulenburg, H., & Félix, M. A. (2017). The Natural Biotic Environment of *Caenorhabditis elegans*. *Genetics*, *206*(1), 55–86. <https://doi.org/10.1534/GENETICS.116.195511>
189. Schwartz, M. L., Wayne Davis, M., Rich, M. S., & Jorgensen, E. M. (2021). High-efficiency CRISPR gene editing in *C. elegans* using Cas9 integrated into the genome. *PLOS Genetics*, *17*(11), e1009755. <https://doi.org/10.1371/JOURNAL.PGEN.1009755>
190. Sengoku, T., Nureki, O., Nakamura, A., Kobayashi, S., & Yokoyama, S. (2006). Structural Basis for RNA Unwinding by the DEAD-Box Protein *Drosophila* Vasa. *Cell*, *125*(2), 287–300. <https://doi.org/10.1016/J.CELL.2006.01.054>
191. Sepsenwol, S., Ris, H., & Roberts, T. M. (1989). A unique cytoskeleton associated with crawling in the amoeboid sperm of the nematode, *Ascaris suum*. *Journal of Cell Biology*, *108*(1), 55–66. <https://doi.org/10.1083/JCB.108.1.55>
192. Shakes, D. C., Wu, J. C., Sadler, P. L., LaPrade, K., Moore, L. L., Noritake, A., & Chu, D. S. (2009). Spermatogenesis-Specific Features of the Meiotic Program in *Caenorhabditis*

elegans. *PLOS Genetics*, 5(8), e1000611.
<https://doi.org/10.1371/JOURNAL.PGEN.1000611>

193. Shaye, D. D., & Greenwald, I. (2016). A network of conserved formins, regulated by the guanine exchange factor EXC-5 and the GTPase CDC-42, modulates tubulogenesis in vivo. *Development (Cambridge)*, 143(22), 4173–4181.
<https://doi.org/10.1242/DEV.141861/VIDEO-3>
194. Sheth, U., Pitt, J., Dennis, S., & Priess, J. R. (2010a). Perinuclear P granules are the principal sites of mRNA export in adult *C. elegans* germ cells. *Development*, 137(8), 1305–1314. <https://doi.org/10.1242/DEV.044255>
195. Sheth, U., Pitt, J., Dennis, S., & Priess, J. R. (2010b). Perinuclear P granules are the principal sites of mRNA export in adult *C. elegans* germ cells. *Development*, 137(8), 1305–1314. <https://doi.org/10.1242/DEV.044255/-/DC1>
196. Shimada, M., Kawahara, H., & Doi, H. (2002). Novel family of CCCH-type zinc-finger proteins, MOE-1, -2 and -3, participates in *C. elegans* oocyte maturation. *Genes to Cells*, 7(9), 933–947. <https://doi.org/10.1046/J.1365-2443.2002.00570.X>
197. Shin, H., Haupt, K. A., Kershner, A. M., Kroll-Conner, P., Wickens, M., & Kimble, J. (2017). SYGL-1 and LST-1 link niche signaling to PUF RNA repression for stem cell maintenance in *Caenorhabditis elegans*. *PLOS Genetics*, 13(12), e1007121.
<https://doi.org/10.1371/JOURNAL.PGEN.1007121>
198. Shinkai, Y., Kuramochi, M., & Miyafusa, T. (2021). New Family Members of FG Repeat Proteins and Their Unexplored Roles During Phase Separation. *Frontiers in Cell and Developmental Biology*, 9, 1818. <https://doi.org/10.3389/FCELL.2021.708702/BIBTEX>
199. Shirayama, M., Stanney, W., Gu, W., Seth, M., & Mello, C. C. (2014). The Vasa Homolog RDE-12 Engages Target mRNA and Multiple Argonaute Proteins to Promote RNAi in *C. elegans*. *Current Biology*, 24(8), 845–851. <https://doi.org/10.1016/J.CUB.2014.03.008>
200. Shukalyuk, A. I., Isaeva, V. v., Shukalyuk, A. I., & Isaeva, V. v. (2012). Molecular and Sub-Cellular Gametogenic Machinery of Stem and Germline Cells Across Metazoa. *Current Frontiers and Perspectives in Cell Biology*. <https://doi.org/10.5772/34896>
201. Singaravelu, G., Chatterjee, I., Marcello, M. R., & Singson, A. (2011). Isolation and in vitro activation of *Caenorhabditis elegans* sperm. *Journal of Visualized Experiments : JoVE*, 47. <https://doi.org/10.3791/2336>
202. Singh, R. N., & Sulston, J. E. (1978). Some Observations On Moulting in *Caenorhabditis Elegans*. *Nematologica*, 24(1), 63–71. <https://doi.org/10.1163/187529278X00074>

203. Skau, C. T., Fischer, R. S., Nussenzweig, A., Steeg, P. S., & Waterman Correspondence, C. M. (2016). *RETRACTED: FMN2 Makes Perinuclear Actin to Protect Nuclei during Confined Migration and Promote Metastasis*. <https://doi.org/10.1016/j.cell.2016.10.023>
204. Smit, R. B., Schnabel, R., & Gaudet, J. (2008a). The HLH-6 Transcription Factor Regulates *C. elegans* Pharyngeal Gland Development and Function. *PLoS Genetics*, *4*(10), 1000222. <https://doi.org/10.1371/JOURNAL.PGEN.1000222>
205. Smit, R. B., Schnabel, R., & Gaudet, J. (2008b). The HLH-6 Transcription Factor Regulates *C. elegans* Pharyngeal Gland Development and Function. *PLOS Genetics*, *4*(10), e1000222. <https://doi.org/10.1371/JOURNAL.PGEN.1000222>
206. Smith, P., Leung-Chiu, W. M., Montgomery, R., Orsborn, A., Kuznicki, K., Gressman-Coberly, E., Mutapcic, L., & Bennett, K. (2002). The GLH Proteins, *Caenorhabditis elegans* P Granule Components, Associate with CSN-5 and KGB-1, Proteins Necessary for Fertility, and with ZYX-1, a Predicted Cytoskeletal Protein. *Developmental Biology*, *251*(2), 333–347. <https://doi.org/10.1006/DBIO.2002.0832>
207. Spichal, M., Heestand, B., Billmyre, K. K., Frenk, S., Mello, C. C., & Ahmed, S. (2021). Germ granule dysfunction is a hallmark and mirror of Piwi mutant sterility. *Nature Communications* *2021 12:1*, *12*(1), 1–15. <https://doi.org/10.1038/s41467-021-21635-0>
208. Spike, C., Meyer, N., Racen, E., Orsborn, A., Kirchner, J., Kuznicki, K., Yee, C., Bennett, K., & Strome, S. (2008a). Genetic Analysis of the *Caenorhabditis elegans* GLH Family of P-Granule Proteins. *Genetics*, *178*(4), 1973–1987. <https://doi.org/10.1534/GENETICS.107.083469>
209. Spike, C., Meyer, N., Racen, E., Orsborn, A., Kirchner, J., Kuznicki, K., Yee, C., Bennett, K., & Strome, S. (2008b). Genetic Analysis of the *Caenorhabditis elegans* GLH Family of P-Granule Proteins. *Genetics*, *178*(4), 1973–1987. <https://doi.org/10.1534/GENETICS.107.083469>
210. Spracklin, G., Fields, B., Wan, G., Becker, D., Wallig, A., Shukla, A., & Kennedy, S. (2017). The RNAi inheritance machinery of *caenorhabditis elegans*. *Genetics*, *206*(3), 1403–1416. <https://doi.org/10.1534/GENETICS.116.198812/-/DC1>
211. Stevens, L. C. (1960). Embryonic potency of embryoid bodies derived from a transplantable testicular teratoma of the mouse. *Developmental Biology*, *2*(3), 285–297. [https://doi.org/10.1016/0012-1606\(60\)90010-5](https://doi.org/10.1016/0012-1606(60)90010-5)
212. Stevens, L. C., & Little, C. C. (1954). Spontaneous Testicular Teratomas in an Inbred Strain of Mice. *Proceedings of the National Academy of Sciences*, *40*(11), 1080–1087. <https://doi.org/10.1073/PNAS.40.11.1080/ASSET/49D810CA-D64A-4869-A634-8DC3A1C4EE5A/ASSETS/PNAS.40.11.1080.FP.PNG>

213. Strome, S., & Updike, D. (2015). Specifying and protecting germ cell fate. In *Nature Reviews Molecular Cell Biology* (Vol. 16, Issue 7, pp. 406–416). Nature Publishing Group. <https://doi.org/10.1038/nrm4009>
214. Strome, S., & Wood, W. B. (1982). Immunofluorescence visualization of germ-line-specific cytoplasmic granules in embryos, larvae, and adults of *Caenorhabditis elegans*. *Proceedings of the National Academy of Sciences*, *79*(5), 1558–1562. <https://doi.org/10.1073/PNAS.79.5.1558>
215. Sulston, J. E., & Horvitz, H. R. (1977). Post-embryonic Cell Lineages of the Nematode, *Caenorhabditis elegans*. *DEVELOPMENTAL BIOLOGY*, *56*, 110–156.
216. Sulston, J. E., Schierenberg, E., White, J. G., & Thomson, J. N. (1983). The embryonic cell lineage of the nematode *Caenorhabditis elegans*. *Developmental Biology*, *100*(1), 64–119. [https://doi.org/10.1016/0012-1606\(83\)90201-4](https://doi.org/10.1016/0012-1606(83)90201-4)
217. Swistowski, A., Peng, J., Liu, Q., Mali, P., Rao, M. S., Cheng, L., & Zeng, X. (2010). Efficient Generation of Functional Dopaminergic Neurons from Human Induced Pluripotent Stem Cells Under Defined Conditions. *Stem Cells*, *28*(10), 1893–1904. <https://doi.org/10.1002/STEM.499>
218. Szklarczyk, D., Gable, A. L., Nastou, K. C., Lyon, D., Kirsch, R., Pyysalo, S., Doncheva, N. T., Legeay, M., Fang, T., Bork, P., Jensen, L. J., & von Mering, C. (2021). The STRING database in 2021: customizable protein–protein networks, and functional characterization of user-uploaded gene/measurement sets. *Nucleic Acids Research*, *49*(D1), D605–D612. <https://doi.org/10.1093/NAR/GKAA1074>
219. Tabara, H., Hill, R. J., Mello, C. C., Priess, J. R., & Kohara, Y. (1999). *pos-1* encodes a cytoplasmic zinc-finger protein essential for germline specification in *C. elegans*. *Development*, *126*(1), 1–11. <https://doi.org/10.1242/DEV.126.1.1>
220. Takahashi, K., & Yamanaka, S. (2006). Induction of Pluripotent Stem Cells from Mouse Embryonic and Adult Fibroblast Cultures by Defined Factors. *Cell*, *126*(4), 663–676. <https://doi.org/10.1016/J.CELL.2006.07.024>
221. Tanaka, S. S., Toyooka, Y., Akasu, R., Katoh-Fukui, Y., Nakahara, Y., Suzuki, R., Yokoyama, M., & Noce, T. (2000). The mouse homolog of *Drosophila Vasa* is required for the development of male germ cells. *Genes & Development*, *14*(7), 841–853. <https://doi.org/10.1101/GAD.14.7.841>
222. Taylor, S. R., Santpere, G., Weinreb, A., Barrett, A., Reilly, M. B., Xu, C., Varol, E., Oikonomou, P., Glenwinkel, L., McWhirter, R., Poff, A., Basavaraju, M., Rafi, I., Yemini, E., Cook, S. J., Abrams, A., Vidal, B., Cros, C., Tavazoie, S., ... Miller, D. M. (2021). Molecular topography of an entire nervous system. *Cell*, *184*(16), 4329–4347.e23.

<https://doi.org/10.1016/J.CELL.2021.06.023/ATTACHMENT/AAD6733E-C282-46D9-980C-A2B0E23A0762/MMC7.XLSX>

223. Thakur, A., Sharma, V., Thakur, A., & Vishal Sharma, C. (2019). An overview of anti-nutritional factors in food. ~ 2472 ~ *International Journal of Chemical Studies*, 7(1).
224. Thomson, J. A., Itskovitz-Eldor, J., Shapiro, S. S., Waknitz, M. A., Swiergiel, J. J., Marshall, V. S., & Jones, J. M. (1998). Embryonic Stem Cell Lines Derived from Human Blastocysts. *Science*, 282(5391), 1145–1147. <https://doi.org/10.1126/SCIENCE.282.5391.1145>
225. Till, J. E., & McCulloch, E. A. (1961). A Direct Measurement of the Radiation Sensitivity of Normal Mouse Bone Marrow Cells 1. *Printed in U.S.A. RADIATION RESEARCH*, 14(2), 213–222.
226. Trounson, A., & McDonald, C. (2015). Stem Cell Therapies in Clinical Trials: Progress and Challenges. *Cell Stem Cell*, 17(1), 11–22. <https://doi.org/10.1016/J.STEM.2015.06.007>
227. Tursun, B., Patel, T., Kratsios, P., & Hobert, O. (2011). Direct conversion of *C. elegans* germ cells into specific neuron types. *Science*, 331(6015), 304–308. https://doi.org/10.1126/SCIENCE.1199082/SUPPL_FILE/TURSUN.SOM.PDF
228. Updike, D. L., Hachey, S. J., Kreher, J., & Strome, S. (2011). P granules extend the nuclear pore complex environment in the *C. elegans* germ line. *The Journal of Cell Biology*, 192(6), 939–948. <https://doi.org/10.1083/JCB.201010104>
229. Updike, D. L., Knutson, A. K. A., Egelhofer, T. A., Campbell, A. C., & Strome, S. (2014). Germ-granule components prevent somatic development in the *C. elegans* germline. *Current Biology : CB*, 24(9), 970. <https://doi.org/10.1016/J.CUB.2014.03.015>
230. Updike, D. L., & Strome, S. (2009). A Genomewide RNAi Screen for Genes That Affect the Stability, Distribution and Function of P Granules in *Caenorhabditis elegans*. *Genetics*, 183(4), 1397–1419. <https://doi.org/10.1534/GENETICS.109.110171>
231. Voronina, E., Seydoux, G., Sassone-Corsi, P., & Nagamori, I. (2011). RNA Granules in Germ Cells. *Cold Spring Harbor Perspectives in Biology*, 3(12), a002774. <https://doi.org/10.1101/CSHPERSPECT.A002774>
232. Wang, J. T., Smith, J., Chen, B. C., Schmidt, H., Rasoloson, D., Paix, A., Lambrus, B. G., Calidas, D., Betzig, E., & Seydoux, G. (2014). Regulation of RNA granule dynamics by phosphorylation of serine-rich, intrinsically disordered proteins in *C. elegans*. *ELife*, 3, 4591. <https://doi.org/10.7554/ELIFE.04591>
233. Ward, S., & Carrel, J. S. (1979). Fertilization and sperm competition in the nematode *Caenorhabditis elegans*. *Developmental Biology*, 73(2), 304–321. [https://doi.org/10.1016/0012-1606\(79\)90069-1](https://doi.org/10.1016/0012-1606(79)90069-1)

234. Ward, S., Roberts, T. M., Strome, S., Pavalko, F. M., & Hogan, E. (1986). Monoclonal antibodies that recognize a polypeptide antigenic determinant shared by multiple *Caenorhabditis elegans* sperm-specific proteins. *Journal of Cell Biology*, *102*(5), 1778–1786. <https://doi.org/10.1083/JCB.102.5.1778>
235. Washington, N. L., & Ward, S. (2006). FER-1 regulates Ca²⁺-mediated membrane fusion during *C. elegans* spermatogenesis. *Journal of Cell Science*, *119*(12), 2552–2562. <https://doi.org/10.1242/JCS.02980>
236. Watts, J. L. (2009). Fat synthesis and adiposity regulation in *Caenorhabditis elegans*. *Trends in Endocrinology and Metabolism: TEM*, *20*(2), 58–65. <https://doi.org/10.1016/J.TEM.2008.11.002>
237. Watts, J. L., & Browse, J. (2002). Genetic dissection of polyunsaturated fatty acid synthesis in *Caenorhabditis elegans*. *Proceedings of the National Academy of Sciences of the United States of America*, *99*(9), 5854. <https://doi.org/10.1073/PNAS.092064799>
238. Weidinger, G., Wolke, U., Köprunner, M., Klinger, M., & Raz, E. (1999). Identification of tissues and patterning events required for distinct steps in early migration of zebrafish primordial germ cells. *Development*, *126*(23), 5295–5307. <https://doi.org/10.1242/DEV.126.23.5295>
239. Weismann, A. (1885). *Die Continuität des Keimplasma's als Grundlage einer Theorie der Vererbung*. Gustav Fischer, Jena . <https://books.google.com/books?hl=en&lr=&id=MEMAAAAQAAJ&oi=fnd&pg=PA1&ots=4KqOwH37HS&sig=RmOOCSTyGXFxoRLFty8NI-6Ijwg#v=onepage&q&f=false>
240. Wenda, J. M., Homolka, D., Yang, Z., Spinelli, P., Sachidanandam, R., Pandey, R. R., & Pillai, R. S. (2017). Distinct Roles of RNA Helicases MVH and TDRD9 in PIWI Slicing-Triggered Mammalian piRNA Biogenesis and Function. *Developmental Cell*, *41*(6), 623-637.e9. <https://doi.org/10.1016/J.DEVCEL.2017.05.021>
241. Wilson, E. B. (1896). *The Cell in development and inheritance*. Macmillan, New York. <https://books.google.com/books?hl=en&lr=&id=zHfjDY5o1GsC&oi=fnd&pg=PA1&ots=E2WL2uXL6X&sig=kA-hX9IMb3IEvf61i-uUw8Cn1Hg#v=onepage&q&f=false>
242. Wood, A. J., Lo, T. W., Zeitler, B., Pickle, C. S., Ralston, E. J., Lee, A. H., Amora, R., Miller, J. C., Leung, E., Meng, X., Zhang, L., Rebar, E. J., Gregory, P. D., Urnov, F. D., & Meyer, B. J. (2011). Targeted genome editing across species using ZFNs and TALENs. *Science*, *333*(6040), 307. https://doi.org/10.1126/SCIENCE.1207773/SUPPL_FILE/WOOD.SOM.REV1.PDF

243. *WormBase : Nematode Information Resource*. (n.d.). Retrieved March 5, 2023, from <https://wormbase.org/#012-34-5>
244. Xiol, J., Spinelli, P., Laussmann, M. A., Homolka, D., Yang, Z., Cora, E., Couté, Y., Conn, S., Kadlec, J., Sachidanandam, R., Kaksonen, M., Cusack, S., Ephrussi, A., & Pillai, R. S. (2014). RNA Clamping by Vasa Assembles a piRNA Amplifier Complex on Transposon Transcripts. *Cell*, *157*(7), 1698–1711. <https://doi.org/10.1016/J.CELL.2014.05.018>
245. Xu, J., Wang, D., Liu, D., Fan, Z., Zhang, H., Liu, O., Ding, G., Gao, R., Zhang, C., Ding, Y., Bromberg, J. S., Chen, W., Sun, L., & Wang, S. (2012). Allogeneic mesenchymal stem cell treatment alleviates experimental and clinical Sjögren syndrome. *Blood*, *120*(15), 3142–3151. <https://doi.org/10.1182/BLOOD-2011-11-391144>
246. Yang, H., Vallandingham, J., Shiu, P., Li, H., Hunter, C. P., & Mak, H. Y. (2014). The DEAD box helicase RDE-12 promotes amplification of RNAi in cytoplasmic foci in *C. elegans*. *Current Biology : CB*, *24*(8), 832–838. <https://doi.org/10.1016/J.CUB.2014.01.008>
247. Yang, N., Yu, Z., Hu, M., Wang, M., Lehmann, R., & Xu, R. M. (2015). Structure of *Drosophila* Oskar reveals a novel RNA binding protein. *Proceedings of the National Academy of Sciences of the United States of America*, *112*(37), 11541–11546. https://doi.org/10.1073/PNAS.1515568112/SUPPL_FILE/PNAS.201515568SI.PDF
248. Yang, W., Dierking, K., Esser, D., Tholey, A., Leippe, M., Rosenstiel, P., & Schulenburg, H. (2015). Overlapping and unique signatures in the proteomic and transcriptomic responses of the nematode *Caenorhabditis elegans* toward pathogenic *Bacillus thuringiensis*. *Developmental & Comparative Immunology*, *51*(1), 1–9. <https://doi.org/10.1016/J.DCI.2015.02.010>
249. Ying, Y., Liu, X. M., Marble, A., Lawson, K. A., & Zhao, G. Q. (2000). Requirement of *Bmp8b* for the Generation of Primordial Germ Cells in the Mouse. *Molecular Endocrinology*, *14*(7), 1053–1063. <https://doi.org/10.1210/MEND.14.7.0479>
250. Yoon, C., Kawakami, K., & Hopkins, N. (1997). Zebrafish vasa homologue RNA is localized to the cleavage planes of 2- and 4-cell-stage embryos and is expressed in the primordial germ cells. *Development*, *124*(16), 3157–3165. <https://doi.org/10.1242/DEV.124.16.3157>
251. Youngman, E. M., & Claycomb, J. M. (2014). From early lessons to new frontiers: the worm as a treasure trove of small RNA biology. *Frontiers in Genetics*, *5*(NOV). <https://doi.org/10.3389/FGENE.2014.00416>
252. Zakrzewski, W., Dobrzyński, M., Szymonowicz, M., & Rybak, Z. (2019). Stem cells: Past, present, and future. *Stem Cell Research and Therapy*, *10*(1), 1–22. <https://doi.org/10.1186/S13287-019-1165-5/FIGURES/8>

APPENDICES

APPENDICE A: SUPPLEMENTAL TABLES AND FIGURES

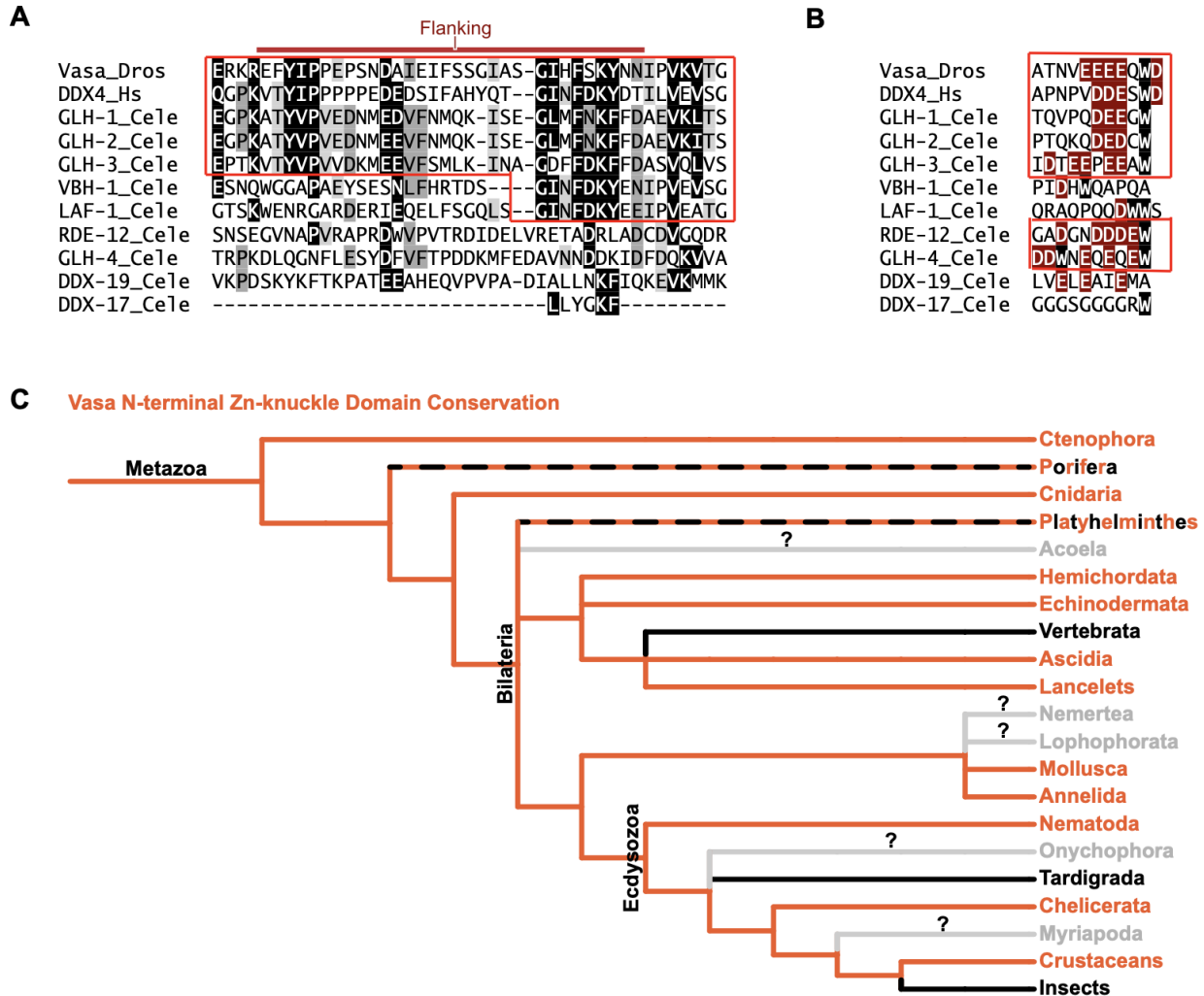


Figure 30: Amino acid sequence conservation between DEAD-box helicase proteins.

A) the flanking domain B) the negatively charged C terminal tryptophan domain. C) The phylogenomic tree showing the conservation of the CCHC zinc-knuckle motif (orange) across Vasa proteins has been updated from (Gustafson and Wessel 2010) using phyloT (phylo.t.biobyte.de) and NCBI taxonomy data. Dashed lines indicate loss of the motif in some species.

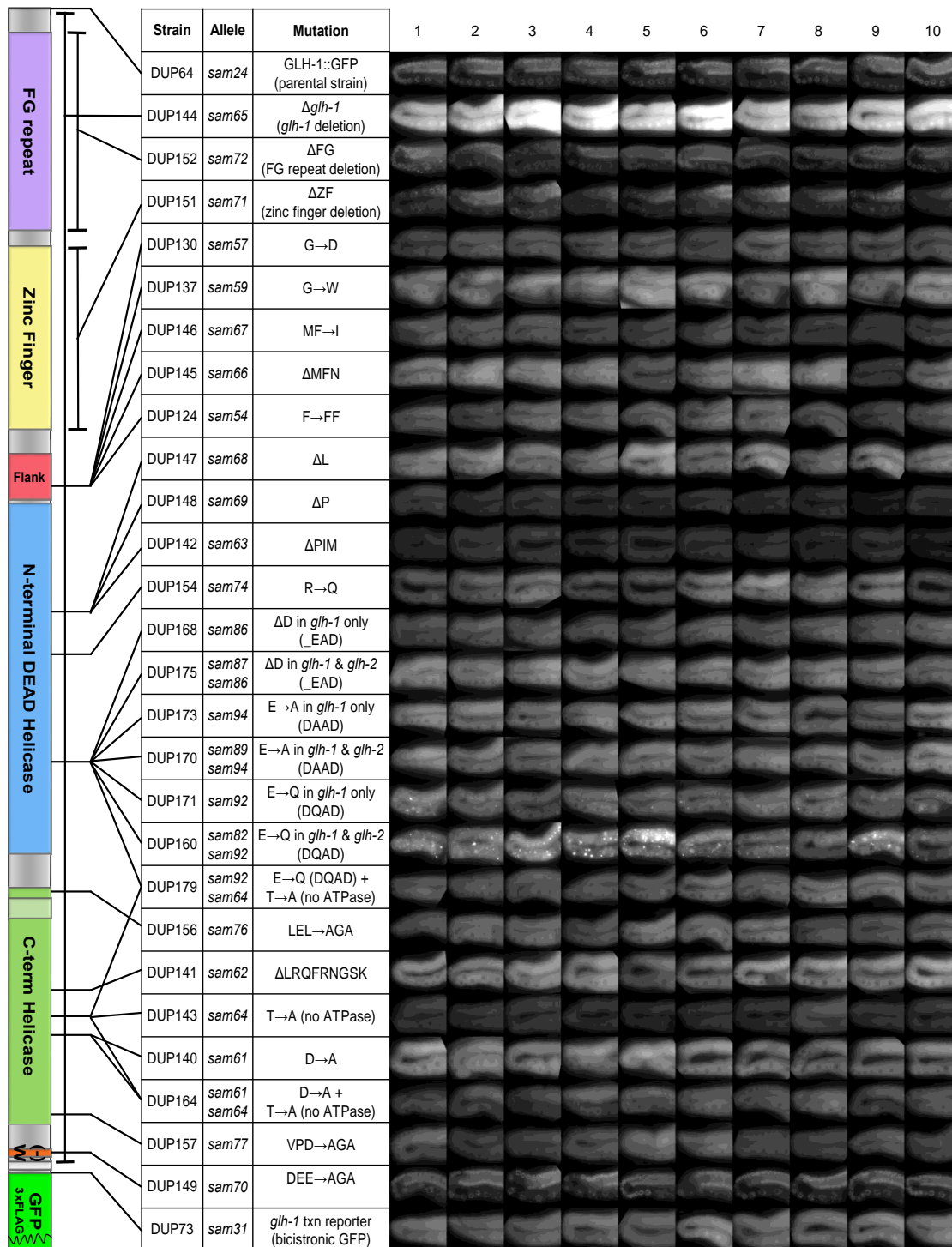


Figure 31: All images used to quantify granularity and expression in Figure 19.

The domain location of the mutation, strain name, allele name and mutation type is indicated.

Ten worms analyzed for each genotype.

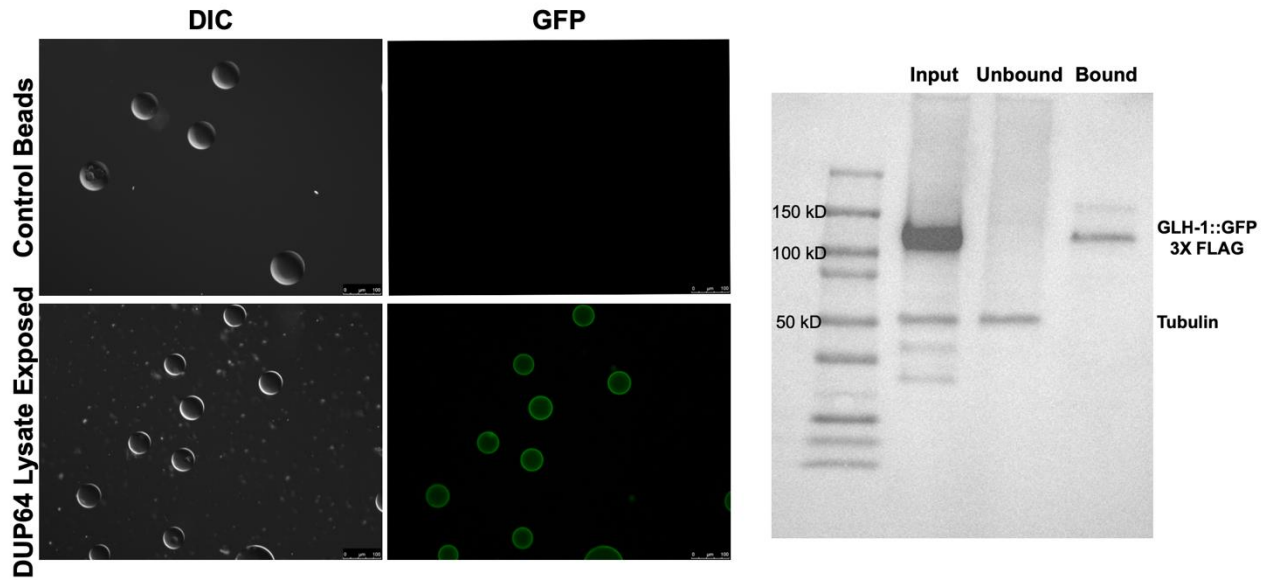


Figure 32: GLH-1 Immunoprecipitation.

Left: Microscope images of control non-antigen exposed anti-DYKDDDDK agarose beads compared to beads exposed to lysate from the GLH-1::GFP::3xFLAG expressing strain. Right: Western blot comparing GLH-1 expression in the input, unbound and elute fraction after immunoprecipitation with protein lysate from the GLH-1::GFP::3xFLAG expressing strain. Results were replicated three times.

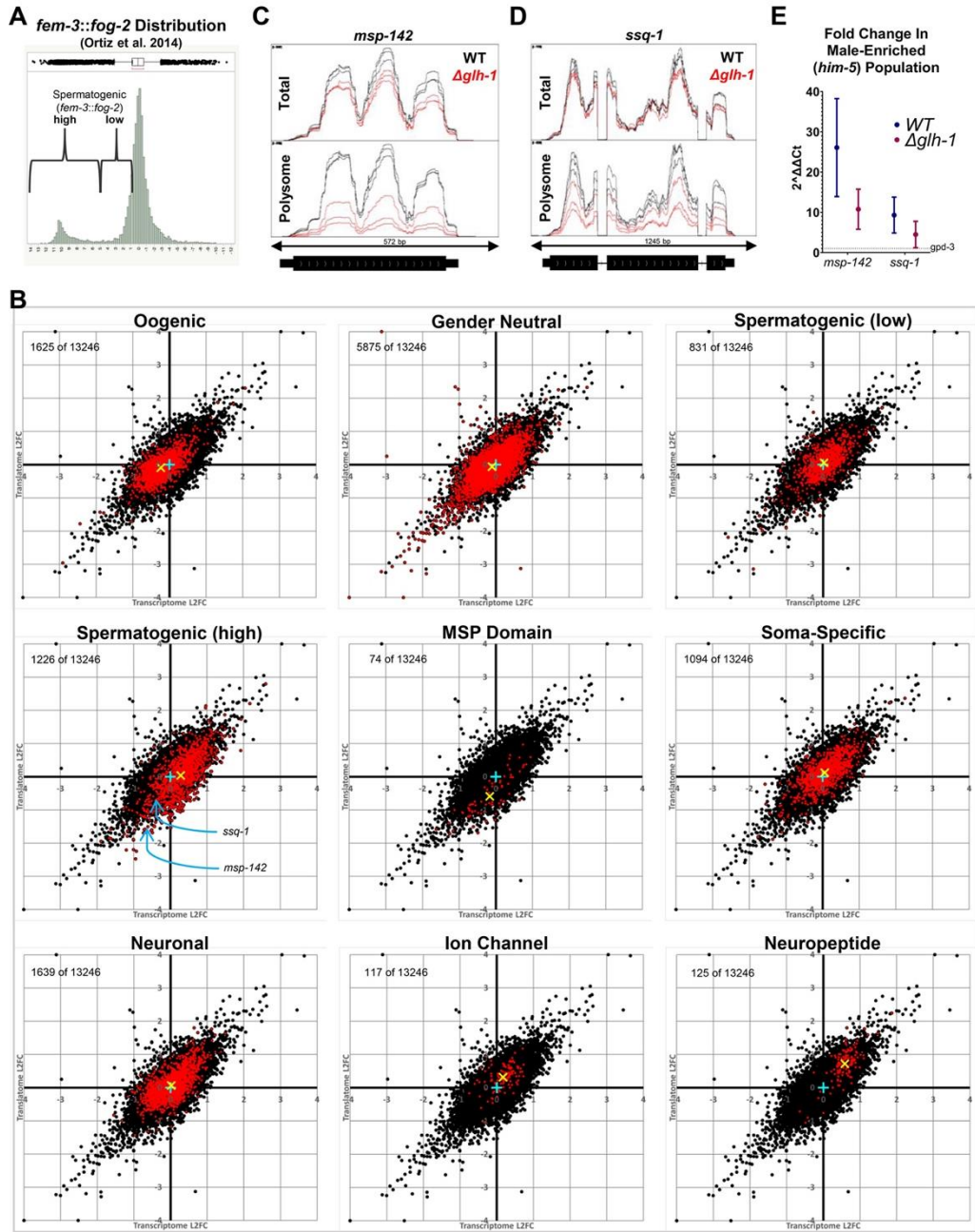


Figure 34:

Allele	Mutation	crRNA(s)	HR template
<i>glh-1(sam65)</i>	Δ <i>glh-1</i>	CTGCGAAAATGTCTGATGGT	TTCTGGAAAATCTTAATTTCTGCGAAAATGTCTAAAGGAGAAGAATTGTTCACTGGAGTTGTCCCAAT
<i>glh-1(sam72)</i>	Δ FG-repeat	TCAGGAGCATCGATGAGTAA GCCAAAACCTGGATTCGGTAG	TTTTGATTAATAAATTTATTTTCAGCCAAAACCTGGAGGGGAAGGAGGACATGGCGGGGAGAGAGAAAACAA
<i>glh-1(sam71)</i>	Δ zinc-finger	GAGGTGGCAACTCTGGTTTT AGAAAGGAAAGAGAGCCGA G	TCAATTGCCAACAGCCAGGACATCGATCGAGTGACGGCGAGCAAGGTCATCGCTCGAATGAGTGCCCCAA
<i>glh-1(sam44)</i>	G→D in flanking	EMS mutagenesis	
<i>glh-1(sam57)</i>	G→D in flanking	CGAAAAACTTGTGAAACATA	ACATGGAGGACGTTTTCAACATGCAGAAAATTCGGAAGATTGATGTTCAACAAGTTTTTCGATGCCGAAGTTAAACTG
<i>glh-1(sam59)</i>	G→W in flanking	CGAAAAACTTGTGAAACATA	ACATGGAGGACGTTTTCAACATGCAGAAAATTCGGAANNNTTGTGTTCAACAAGTTTTTCGATGCCGAAGTTAAACTG
<i>glh-1(sam67)</i>	MF→I in flanking	CGAAAAACTTGTGAAACATA	likely non-homologous end joining (NHEJ)
<i>glh-1(sam66)</i>	Δ MFN in flanking	CGAAAAACTTGTGAAACATA	likely NHEJ
<i>glh-1(sam54)</i>	F→FF in flanking	CGAAAAACTTGTGAAACATA	likely NHEJ
<i>glh-1(sam68)</i>	Δ L in Walker I	GACGAGTCATGATAGGCAG A	likely NHEJ
<i>glh-1(sam69)</i>	Δ P in Walker I	GACGAGTCATGATAGGCAG A	likely NHEJ
<i>glh-1(sam63)</i>	Δ PIM in Walker I	GACGAGTCATGATAGGCAG A	likely NHEJ
<i>glh-1(sam74)</i>	R→Q in Motif Ia	TGATCAGCGAGTTCGCGAGT	GGTTGCTATCCCGTTGCATCATCTTGACTCCAACAACAAGAACTCGCTGATCAAATTTACAACGAGGGAAGAAAG
<i>glh-1(sam86)</i>	Δ D (EAD) in Walker II	*CCGCTTCTTTGTTCTTGACG	likely NHEJ
<i>glh-2(sam87)</i>	Δ D (EAD) in Walker II	*CCGCTTCTTTGTTCTTGACG	likely NHEJ
<i>glh-1(sam94)</i>	E→A (DAAD) in Walker II	*CCGCTTCTTTGTTCTTGACG	CATCAAGCTTGACAAATGCCGCTTCTTTGTTCTTGACGAGCTGATCGTATGATCGATGCTATGGGATTCGGAAC
<i>glh-2(sam89)</i>	E→A (DAAD) in Walker II	*CCGCTTCTTTGTTCTTGACG	CATCAAGCTTGACAAATGCCGCTTCTTTGTTCTTGACGAGCTGATCGTATGATCGATGCTATGGGATTCGGAAC
<i>glh-1(sam92)</i>	E→Q (DQAD) in Walker II	*CCGCTTCTTTGTTCTTGACG	CATCAAGCTTGACAAATGCCGCTTCTTTGTTCTTGACCAAGCTGATCGTATGATCGATGCTATGGGATTCGGAAC
<i>glh-2(sam82)</i>	E→Q (DQAD) in Walker II	*CCGCTTCTTTGTTCTTGACG	CATCAAGCTTGACAAATGCCGCTTCTTTGTTCTTGACCAAGCTGATCGTATGATCGATGCTATGGGATTCGGAAC
<i>glh-1(sam76)</i>	LEL→AGA in KGB site	GACAAACTCTAGAGCTTCT	TCGAGAGATGCGAAAGAAGCGAGAAGAAGGACAAACTGCCGGCGCTCTGGGAATCGATATCGACAGTTACACGACCGGAGA
<i>glh-1(sam62)</i>	Δ LRQFRNGSK b/w IV & V	GCTACTGCGGTGCTGAACG	likely NHEJ
<i>glh-1(sam64)</i>	T→A just before Motif V	GCTACTGCGGTGCTGAACG	AATTCGAAATGGATCGAAACCTGTTCTTATTGCTGCTGCGGTCGAGAGAGGACTTGATATCAAAGGAGTGGATCATGTCA TCAA
<i>glh-1(sam61)</i>	D→A in Motif V	GCTACTGCGGTGCTGAACG	GGATCGAAACCTGTTCTTATTGCTACTGCGGTCGAGAGAGGACTTGATATCAAAGGAGTGGATCATGTCACTCAACTATGAC A
<i>glh-1(sam77)</i>	VPD→AGA in eIF5b site	GCAGACCTTGATCCAGTC	ACTTGTGGTGTCTCTGCCGACGACAACAGATTGCCGGCGCTGGATGCAAGGTGCTGCTGGAGGCAATTACGGAG
<i>glh-1(sam70)</i>	DEE→AGA in (-)W terminus	TCAAGTCCCAGGACGAG G	ATTTGGTCCAGTGTACAACTCAAGTCCCAGCGCCGCGGGTGGGAGCATCGGGAGCCTCAGGAGCATCGA *crRNA targets both <i>glh-1</i> & <i>glh-2</i>

Table 2: CRISPR/Cas9 reagents for generating *glh-1* alleles.

CRISPR/Cas9 reagents for generating *glh-1* alleles

APPENDICE B: DEPOSITED DATA

Data in chapter IV can accessed in the footnotes of (Marnik et al. 2019),
<https://www.ncbi.nlm.nih.gov/pmc/articles/PMC6827368/>

Raw RNA-seq data flies in chapter V can be accessed on NCBI GEO GSE148737 (BioProject ID PRJNA625528)

BIOGRAPHY OF THE AUTHOR

Jesse Rochester, born in August 1994, in Fort Kent, Maine. After graduating from Presque Isle High School in June 2012, he pursued a Bachelor of Biology from the University of Maine Fort Kent, completing the degree in May 2016. During his undergraduate studies, he demonstrated academic excellence and received the Biology Award, an honor bestowed upon students expected to contribute significantly to the field of biology in the future.

Rochester's early career in research began as an undergraduate research assistant under the mentorship of Dr. Peter Nelson at the University of Maine Fort Kent. There, he spent two years conducting ecology research that included tracking subtle changes in climate change using LiDAR and radio spectrometry in the Brooks Range of Alaska and the northern Atacama Desert of Chile, as well as researching an extreme endemic plant of the St. John River basin, which was later published in the IUCN red list of threatened species (Rochester, 2018).

After completing his bachelor's degree, Rochester joined the laboratory of Dr. Dustin Updike at Mount Desert Island Biological Laboratories, where he studied germ granule components of the *C. elegans* germ line for two years before joining the Updike lab as a direct-admit graduate student with the Graduate School of Biomedical Science and Engineering at the University of Maine in 2018. During his time in the Updike lab, Rochester co-authored three journal articles titled "PQN-75 is expressed in the pharyngeal gland cells of *Caenorhabditis elegans* and is dispensable for germline development" (Rochester et al., 2017), "Germline Maintenance Through the Multifaceted Activities of GLH/Vasa in *Caenorhabditis elegans* P Granules" (Marnik et al., 2019), "GLH-1/Vasa represses neuropeptide expression and drives spermiogenesis in the *C. elegans* germline" (Rochester et al., 2022), and was awarded a NIH T32 training grant in 2019.

Jesse Rochester is a candidate for the Doctor of Philosophy degree in Biomedical Science from the University of Maine in August 2023.